Electroding Methods for *in situ* Reverse Osmosis Sensors

Kahlil Thomas Ernest Detrich

Thesis submitted to the faculty of the Virginia Polytechnic Institute and State University
in partial fulfillment of the requirements for the degree of

Master of Science

In

Mechanical Engineering

Nakhiah C. Goulbourne, Chair
Daniel J. Inman
Pavlos P. Vlachos

January 28th, 2010
Blacksburg, Virginia

Keywords: *in situ* sensing, reverse osmosis membrane, platinized polymer graft, fouling, electrical impedance spectroscopy

Electroding Methods for *in situ* Reverse Osmosis Sensors

Kahlil Thomas Ernest Detrich

Abstract

The purpose of this work is to develop and evaluate electroding methods for a reverse osmosis (RO) membrane that results in an *in situ* sensor able to detect RO membrane protein fouling. Four electroding techniques were explored: *i*) gold exchange-reduction, *ii*) encapsulated carbon grease, *iii*) "direct assembly process" (DAP), and *iv*) platinized polymer graft. The novel platinized polymer graft method involves chemically modifying the RO membrane surface to facilitate platinization based on the hypothesis that deposition of foulant on the platinized surface will affect platinum/foulant/solution interfacial regions, thus sensor impedance. Platinized polymer graft sensors were shown to be sensitive to protein fouling.

Electrodes were characterized by their electrical properties, SEM and XPS. Assembled sensors were evaluated for sensitivity to electrolyte concentration and protein fouling. Micrographs showed coating layers and pre-soak solution influence gold exchange-reduction electrode formation. High surface resistance makes gold exchange-reduction an unsuitable method. Concentration sensitivity experiments showed carbon grease and DAP electroding methods produce unusable sensors. Carbon grease sensors have time-dependent impedance response due to electrolyte diffusion within the micro-porous polysulfone support. DAP electroded sensors proved quite fragile upon hydration; their impedance response is transient and lacks predictable trends with changes in concentration. A parametric study of the platinized polymer graft method shows amount of grafted monomer correlates to grafting time, and deposited platinum is a function of exchange-reduction repetitions and amount of grafted monomer. Platinized polymer graft sensors were fouled in both dead-end and cross-flow RO systems, and their impedance trends, while varying between sensors, indicate protein-fouling sensitivity.

Acknowledgements

The work presented in this thesis was not done in isolation. Firstly, I would like to thank Dr. Nakhiah Goulbourne, my advisor, who was the motivating force behind this research. She provided funding and, more importantly, academic guidance and insight; she taught me how to ask the right questions and find the right answers. Beth Howell provided much support through her administration of the project and help navigating the oftentimes-tortuous paths of HokieMart and reimbursements. From a research standpoint, I had much assistance with various stages of the project. Dr. Andy Duncan was an immense help with the finer points of the "direct assembly process" and a walking encyclopedia of polymeric knowledge. Minjae Lee graciously loaned chemistry equipment and taught me the necessary techniques for making the gold complex used in the gold exchange-reduction method. Dr. Judy Riffle provided insight and advice for the grafting portion of platinized polymer graft sensor development. Steve McCartney (SEM), John McIntosh (FIB-SEM) and Dr. Jerry Hunter (XPS) at the NCFL and Vicki Long were indispensible in characterizing the electrodes. I would also like to thank Dr. Pavlos Vlachos and Dr. Dan Inman for graciously serving on my committee.

A big "thank you!" also goes to Dr. Dan Inman for his support, comedic wit and for making CIMSS the wonderful lab that it is. Along that vein, I owe a large debt of gratitude to my colleagues in CIMSS for both their help and their humor. Bantering with Andy Sarles kept my Appalachain twang well polished. He was also an indispensible resource in working with electrical impedance spectroscopy and the intricacies of AutoLab. Political and religious discussions with Austin Creasy provided a nice contrast with the more black and white (and staid) world of engineering, and he taught me the art of milling. Onur Bilgen and Dr. Pablo Tarazaga helped me perfect my lab birdcalls and kept the lab running smoothly and with healthy dose of humor. Dr. Alper Erturk's proclivity for research productivity and discussions on the "why" of academia kept me inspired. Extracurricular activities with Steve Anton and Devon Murphy made long lab hours bearable while Jacob Davidson kept me in shape, dancing and was a programming whiz. In addition, Josh Stenzler, Seyul Son and Justin Klein helped make the past few years memorable and fun.

I want to thank Jim and Sue Stade for their support, hospitality and chicken/cat-sitting. My parents, Bob and Donna, provided me encouragement, advice and a splendid "retreat" when I

needed a break from academic rigors and Blacksburg. Finally, Natalie Stade has been a constant companion, breath of fresh air, exercise motivator and a welcomed distraction. She has tolerated me with an unbelievable amount of patience, love and interstate travel.

This research was funded, in part, by a grant from the National Science Foundation PFI: Partnerships for Water Purification (0650277). The author created all figures and took all of the photographs in this document.

Table of Contents

Table of Figures

Table of Tables

1. INTRODUCTION

The purpose of this research is to explore and develop electroding methods for a thin film composite ionomer that may result in a sensor able to detect protein fouling of a reverse osmosis (RO) membrane using electrical impedance spectroscopy. We fabricated four types of contact electrodes: *i*) encapsulated carbon grease, *ii*) DAP – gold foil and RuO_2/Nafion laminates based on a "direct assembly process", *iii*) gold exchange-reduction – gold nanoparticles deposited using an exchange-reduction reaction, and *iv*) platinized polymer graft – discontinuous platinization of a modified polyamide thin film. The electrodes were characterized using their electrical properties, SEM and XPS. The carbon grease and DAP sensors' electrolyte concentration sensitivity were probed with electrical impedance spectroscopy (EIS). EIS was also used to evaluate the response of platinized polymer graft sensors to protein fouling in both dead-end and cross-flow RO systems. The ultimate goal of this research is to develop an *in situ* sensor sensitive to chemical degradation and various membrane foulants to facilitate a proactive rather than reactive approach towards RO system operation. Real-time detection will allow for membrane cleaning, pretreatment adjustment of feedwater and membrane replacement as needed rather than waiting for a decrease in membrane performance or membrane failure. This will lead to improved system operation efficiency and decreased operating expenditures.

This chapter provides an overview of reverse osmosis membrane technology, *in situ* sensing techniques used in RO research, sensing techniques based on electrical impedance spectroscopy and polymer electroding methodologies.

1.1. Motivation

As recently as 2004, over 1 billion people lacked access to an improved water supply, and as global demand increases, clean water will become an ever more precious commodity[1]. Reverse osmosis has emerged as the most energy efficient method for desalination and wastewater treatment; however, maintenance and replacement of the semipermeable, thin film composite ionomer membrane modules used in modern RO systems significantly raise operating costs and face several challenges[2]. These thin film composites are susceptible to chemical degradation from water pretreatment and fouling due to feedwater chemistries. Monitoring the membranes' condition in real-time is likely to decrease the high operating costs by allowing maintenance and replacement to be tailored to the conditions of the system rather than relying on

scheduled maintenance and/or membrane failure. This thesis presents a study of electrode techniques for developing an *in situ* sensor based on the RO membrane. Specifically, electrical impedance spectroscopy is utilized to detect changes in the interfacial regions of the sensor as a measure of salt concentration and protein fouling.

1.2. Reverse osmosis and semipermeable membrane development

RO is a process that uses hydraulic pressure to force solvent from a high concentration solution (feedwater) to a lower concentration solution (permeate) through a semipermeable membrane that prevents passage of solutes. Rather than equalizing the osmotic pressure due to disparate concentrations (or chemical potentials) of the separated solutions as is energetically favorable, the energy applied to the system overcomes the osmotic pressure to transport solvent against this gradient. RO applications are varied and include dialysis, the fruit juice and dairy industries and, most relevant to our research, desalination and wastewater treatment.

Desalination utilizing reverse osmosis and a semipermeable membrane was first explored by Reid and Breton in the late 1950's using a dead-end stirred cell configuration and a cellulose acetate membrane[3]. Building on their work, Loeb and Sourirajan discovered that key to the salt rejection properties of cellulose acetate membranes was their asymmetric morphology and, indeed, preferentially rejected solutes in one direction[4]. By controlling the membrane asymmetry with hand casting, they were able to greatly improve membrane performance as compared to the modified commercial membranes used by Reid and Breton. Consequently, Loeb and Sourirajan are credited with developing the first cellulose acetate membranes with high enough permeate flux and salt rejection as to be commercially practicable[4]. Further developments in membrane technology led to novel membrane geometries and polymeric membrane materials beyond cellulose acetate[5-8]. Cadotte improved on high performance membrane construction using interfacial polymerization onto a supporting layer to create a thin film composite structure[9-10]. Larson, Cadotte and Petersen later developed a fully aromatic polyamide formed by an interfacial polymerization reaction[11]. Recent research has explored membrane surface modification with coatings, polymer grafts and novel chemistries to further improve performance and increase chemical and fouling resistance[12-17]. Despite the ongoing search for RO membrane improvements, highly cross-linked, interfacially polymerized aromatic polyamide thin film composites remain the industry standard.

1.3. Polyamide membrane chemistry and morphology

Current commercial membranes typically consist of a polyamide thin film interfacially polymerized on a porous polysulfone support that has been cast on a non-woven backing layer (Figure 1). The aromatic polyamide thin film composite membranes used in this research are based on DOW's FT30 crosslinked aromatic polyamide thin films formed by the reaction of 1,3 phenylene diamine and trimesoyl chloride[18]. These membranes have been characterized extensively by two groups. Freger et al. studied the heterogeneous morphology of commercial thin film membranes and showed three distinct regions having different charges, chemistries and densities due to interfacial polymerization[19-20]. The outermost layer is rich in carboxyl endgroups and negatively charged while the innermost layer is rich in positively charged amine endgroups. Between the two oppositely charged layers is a much denser thin layer that may determine the flux and salt rejection properties of the membrane[19-20]. Tang et al., using XPS, TEM, ATR-FTIR and streaming potential, showed strong evidence of an aliphatic polymeric alcohol coating on certain commercial membranes[21]. The gold exchange-reduction electrodes mentioned earlier in this chapter exploited the carboxyl endgroups of the polyamide and both coated and uncoated membranes were used.

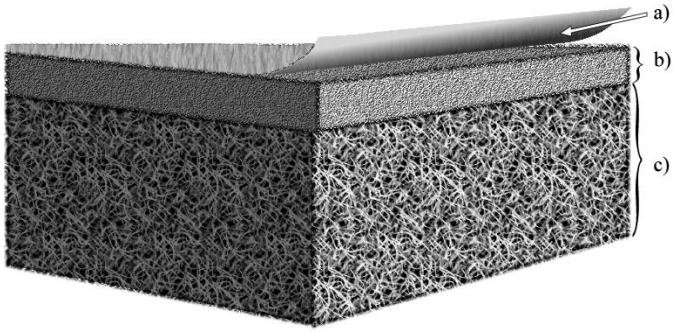

Figure 1: Schematic of a thin film composite membrane - a) polyamide ~ 0.2 μm; b) polysulfone 40 μm; c) non-woven backing 120 μm.

1.4. Membrane challenges

Cross-linked polyamide RO thin films are fairly chemically resistant and mechanically robust but continue to present problems in commercial RO systems. Feedwater is typically pretreated with biocide, most commonly chlorine, to decrease biofouling. The addition of chlorine necessitates its removal before reaching the RO stage because even trace amounts of an oxidizer such as chlorine have been shown to degrade the polyamide thin film, resulting in membrane failure[22-

24]. The extra steps involved with chlorine removal obviously increase overall system complexity and cost. Soice et al. attributed membrane failure to two different mechanisms[23]. Using pendant drop mechanical analysis, they showed that chlorine exposure at a constant pH decreased the ductility of the polyamide thin film possibly due to amide or aromatic ring chlorination. Thin film exposure to chlorine at low pH followed by a caustic pH, such as in a cleaning cycle, showed significant "loosening" of the membrane due to either morphological changes or polymer chain scission. Kwon et al. tested a commercial aromatic polyamide membrane over a range of pH and chlorine concentrations[24]. Their results showed a change in surface charge and chemistry attributed to chlorination of amide bonds and, to some degree, the aromatic ring. They concluded membrane failure is from a weakening of the hydrogen bonds responsible for some of the mechanical strength of the polyamide.

Along with chemical degradation, significant effort is being devoted to understanding and predicting other phenomena that decrease RO membrane performance (defined as a decrease in permeate flux or a decrease in salt rejection). The ultimate goal of these efforts is to maximize operating efficiency while minimizing operating cost. Concentration polarization and fouling are two primary mechanisms that decrease membrane performance and lead to failure (Figure 2). Concentration polarization describes the formation of a boundary layer of higher solute concentration at the membrane surface than that of the bulk feedwater due to solutes being rejected by the membrane faster than can diffuse back into the bulk feedwater. As well as decreasing permeate flux by increasing the local osmotic pressure; concentration polarization causes an apparent decrease in salt rejection. Furthermore, concentration polarization of less soluble salts can lead to scale formation on the membrane surface, which fouls the membrane and decreases its performance[25-26]. In addition to scaling, RO membranes are susceptible to fouling by proteins, microorganisms, and colloids that invariably reach the RO modules because of imperfect feedwater pretreatment[2, 27-31]. The fouling layers decrease membrane performance by increasing the need for chemical cleaning, decreasing permeate flux due to hydraulic resistance, and decreasing salt rejection[32]. Protein fouling is associated with RO treatment of wastewater. Several groups have studied protein fouling using bovine serum albumin (BSA) as a model protein and concluded membrane roughness as well as surface morphology play an important role in membrane fouling[33-34]. Ang and Elimelech's research with protein fouling showed a strong correlation between foulant-foulant electrostatic forces as

measured by atomic force microscopy and long term permeate flux decline[35].

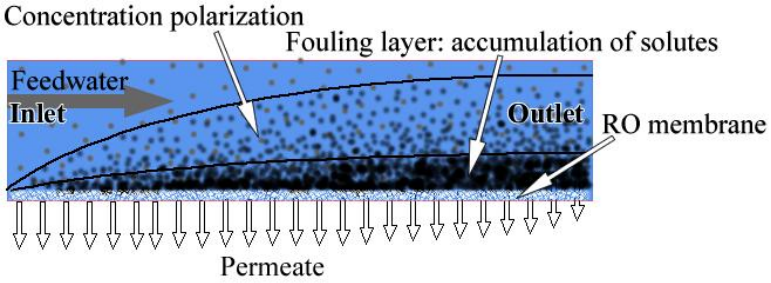

Figure 2: Development of concentration polarization and foulant layer formation in an RO cross-flow system.

One successful tactic developed within the past decade or so to decrease RO membranes' susceptibility to fouling has been to modify the surface of the polyamide thin film because of its importance in determining fouling properties. Several approaches have been taken including dip coating to reduce surface roughness[15, 36] and grafting monomers to tweak the surface charge and morphology of the polyamide thin film[13-14, 37-38]. The research presented in this thesis capitalizes on Belfer et al.'s recipe for grafting sulfopropyl methacrylate to the RO membrane. Rather than trying to improving fouling resistance, we selected the specific monomer for its chemical structure in order to electrode the membrane and make a sensor. The details of this approach will be discussed in later sections and chapters.

1.5. *In situ* sensing approaches

The ability to detect membrane fouling and degradation prior to membrane failure is paramount for any sensor. Over the years, numerous approaches for an *in situ* RO membrane sensor have been explored; however, relatively few were meant for implementation in a commercial system. Predominately, *in situ* laboratory techniques have been developed to probe the physico-chemical mechanisms responsible for concentration polarization, fouling and membrane degradation and were reviewed and critiqued in a paper by Chen[39]. Several optical techniques have been applied to detect either concentration polarization or membrane fouling, but all require specialized cross-flow cells that would be difficult to incorporate into the spiral wound membrane configurations predominantly used in modern RO plants[40-42]. Moreover, the light deflection techniques used to quantify concentration polarization would not simultaneously work to detect fouling as the fouling layer would scatter or absorb light rather than only change the refractive index. The techniques employing laser triangulation[43], light absorption[44-45] or

optical microscopy[46-49] to monitor fouling layer formation would likewise be unable to quantify salt concentration at the membrane surface. Nuclear magnetic resonance[50-52] and labeling with radioisotopes[53] are impractical for commercial implementation. Ultrasonic time-domain reflectometry has been used to detect foulant layer formation by measuring the time delay between signals reflected from the foulant layer surface and the membrane layer surface due to a change in acoustic impedance of the system[54-57]. Current limitations of this technique include resolutions of foulant layer on the order of microns and an inability to detect membrane degradation. Electrical impedance spectroscopy is another more promising method being applied to *in situ* RO research[58-59]. It has several advantages for RO sensing applications including requiring minimal modification of the membrane system (adding the electrodes), being a widely studied sensing technique in other applications and easily automated. Most importantly, EIS results can be correlated to phenomena occurring at interfaces as well as changes in material properties implying it may be able to differentiate between various phenomena (i.e. concentration polarization, fouling and membrane degradation).

1.6. Electrical impedance spectroscopy

As previously mentioned, EIS is a technique widely used to study electrochemical interactions as well as material properties and has been effectively employed as a sensing method for many applications. In this thesis, EIS was utilized as a means for detecting changes (such as fouling) occurring at the surface of an RO membrane. The following paragraphs will provide an overview of EIS theory and its sensing applications directly related to the approaches explored in the research presented in this thesis.

The basic approach of EIS is to apply a small alternating potential to a system through a range of frequencies while simultaneously measuring the resulting current response through the system. If the amplitude of the applied voltage lies within a pseudo-linear region of the system, the resulting current will be at the same frequency as the applied voltage and have a magnitude and phase shift related to the system impedance. Impedance, analogous to Ohm's law, is the ratio of the applied voltage divided by the measured current response and is a function of voltage frequency

$$Z = \frac{V_0}{i_0}\frac{\sin(\omega\, t)}{\sin\,(\omega\, t - \varphi)} = Z_0\frac{\sin(\omega\, t)}{\sin\,(\omega\, t - \varphi)} \quad (1)$$

where V_0 is the magnitude of the applied voltage, i_0 is the magnitude of the current response, Z_0 is the impedance magnitude $\left(\frac{V_0}{i_0}\right)$, ω is the radial frequency (rad/s) and φ is the current's phase shift (rad).

From this equation, a Bode plot of the frequency response of the sensor can be plotted with Z_0 and φ as a function of ω. Assuming the current has a pseudo- linear response to voltage and is time invariant, the resulting impedance spectra provides insight on the mass transport of ions, reaction rates, dielectric properties, composition, defects, among other phenomena of the system[60]. The impedance response can be represented by a suitable combination of electrical elements: resistors, capacitors and constant phase elements[61]. In the sensing experiments, we anticipated that EIS could be used to probe the heterogeneous interfacial regions between the membrane, electrode, foulant and aqueous solution. Developing an equivalent circuit is a popular method for analyzing EIS results; and, although useful for representing the measured response, an equivalent circuit by itself does not provide insight into the physical mechanisms responsible for the observed trends. Examining the mechanisms affecting sensor response was beyond the scope and intent of this thesis, so rather than fitting an assumed circuit model to probe physical phenomena, the impedance spectra were analyzed qualitatively for trends related to changes at the sensor surface.

As mentioned in the preceding paragraph, the impedance response of a sensor can provide valuable insight into its physical properties, processes and interfacial regions. Because of this, EIS is commonly used in biosensing applications and, to some extent, to investigate RO membrane transport and rejection mechanisms. Bason et al. extensively studied the transport mechanisms and diffusion coefficients through RO polyamide thin films required by current RO transport models[62]. In their work, the polyamide layer was adhered to a glassy carbon working electrode after swelling with N,N-dimethyl formamide; the supporting polysulfone layer was removed with subsequent solvent washings exposing the polyamide interlayer to the surrounding solution. A platinum wire immersed in the surrounding solution acted as the auxiliary electrode and a Ag/AgCl KCl half cell was the reference electrode. With this three-electrode configuration, they measured the ion permeability of the polyamide membrane for both an inactive salt (KCl) solution and an electroactive ion couple (ferri- and ferrocyanide). The relevant results of their experiments as related to this research showed a decrease in impedance

due to an increase in KCl concentration in the 10 Hz to 10 kHz frequency range. They attributed the change in membrane resistance directly to ion permeability of the membranes, the diffusion of the salt through the membrane. Our initial sensor methodologies were targeted towards detecting changes in electrolyte concentration to establish a baseline response from which other phenomena (i.e. fouling) could be distinguished as well as evaluate the sensors' viability in detecting concentration polarization.

The platinized polymer graft sensors developed in this thesis were evaluated for sensitivity to protein fouling. Park et al. probed the change in electrical properties of an ion-exchange membrane with different degrees of protein fouling (BSA) as well as different protein concentrations in the surrounding solutions using EIS and a non-contact four electrode system[63]. They used a two chamber test setup with the ion exchange membrane dividing the chambers. Voltage was applied via two large planar Ag/AgCl working electrodes and current was measured with two reference electrodes immersed in Luggin capillaries and separated by the membrane plus a 6 mm gap. Their experimental results fit to an equivalent circuit showed the resistance increasing with deposition of protein from 74 to 82 Ω (about 11%) for the frequencies measured (6.8 mHz to 104 kHz) while the observed capacitance did not perceptibly change. Using an in-plane rather than through-thickness impedance approach, Gaedt et al. sputtered a 60 nm thick platinum electrode on a polysulfone ultrafiltration membrane to infer surface roughness and membrane porosity from the platinum-solution interfacial electrical properties[59]. They proposed that their in-plane sputtered electrode could also be utilized as a sensor employing EIS to monitor the response as the solution-platinum interface becomes a solution-foulant-platinum interface. Unfortunately, the sputtered layer significantly decreased the water flux by reducing the porosity of the polysulfone, and their investigation ended there. Similar to Gaedt et al.'s proposal, DeSilva et al. used EIS and a thin, discontinuous platinum film on a silicon dioxide substrate as an in-plane biosensor for Staphylococcus enterotoxin B[64]. The platinum film, deposited using electron beam evaporation, was coated with the toxin's antigen for binding specificity. Their results showed an irreversible 86% decrease, from 1.6 kΩ to 220 Ω, in sensor impedance at 100 Hz resulting directly from protein (enterotoxin B) binding to its antigen on the discontinuous electrode surface. We have developed a platinized polymer graft sensor that has a discontinuous platinum film similar to DeSilva et al.'s sensor but does not incorporate protein-specific binding sites.

1.7. Electroded polymers

Four electrode fabrication techniques were investigated in this thesis: *i*) compliant electrodes with carbon grease, *ii*) penetrating electrodes following a "direct assembly process", *iii*) chemically deposited gold employing an exchange-reduction process, and finally *iv*) chemically deposited platinum using a newly developed platinized polymer graft method. The purpose of electroding the RO membrane was to create an *in situ* sensor and use EIS to detect changes in interfacial properties and interactions. Fabricating the electrode on the RO thin film composite membrane proved the most challenging and critical aspect of the research. As such, we will outline RO electrode requirements and give an overview of polymer electroding applications and techniques that provide the foundation for the methodologies developed in this work.

1.7.1. Electrode requirements for *in situ* RO sensor

The electroding method is crucial in the development of a truly *in situ* sensor for an RO system. An ideal electrode system will be: *i*) sensitive to the onset of fouling and changes in concentration polarization, *ii*) capable of detecting membrane degradation, *iii*) mechanically robust to withstand hydraulic pressures and feedwater velocities, *iv*) chemically resistant to feedwater conditions and cleaning protocols. Furthermore, the sensor should accomplish these tasks without significantly interfering with membrane performance (solute rejection and permeate flux). The final motivation for using the RO membrane itself as the sensor is to reduce the introduction of extraneous elements to the system.

1.7.2. Basis for electroding methodologies

Previous electroding methods applied to RO membranes have failed to meet the sensor requirements. In Bason and Freger's experiments, the polyamide thin film lacking the polysulfone support layer proved to be mechanically unstable even when supported by a glassy carbon surface[62]. Sputtering platinum on the active layer of an ultrafiltration membrane significantly decreased membrane performance and failed to probe membrane properties [59]. Finally, non-contact through-thickness electrodes as used by Park et al. would be difficult to implement as an *in situ* sensor in typical RO membrane systems[63]. Keeping these prior attempts in mind, we looked to other applications employing electroded polymers.

As a first approach, RO membranes were electroded with compliant electrodes. Compliant electrodes are light, easily fabricated electrodes used in conducting electrical components and,

more recently, in dielectric elastomer transducers. Dielectric elastomer transducers utilize flexible and conductive electrodes to generate large strains through the application of an electric field between two electrodes separated by an incompressible elastomeric dielectric membrane. Experiments performed by Fox and Goulbourne, Pelrine et al. and Carpi et al. showed carbon grease to be an effective electrode[65-67]. In our research, carbon grease electrodes were explored because of their straightforward fabrication and low cost, and it was thought the conductive grease might make sufficient contact with the relatively rough and folded surface of the polyamide thin film to detect changes in its electrical properties due to electrolyte concentration sensitivity in the surrounding solution. Ultimately, this proved not to be a viable method for making a robust RO sensor.

A second method investigated was electrodes based on a "direct assembly process" (DAP) commonly used in electroding Nafion™, a commercial perfluorosulfonic acid ionomer. These electrodes, like those of dielectric elastomer transducers, are compliant; however, the DAP is less straightforward and more expensive. The approach used in this thesis followed a method developed for ionic polymer metal composites (IPMC) by Akle et al. [68]. In their approach, a conducting dispersion of ruthenium oxide and Nafion is melt-pressed into the substrate ionomer membrane to form a conductive penetrating network. Surface conductivity of the electrode is further enhanced by either chemically plating platinum using an impregnation-reduction technique followed by gold electroplating or melt-pressing a layer of gold foil to the electrode. In the end, RO membrane DAP electrodes failed to sufficiently meet sensor requirements outline in the previous section.

A method developed early in the evolution of IPMC electrodes was to chemically reduce rather than melt-press the electrodes [69]. Flemion™ is a perfluorocarboxylic acid ionomer used as a substrate for IPMC transducers and is electroded using an impregnation-reduction electroding method [70-71]. In the electroding recipe presented by Oguro et al., gold salt penetrates the perfluorocarboxylic acid ionomer and exchanges with the cation ionically bound to the negatively charged carboxylate groups of Flemion. The Flemion membrane impregnated with gold salt is subsequently placed in a chemically reducing solution to convert the cationic gold compound to elemental gold. The RO polyamide thin film contains carboxyl rich regions on its

outermost surface, and we attempted to use Oguro et al.'s recipe to exploit the membrane chemistry in making a sensor.

Our final sensor design, inspired in part by DeSilva's biosensor mentioned previously, used a platinum exchange-reduction recipe to deposit platinum nanoparticles at the sulfonate endgroups of a monomer grafted to the polyamide thin film. This platinized polymer graft electrode was based on an impregnation-reduction recipe used in electroding Nafion IPMCs. The method is similar to that used for Flemion-based IPMCs. *Platinum* salt exchanges with cations on *sulfonate* groups rather than *gold* salt exchanging with cations on the *carboxylate* groups as in the case of Flemion electroding. The Nafion membrane impregnated with platinum salt is subsequently placed in a chemically reducing solution to convert the platinum salt to elemental platinum. By repeating the impregnation-reduction steps, the morphology and conductivity of the electrode can be somewhat controlled.

1.8. Scope of Thesis

This thesis provides a foundation for the development of a novel *in situ* reverse osmosis sensor capable of detecting the onset of fouling, and ultimately membrane degradation and concentration polarization.

Preliminary research used carbon grease and the "direct assembly process" to electrode sensors for detecting variable electrolyte concentrations. It was hypothesized that diffusion of electrolyte through the thin film composite and between the through-thickness electrodes would affect sensor impedance due to solution resistance and double layer capacitance. Results suggested the carbon grease sensor's response was due to diffusion of the electrolyte solution through the porous polysulfone support rather than directly measuring a change in electrical properties of the active polyamide thin film layer. DAP sensors lacked the durability required for sensing experiments and were not pursued further.

Electrodes made using a gold exchange-reduction method indicated the high degree of cross-linking in the polyamide thin film limits the concentration of carboxyl groups able to participate in the gold exchange reaction. Results also showed that the presence of a coating layer on the polyamide influenced gold deposition.

Finally, a novel platinized polymer graft sensor was fabricated, and protein fouling experiments were carried out to evaluate its response using both dead-end and cross-flow RO filtration experimental configurations. It was anticipated that the addition of a platinized polymer graft would sensitize the surface of the polyamide thin film to adsorption of foulants, specifically BSA (a commonly used model protein). The morphology of the platinized area from SEM results (presented in Section 3.4.1) was shown to consist of discontinuous platinum nanoparticles (~20 nm diameter) on the surface of the polyamide thin film. These conductive islands provide a preferential current path with the electric field applied when using EIS. With the adsorption of a fouling layer, the interfacial regions of platinum/foulant/solution separating the islands would certainly manifest themselves as changes in sensor impedance. The characteristically large surface area to volume of nanoparticles provides a relatively large interfacial area to be probed by EIS, in turn leading to increased sensitivity. It was expected that the impedance response of the sensor would change with adsorption of protein to the surface. Parametric studies on the influence of reaction times and layer deposition were performed; the results will be presented in Chapter 3.4. An initial cross-flow experiment showed the platinized polymer graft to be somewhat durable when exposed to very high pressures and flow rates. EIS results indicated the platinized polymer graft sensors were sensitive to fouling, but their responses were inconsistent varying significantly between sensors and experimental conditions. Results will be presented and discussed in Chapter 5.

Chapter 2 outlines the electroding fabrication materials, methods and recipes. In Chapter 0, the results of electrode characterization using electrical resistance, qualitative and quantitative durability analysis and microscopy are presented. Following electrode characterization, Chapter 4 discusses the results of the concentration polarization sensing experiments for the carbon grease and DAP sensors. The results of protein fouling experiments using the platinized polymer graft sensors are communicated in Chapter 5. The thesis concludes in Chapter 6 with a summary of the work done so far, contributions to the field of *in situ* sensing in reverse osmosis systems and future directions further research could continue based on the research completed thus far.

2. POLYMER ELECTRODING METHODS

The goal of this study is to determine an optimal electrode methodology and to assess sensor performance as a function of membrane fouling. In this chapter, four electrode fabrication techniques will be described. The first two techniques explored involve contact and interpenetrating electrodes – specifically, using carbon grease and a direct assembly process. A third electroding technique, gold exchange-reduction, chemically deposited gold clusters on the RO membrane surface. The fourth method deposited conductive platinum nanoparticles on a chemically modified RO surface; this technique involved a grafting process to facilitate chemical deposition of the platinum. The following section will describe the RO membranes used. Subsequent sections will outline fabrication methods for each type of sensor.

2.1. RO membranes

The electroding approaches were applied to one or more of several well-characterized commercial RO membranes. Three different RO membranes (SW30HR, BW30LE, and BW30) were supplied by DOW Filmtec^{TM}. All three membranes' active thin films are based on DOW's FT-30 aromatic polyamide membrane formed by interfacial polymerization of 1,3 phenylene diamine and the tri acid chloride of benzene. The membranes are highly crosslinked because of the three functional groups on the benzene ring and have both amine and carboxylate endgroups. The SW30HR membrane is meant for seawater desalination at high operating pressures (greater than 2.5 MPa); the BW30 and BW30LE membranes are tailored for desalinating brackish water and operate at much lower pressures (0.5 – 1 MPa)[18]. Tang et al. showed that both BW30 and SW30HR membranes have a layer containing aliphatic alcohol groups coating the polyamide thin film while the BW30LE membranes are not coated[21]. The presence or absence of the coating determined to some extent which samples were used in the electroding approaches. The thin film composite membranes were stored as received in dark, dry and room temperature conditions and typically boiled in DI water to clean before use.

2.2. Carbon grease electrode fabrication

Carbon grease is a commonly employed contact electrode in used in the fabrication of electromechanical transducers. Specifically, carbon grease is used as an effective compliant electrode for dielectric elastomer actuators and sensors[72]. As a first approach, mechanically

robust carbon grease electrodes encapsulated with epoxy were fabricated in both through-thickness and surface configurations.

The following steps were applied to both SW30HR and BW30LE membranes. The non-woven backing layer was mechanically removed prior to electroding. For the through-thickness configuration, a layer of carbon grease was painted uniformly on a 25 mm^2 area (~ 0.5 µL) of both the polyamide and polysulfone sides (Figure 3a). The in-plane electrodes consisted of two 25 mm^2 carbon grease areas separated by 4 mm (Figure 3b). Electrical leads were attached via wires soldered to stainless steel coupons smaller than the painted electrode. The stainless steel coupon/electrical lead assembly was carefully clamped onto the carbon electrode and epoxied in place (Scotch-Weld DP105, 3M) with the epoxy border extending 1mm beyond that of the carbon grease. The epoxy provided strain relief for the lead attachment, stabilized the carbon grease in the presence of water and electrically insulated the electrode from the surrounding environment. Figure 3c shows a fully assembled electrode on the polyamide side of a membrane. After the epoxy had fully cured, the electroded samples were placed in deionized water for two hours for cleaning prior to implementation.

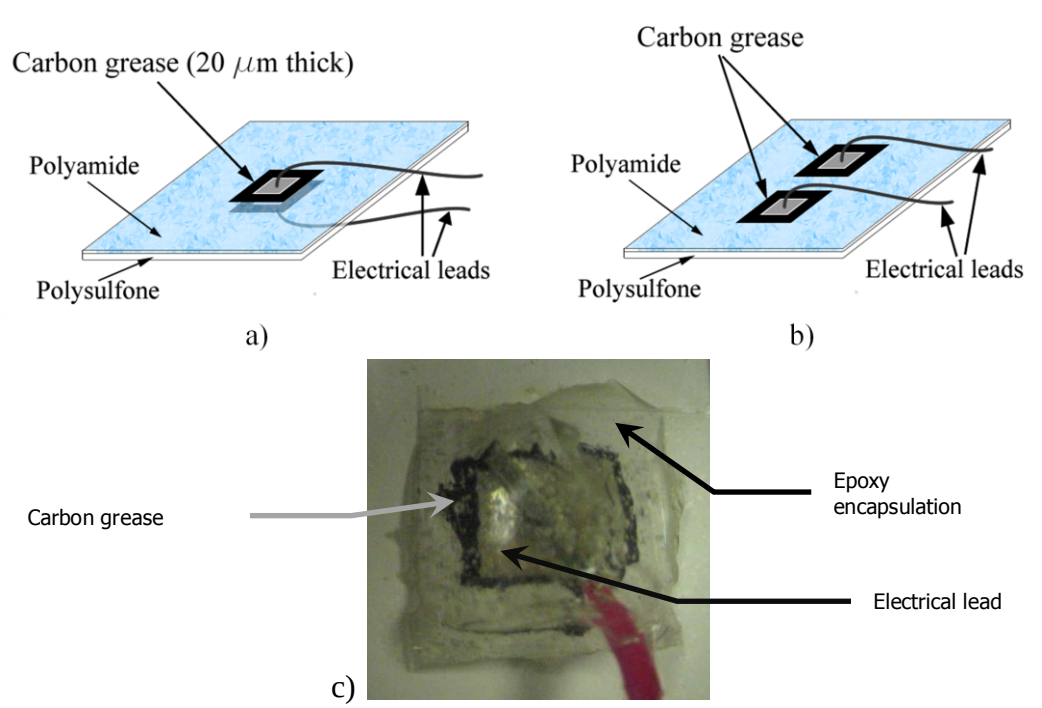

Figure 3: Carbon grease electrode construction – a) through-thickness, b) in-plane, and c) shows a fully fabricated sensor.

2.3. Direct assembly process electrode fabrication

The second method explored uses an asymmetric Direct Assembly Process (DAP) to electrode the polyamide side of the membrane while melt-pressing gold foil to the polysulfone side to create a through-thickness sensor. As discussed in Chapter **Error! Reference source not ound.**, DAP electrodes were originally developed for fabricating IPMCs with mechanically stable, highly conductive surfaces with a more controlled geometry and morphology than those created using impregnation-reduction methods[68]. These sensors used the same electrode geometry and size as the carbon grease electrodes (square, 25 mm^2).

Similar to the carbon grease electrodes, both SW30HR and BW30LE membrane samples were electroded following removal of the non-woven backing layer and boiling in deionized water for cleaning. Following Akle et al.'s DAP electroding recipe, a conducting dispersion (40 vol% RuO_2) was created[68]. A 5% Nafion dispersion (Fuel Cell Store) (90 mg) was added to 23 mg of electronic grade ruthenium oxide (RuO_2) (Alfa Aesar), deionized water (56 mg) and isopropyl alcohol (43 mg) for each sample. It was assumed 30% was lost due to overspray and the layer was 15 microns thick when calculating the volume of conductive dispersion required. The mixture is sonicated for at least one hour to ensure the RuO_2 particles are well dispersed and then sprayed on the polyamide thin film with an airbrush. As a modification to Akle et al.'s process, the conducting dispersion was applied in one step rather than several with heat and pressure applied between repetitions. To facilitate a one step application and to prevent puddling and running, a heat lamp evaporated the water and isopropyl alcohol from the conductive dispersion during application. The membrane was then completely dried *in vacuo* at 100^{o}C leaving a 25 mm^2 RuO_2/Nafion layer on the membrane. Prior to applying gold foil (500 nm thick, Arrow Springs), a thin film of a Nafion and isopropyl alcohol solution (50 wt%) is brushed on the RuO_2/Nafion layer as previous attempts had shown this improved gold foil adhesion. The gold foil is subsequently melt-pressed onto the RuO_2/Nafion layer and onto the polysulfone support layer for 90 s at 180-185^{o}C and 8.9 MPa (1290 psi). This temperature is higher than the glass transition temperature of both polysulfone and Nafion, thus improving the mechanical bond of gold to the two polymers. Figure 4 shows both a schematic of the DAP electrode and images of the electroded polyamide side (b) and polysulfone side (c).

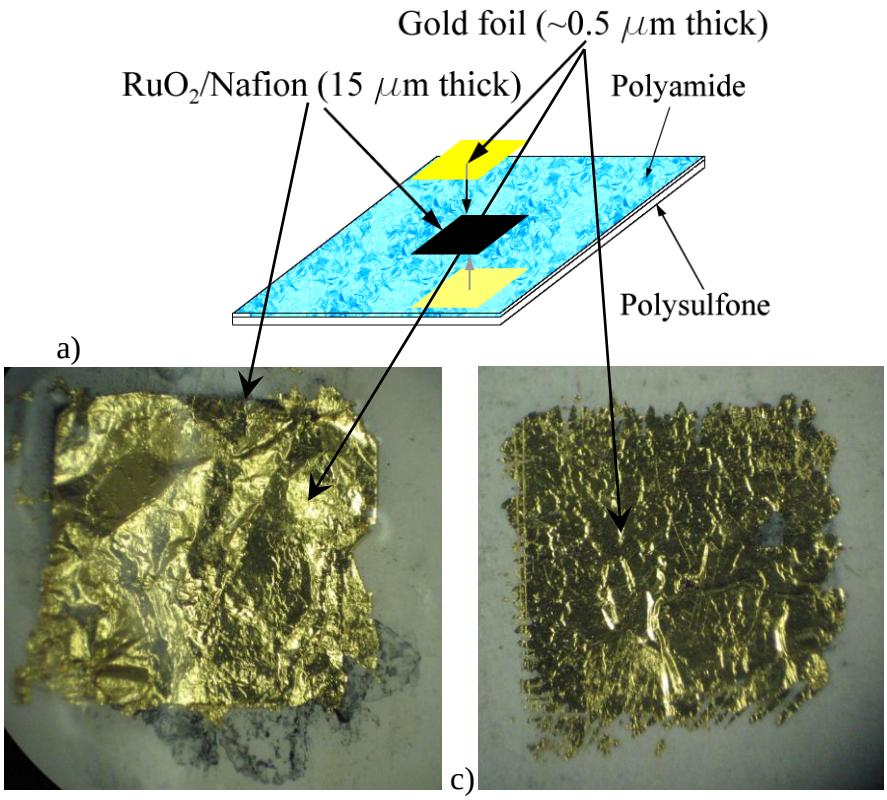

Figure 4: Melt-pressed DAP electrode schematic (a) and actual sensor on a SW30HR membrane – polyamide DAP electrode (b), polysulfone melt-pressed gold foil (c).

2.4. Gold exchange-reduction

Chemically depositing an electrode directly to the active layer was a third method explored. The polyamide thin film is chemically heterogeneous due to interfacial polymerization; a carboxyl rich region comprises the surface of the polyamide[20]. Impregnation-reduction of a gold complex on another carboxyl containing ionomer, Flemion, has been used successfully to fabricate an ionic polymer metal composite electrode[71]. We applied this approach to the RO membranes studied in this research to take advantage of the fabrication technique developed specifically for carboxyl rich surfaces.

All three RO membranes (SW30HR, BW30LE and BW30) were used to qualitatively evaluate the influence of the aliphatic alcohol coating on gold exchange-reduction process. As with previous methods, the nonwoven backing layer was carefully removed and the samples were boiled in deionized water to clean. The gold complex, dichloro-(phenanthroline) gold(III) chloride, was created in-house following Harris' recipe using 10-phenanthroline dihydrate, sodium tetrachloroaurate(III) and ammonium chloride (Alfa Aesar)[73]. The gold complex has

been shown to exchange most effectively if the hydrogen ions on the carboxyl groups have been first replaced with potassium ions[74]. To determine how best to exchange protons for potassium ions and establish whether this step was required, the membrane samples were soaked in aqueous solutions of potassium chloride (1 M), potassium hydroxide (1 M) or deionized water for 17 hours with stirring. After ion exchange, they were placed in deionized water to remove any excess solution. The membranes were then sonicated in a 10 mM aqueous solution of the gold complex for 6 hours and soaked for an additional 66 hours at ambient temperature to exchange the K^+ ions with the gold complex. After rinsing with deionized water, samples were placed in 150 mL of deionized water with 25 mL of 0.4 M reducing solution of sodium sulfite added. An additional 25 mL of the reducing solution was added 80 minutes later, and the membranes were soaked in the stirred solution for 6 hours. The entire process was repeated once beginning with the potassium ion exchange.

2.5. Platinized polymer graft electrode fabrication

The final electroding approach taken was to graft a monomer to the backbone of the polyamide thin film that terminates in a sulfonate group. The addition of a sulfonate groups enables platinum exchange-reduction to be used to platinize the modified surface. The redox grafting reaction was based on research to modify the surface of RO membranes to improve fouling resistance[37-38]. By carefully selecting an appropriate monomer to graft, we were able to platinize the membrane surface to create a novel sensor. The fabrication process is outlined in the following section.

To minimize extraneous effects, BW30LE (no coating layer) was used for all platinized graft sensors. As this was to be implemented as an in-plane sensor, the non-woven backing layer was not removed to maintain the membranes' structural integrity and minimize the introduction of defects. Each sample was cleaned by boiling in deionized water for at least 30 minutes prior to grafting. The redox grafting procedure was based on a method developed by Freger et al. at room temperature (23° ± 2° C) [12]. Sulfuric acid (EMD Chemicals, Inc.) was added to deionized water to lower the pH to 1.8 (0.0158 M) as this was shown to improve monomer grafting. The redox reactants potassium persulfate (Sigma-Aldrich) (0.01 M) and sodium metabisulfite (Sigma-Aldrich) (0.01 M) were stirred into the solution until all solids were dissolved. The monomer to be grafted, 3-sulfopropyl methacrylate (SPM) potassium salt (98%

Aldrich) (0.5 M), was then added. After mixing thoroughly, the grafting solution was poured in a fixture that only exposed the polyamide thin film to the solution. The solution was covered for duration of the graft polymerization. After grafting and removal of excess solution, the modified area was rinsed three times spraying the surface with a stream of deionized water to remove any unreacted reagents.

Immediately after grafting SPM to the polyamide, a platinum salt solution, tetraammineplatinum (II) chloride (Aldrich), at a concentration of 5 mg/mL of deionized water (14.2 mM) was poured into the grafting fixture and allowed to sit unstirred. The platinum salt exchanged with potassium cations on the sulfonate functional group of the grafted SPM. The platinum salt solution was then removed and the membrane rinsed with deionized water one time without directly spraying the surface to remove excess solution. A reducing solution of 0.1 % wt sodium borohydride then covered the grafted and exchanged polyamide surface to chemically reduce the platinum salt to platinum.

Platinized polymer graft sensors were made following the above procedures. The grafting reaction progressed for 3 hours unless otherwise noted. Platinum exchange typically took place for 2 hours and the reducing step for half an hour. The exchange and reduction steps were repeated until the desired degree of sensor platinization had been achieved; as we will show, the amount of platinum deposited is determined by, among other factors, the number of exchange-reduction repetitions.

A parametric study was undertaken to observe the effects of varying grafting, exchanging and reducing times and repetitions on the degree of platinization. A 36 well fixture was used allowing simultaneous and independent fabrication of multiple samples. An initial study varying the effects of time exposure and repetitions of the various stages in fabrication did not produce any statistically significant variation due to small sample size. The experimental outline of a subsequent parametric study with at least three distinct samples for each time combination is shown below in Table 1. The results of this study and subsequent characterization with x-ray photoelectron spectroscopy (XPS) and scanning electron microscopy (SEM) will be presented and discussed in the following chapter.

Table 1: Experimental outline of platinized polymer graft sensor parametric study (time in hours: minutes).

SPM grafting	Pt^{2+}/K^{+} exchange	Pt^{2+}/Pt reduction	Exchange-reduction repetitions
2:00	2:00	0:30	1, 2, 3
2:00	4:00	4:00	1, 2, 3
4:00	2:00	0:30	1, 2, 3, 4
4:00	4:00	4:00	1, 2, 3

Attaching the electrical leads for sensors used in fouling experiments proved nontrivial. Initial approaches attaching two parallel strips of copper tape to the platinized area and encapsulating with both Kapton tape and silicone delaminated when exposed to RO operating conditions. Silver paint (Fullam 14810) was finally used due to its low resistivity (< 0.1 Ω/cm) and excellent adhesion to the platinized polyamide. Three parallel strips ~3 mm apart were applied along the length of the platinized area (65 mm). These were then encapsulated with a UV cure epoxy (Loctite 3104) to minimize stray current through the solution. Two electrical leads of the same geometry and construction were applied to an unplatinized area of the membrane as a control. Fine gauge copper wire was bonded to the silver paint with the UV cure epoxy. The resistances of the electrical connections were measured throughout fabrication to ensure conductivity between the electrical leads and silver paint. Contact between the electrical leads and the o-rings of the cross-flow test cell, squeezed by the clamping pressure required to adequately seal the cross-flow cell, required an additional layer of Kapton tape for further support. The sensor assembly is shown in Figure 5. Having three electrical leads allows two sensors to be simultaneously tested by applying potentials between the center lead and the two outer ones. This also proved beneficial when the encapsulation of one of the outer leads failed, as the test would continue using the other "half" of the assembly.

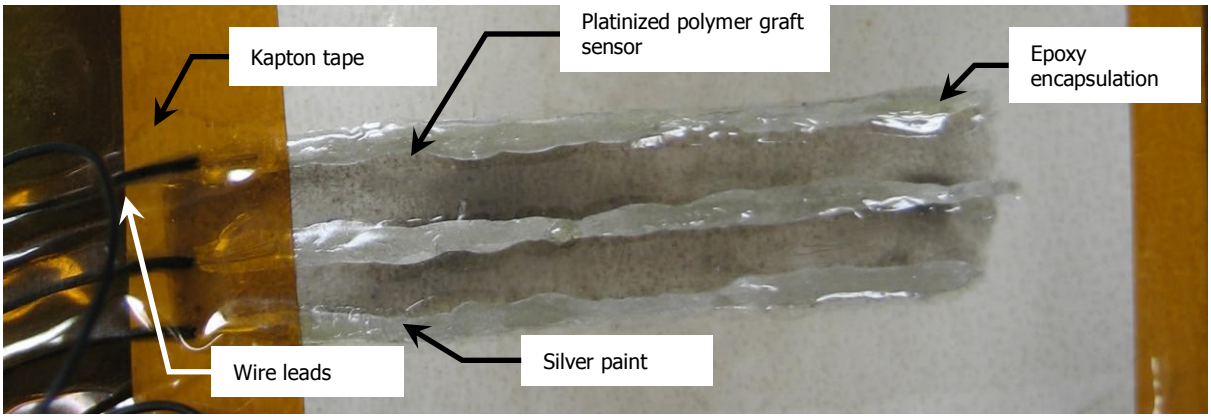

Figure 5: Fully constructed platinized polymer graft sensor with electrical leads attached and encapsulated.

3. ELECTRODE CHARACTERIZATION

Sensors fabricated using the four methods outlined in Chapter 2 are characterized in this chapter. The different electrodes were evaluated with respect to surface resistivity. The dry surface resistances of the carbon grease and DAP electrodes were measured using a multimeter (U1241A, Agilent) connected to a custom-built fixture (Figure 6). In the case of the platinized polymer graft sensors, the resistances were out of range of the multimeter, so EIS with a potentiostat/galvanostat (Autolab PGSTAT12, Eco Chemie) was used to quantify surface impedance. Sensor durability was assessed by visual inspection and in one case, x-ray photoelectron spectroscopy (XPS). Durability of the carbon grease and DAP electrodes was qualitatively monitored throughout sensor fabrication and concentration sensing experiments by visually inspecting the adhesion between the different layers of the electrode assembly. The durability of the platinized polymer graft sensors was inferred using XPS to quantify the relative amounts of platinum and grafted monomer on the polyamide thin film prior to and after exposure to severe RO cross-flow conditions. A parametric study of the newly developed platinized polymer graft method was undertaken to begin determining optimal platinization conditions. XPS was used to quantify the amount of monomer grafted and platinum deposited on the samples from the study. Scanning electron microscopy (SEM) was used to qualitatively assess the distribution and size of the nanoparticles deposited with the exchange-reduction methods.

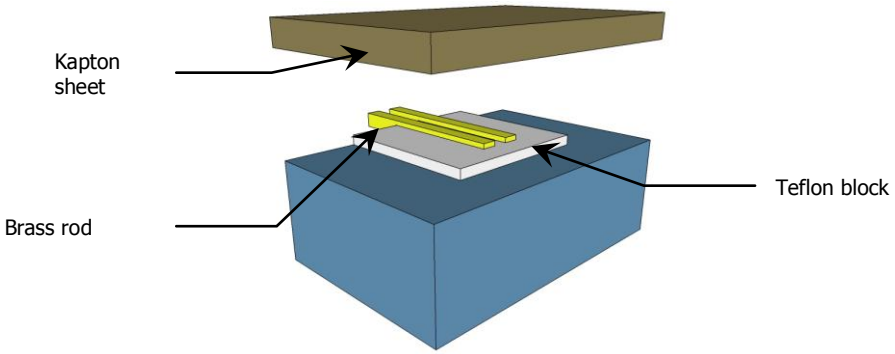

Figure 6: Fixture used to measure surface resistance. A rigid Kapton sheet clamps the electroded area against the brass rods using a binder clip ensuring consistent contact force. The brass rods are imbedded in an insulating Teflon block.

Summary of electrode characteristics:

1. The carbon grease electrodes prior to encapsulation had an average surface resistance from 27 – 32 kΩ mm/mm on the polyamide side and 16 – 30 kΩ mm/mm on the polysulfone. They proved to be quite durable upon encapsulation throughout the concentration sensing experiments.
2. The RuO2/Nafion layer of the DAP electrodes had a surface resistance less than 2 kΩ mm/mm. After melt-pressing gold foil to the electrode the, surface resistance fell below 0.3 Ω mm/mm. The gold foil adhesion to the RuO_2/Nafion layer proved to be inadequate during the concentration fouling experiments.
3. The gold exchange-reduction electrode surface resistances were out of range of the multimeter. An aliphatic polymeric alcohol coating present on two of the three types of membranes electroded appeared to inhibit formation of the electrode. Soaking the membranes in a strong base containing potassium ions prior to the exchange-reduction process created uniformly distributed gold nanoparticles tens of nanometers in diameter.
4. The surface resistance of platinized polymer graft sensors averaged ~23 GΩ mm/mm and had a capacitance of 8.5 pF as measured by EIS. The XPS results of the parametric study showed the amount of monomer grafted to the membrane increased 20% when doubling the length of exposure to the grafting solution from two to four hours. The amount of platinum deposited on the grafted membrane increased 101% with three repetitions of the exchange-reduction steps as compared to only doing one exchange reduction step. The amount of monomer grafted to the surface also had a statistically significant effect on the degree of platinization.

3.1. Carbon Grease

The carbon grease electrodes were initially evaluated for mechanical stability during testing and for electrical viability by measuring surface resistance prior to applying epoxy. The carbon grease electrodes with the epoxy encapsulation were, as expected, quite stable with no deterioration or delamination of the sensor upon hydration or during testing.

The results of in-plane resistance measurements proved to be less straightforward than expected. If measured immediately following carbon grease application, the electrode's resistance dropped continuously as the non-conductive silicone oil in it spreads as a visible film on the polyamide

surface or, in the case of the porous polysulfone layer, absorbed. To achieve stable resistance measurements, the carbon grease electrodes were placed under a heat lamp at 35°C for at least 2 hours to rapidly facilitate the silicone oil flow. The measured values were normalized (R_n) to the geometry of the fixture using

$$R_n = R_{exp} * \frac{l}{d} \quad (2)$$

where R_{exp} is the measured resistance, l is the length of contact between conductive bar and the carbon grease, and d is the distance between the two conductive bars.

Figure 7 shows the normalized average surface resistances of carbon grease electrodes on each side (polyamide and polysulfone) for both BW30LE and SW30HR membranes. Seven samples of each category were measured twice with the electrodes rotated 90° between measurements. Rotating between measurements improved confidence in the data because unintended discontinuities in the electrode were observable as a significant change in resistance after rotating. The resistances were generally ~10 kΩ with no obvious trends with regards to membrane type or surface tested.

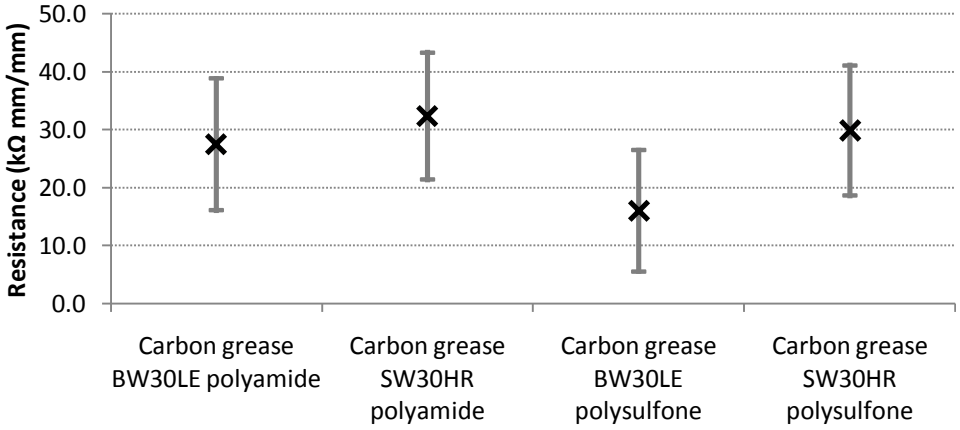

Figure 7: Normalized average surface resistance for carbon grease electrodes. Error bars are ± 1 standard deviation of data.

3.2. DAP electrodes

The surface resistance of the RuO_2/Nafion penetrating electrode was measured in the same manner as the carbon grease electrodes. Four samples were measured twice each, rotated 90° between measurements. The DAP electrodes' surface resistances were an order of magnitude

less than the carbon grease electrodes (< 2 kΩ mm/mm) without the gold foil layer. After melt pressing the gold foil to complete DAP fabrication, their surface resistance fell further, to less than 0.3 Ω mm/mm. The type (BW30LE or SW30HR) of membrane being electroded did not appear to affect surface resistance.

As with the carbon grease electrodes, the DAP electrodes were evaluated qualitatively for mechanical stability during testing and for electrical viability by measuring surface resistance. The DAP electrode assembly proved to be significantly more fragile that the carbon grease electrodes; the gold foil delaminated from the RuO2/Nafion layer upon hydration despite careful handling. However, the delamination tended to be incomplete. Figure 8 shows a cross section of DAP electroded membrane with the gold foil imperfectly adhered to the conductive dispersion. Adhesion of the melt-pressed gold foil relies on mechanical bonding to the RuO_2/Nafion layer and, more than likely, specifically to the Nafion. Additionally, RuO_2/Nafion layer adhesion to the membrane depends on it penetrating and/or mixing with the substrate when melt-pressed. The polyamide thin film has a high T_g (>200^o C), so it is doubtful the conducting dispersion bonded adequately to the polyamide thin film with melt-pressing at 185°C. Indeed, a truly penetrating RuO_2/Nafion electrode would compromise the active layer's salt rejection performance because the active layer is so thin (tens of nm)[20], and an *in situ* sensor that allows salt passage through the RO membrane is undesirable. Consequently, the delamination of the gold foil was likely due to poor mechanical bonding between the various layers of the DAP electrode (gold foil to RuO_2/Nafion to polyamide). Conversely, the gold foil melt-pressed to the polysulfone support layer did prove to be reliably durable as the temperatures used were above that of the T_g of polysulfone.

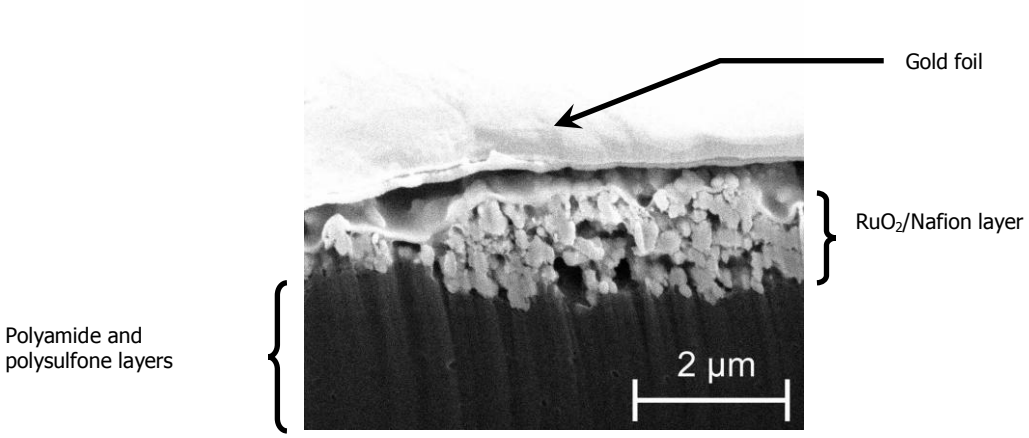

Figure 8: Micrograph of the polyamide side of a DAP electroded membrane cross-section. FIB-SEM: 5 kV, Inlens detector.

3.3. Gold exchange-reduction

The gold exchange-reduction membrane resistance was too large to measure with a hand-held multimeter. However, the membrane samples developed a light pink hue (consistent with the presence of gold nanoparticles) after being placed in the reducing solution. To verify the presence of gold and the influence of membrane type and method of ion exchange, the samples were qualitatively analyzed using scanning electron microscopy (SEM) with secondary and backscattered electron detectors. Higher electron densities (gold particles) appear as brighter areas in Figure 9 – Figure 11.

3.3.1. Influence of membrane

Results showed gold particles to be on all membranes presoaked in the KOH solution; however, the gold particle size and density varied (Figure 9). Both BW30LE and SW30HR have large numbers of gold nanoparticles less than 50 nm, whereas the BW30 sample particles are quite sparse but large. BW30 and SW30HR membranes were shown to contain a coating rich in aliphatic polymeric alcohol groups by Tang et al[21] which may play a role in the gold exchange-reduction reactions as they had the largest gold particles (greater than 500nm). Particle size did not correlate to particle density as BW30 had the lowest number of particles overall, while SW30HR had dense clusters of gold nanoparticles surrounded by less populated regions (Figure 9a and Figure 10). Further analysis is required to determine the relative amounts of gold deposited. Interestingly, Tang's research showed the SW30HR coating to be non-uniform over the surface while BW30 XPS results suggested the coating to be relatively thick;

the polyamide thin films of all three types of membranes used in our experiments were shown to have chemical compositions consistent with one another[21]. Our results suggest the aliphatic polymeric alcohol coating decreased the effectiveness of the exchange-reduction process, perhaps by decreasing the number of carboxylic endgroups available to participate in the reaction. It is hypothesized that the gold clusters on SW30HR's surface (Figure 10) may be located in areas where the polymeric coating was absent or too thin to inhibit exchange-reduction; whereas, BW30's thicker coating inhibited exchange-reduction more uniformly.

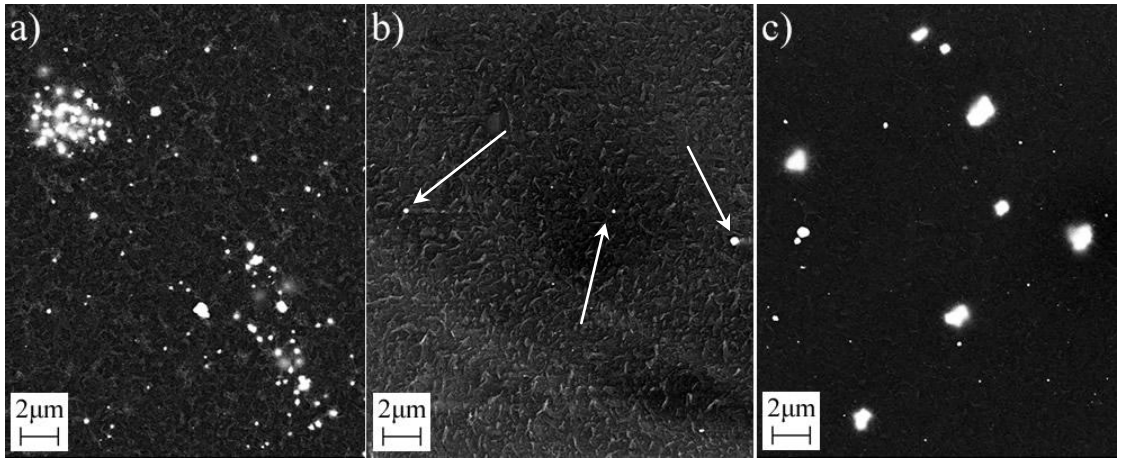

Figure 9: Representative areas showing large gold nanoparticles on polyamide thin film surfaces after exchange-reduction with KOH presoak: a) SW30HR – clusters of particles >500 nm; b) BW30LE – arrows point to particles <500 nm; c) BW30 – particles >500 nm. SEM: 20kV, Backscattered detector.

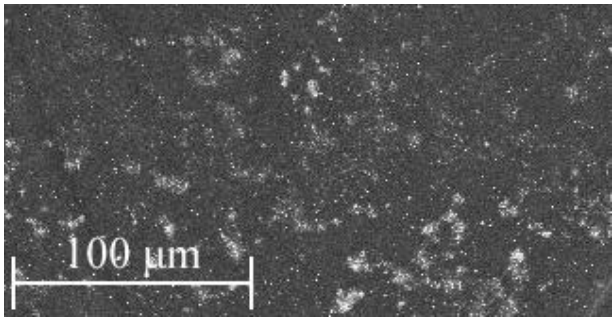

Figure 10: Gold nanoparticle clustering on SW30HR polyamide thin film after exchange-reduction with KOH presoak. SEM: 20kV, Backscattered detector.

3.3.2. Influence of ion exchange

The effect of exchanging the proton on the carboxyl group with a potassium ion was explored using KOH or KCl and, as a control with no ion exchange, deionized water. The results for the

BW30LE samples showed the protons exchanged using KOH has many small gold particles within the membrane (Figure 11a). The KCl-exchanged membrane has larger and fewer gold particles on the polyamide surface (Figure 11b), and the sample without any ion exchange showed a small number of fine particles within the membrane (Figure 11c). The results imply that a strong base, KOH, exchanges potassium ions with the membrane best as many small particles uniformly dispersed are desired for uniformity of electric field upon implementation as an electrode for EIS. Coronell et al. in a study to quantify the number of functional groups on the polyamide thin film showed that maximum ion exchange occurred at pH > 10 [75]. Despite these encouraging results, a higher particle density is required for adequate conductivity. The number of carboxyl groups available to participate in the gold exchange-reduction process may be limited due to the high degree (94%) of crosslinking of the polyamide [75].

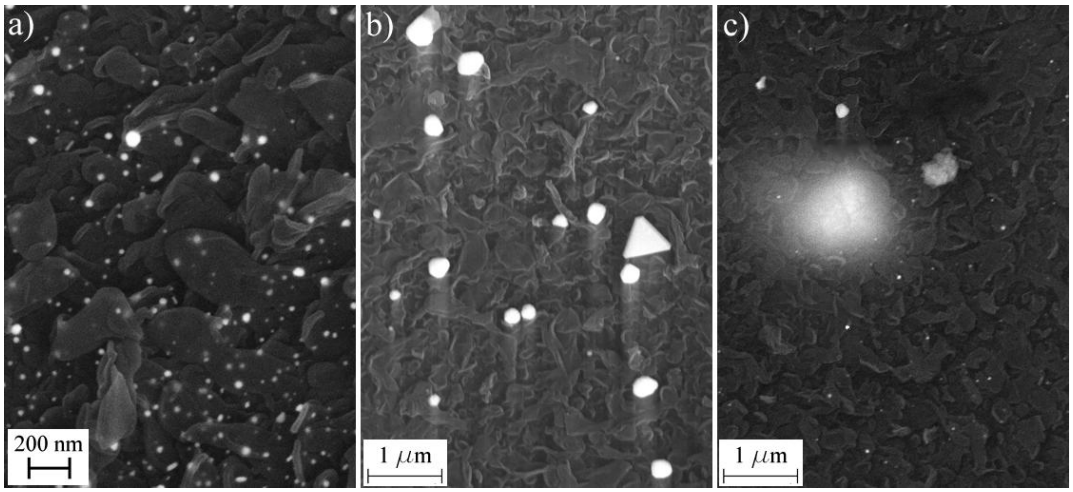

Figure 11: Gold nanoparticles on BW30LE polyamide surface after exchange-reduction with presoak solution of: a) KOH; b) KCl*; c) H_20. The fuzzy glow in c) is large gold particle beneath the polyamide surface. SEM: 20kV, Backscatter detector, (* secondary electron detector)

3.4. Platinized polymer graft

The platinized polymer graft method was a new approach for metalizing polymers. A parametric study was conducted and the results analyzed to assess the degree of platinization. The parameters varied were: *i*) time exposed to grafting solution, *ii*) time of platinum salt exchange, *iii*) time of platinum reduction, and *iv*) repetitions of the exchange-reduction steps. Table 1, in Chapter 2.5, shows the parameter values varied. Initially, electrode resistance and capacitance of

the samples from the parametric study, calculated using EIS, were used as metrics to correlate the degree of platinization to the effects of the parameters varied. This data did not yield meaningful results, as there was no correlation between electrical properties and amount of platinum deposited. Hence, XPS was used as a means of quantifying the relative concentrations of platinum and grafted monomer.

3.4.1. Monomer grafting

The relative amounts of monomer (SPM) grafted to the polyamide thin film samples during the parametric study were quantified using x-ray photoelectron spectroscopy (XPS) to detect sulfur (S_{2p} as % atomic concentration) because the grafted monomer contained sulfonate endgroups. XPS is surface sensitive with a penetration depth not exceeding the thickness of the polyamide thin film. Surface sensitivity was required because had the penetration depth exceeded the polyamide, the sulfur in the polysulfone support layer would have dominated, masking any information on the amount of SPM on the polyamide in the signal. The averaged results (7 samples for both 2 and 4 hours) showed sulfur on the polyamide increased 20% with a doubling of the time exposed to the grafting solution (Table 2). Analysis of variance (ANOVA) of the data gave a p-value of 0.0695; the p-value is the smallest level of significance that would lead to the rejection of the null hypothesis, namely, that grafting time does not affect the atomic concentration of sulfur on the electrode surface. It may be expected that doubling the time of grafting would double the amount of monomer grafted; however, it is possible that the grafting polymerization reaction has approached equilibrium after two hours. More data concerning different grafting times are needed to determine an optimal length of time for the grafting step.

Table 2: Sulfur concentration of platinized polymer graft parametric study using XPS.

Grafting time (hr)	Sulfur - atomic concentration	1 Standard Deviation
2	1.23%	±0.28%
4	1.48%	±0.25%

3.4.2. Surface resistance and degree of platinization

Like the gold exchange-reduction samples, the surface resistance of the platinized membrane was beyond the range of the multimeter. Instead, an impedance analyzer (Autolab PGSTAT12, Eco Chemie) and the fixture (to measure surface resistance) illustrated in Figure 6 were used to measure surface impedance by applying a 100 mV (rms) sinusoidal voltage from 50 mHz to 1

kHz. The frequency response results closely matched the response of a parallel resistor-capacitor circuit; Figure 12: shows a typical impedance spectrum. Resistance and capacitance were calculated with MATLAB by curve fitting the complex impedance data (Z) to the model given by Equation (3), where R is the sample resistance, ω is radial frequency (rad/s), C is the sample capacitance and $j = \sqrt{-1}$.

$$\frac{1}{Z} = \frac{1}{R} + j\omega C \quad \Rightarrow \quad Z = \frac{R}{1 + j\omega CR} \tag{3}$$

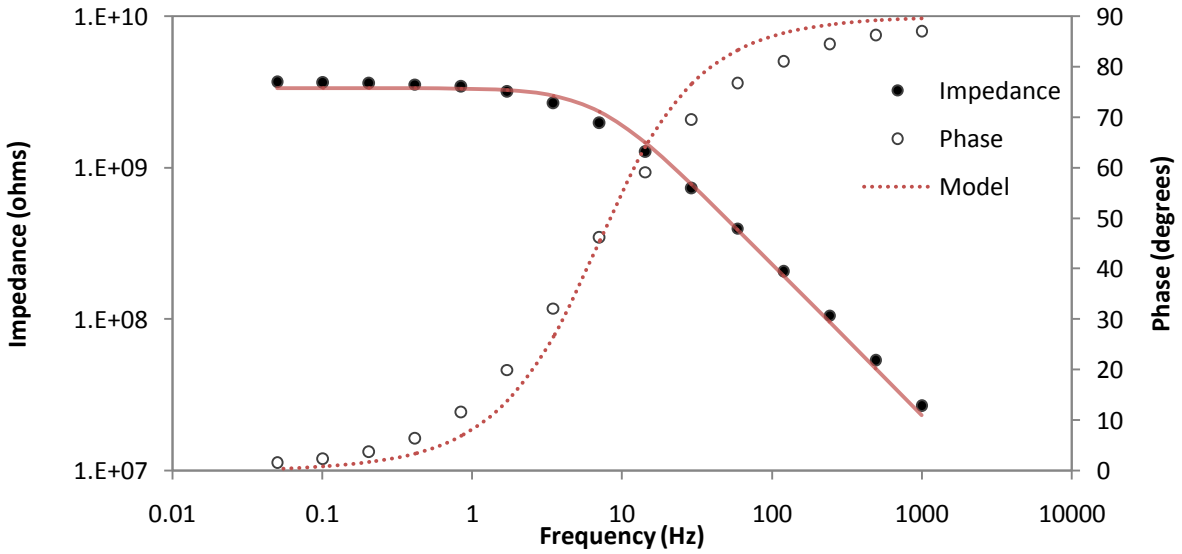

Figure 12: Typical impedance response of a dry platinized polymer graft sensor with silver paint applied for electrical leads (Parametric study, 2nd run, well #1b). The solid circles correspond to the impedance while the hollow circles indicate phase. The red lines are fits of the model to the experimental data.

It was hypothesized that the surface impedance of the platinized region would serve as a metric for the quantity and distribution of platinum deposited on the samples (see Table 1). The resistance and capacitance values determined by fitting Equation (3) to the sample impedance averaged 86 GΩ mm/mm and 6 pF respectively (labeled "Bare electrode" in Figure 13). Impedance measurements of the fixture itself and an unplatinized area of the membrane were taken as experimental controls. The results showed the resistance and capacitance of the fixture and membrane to lie within the range of values for the platinized polymer graft samples. Evidence strongly indicates that the bare electrode impedance results were imprecise and likely artifacts of the fixture impedance (Figure 13).

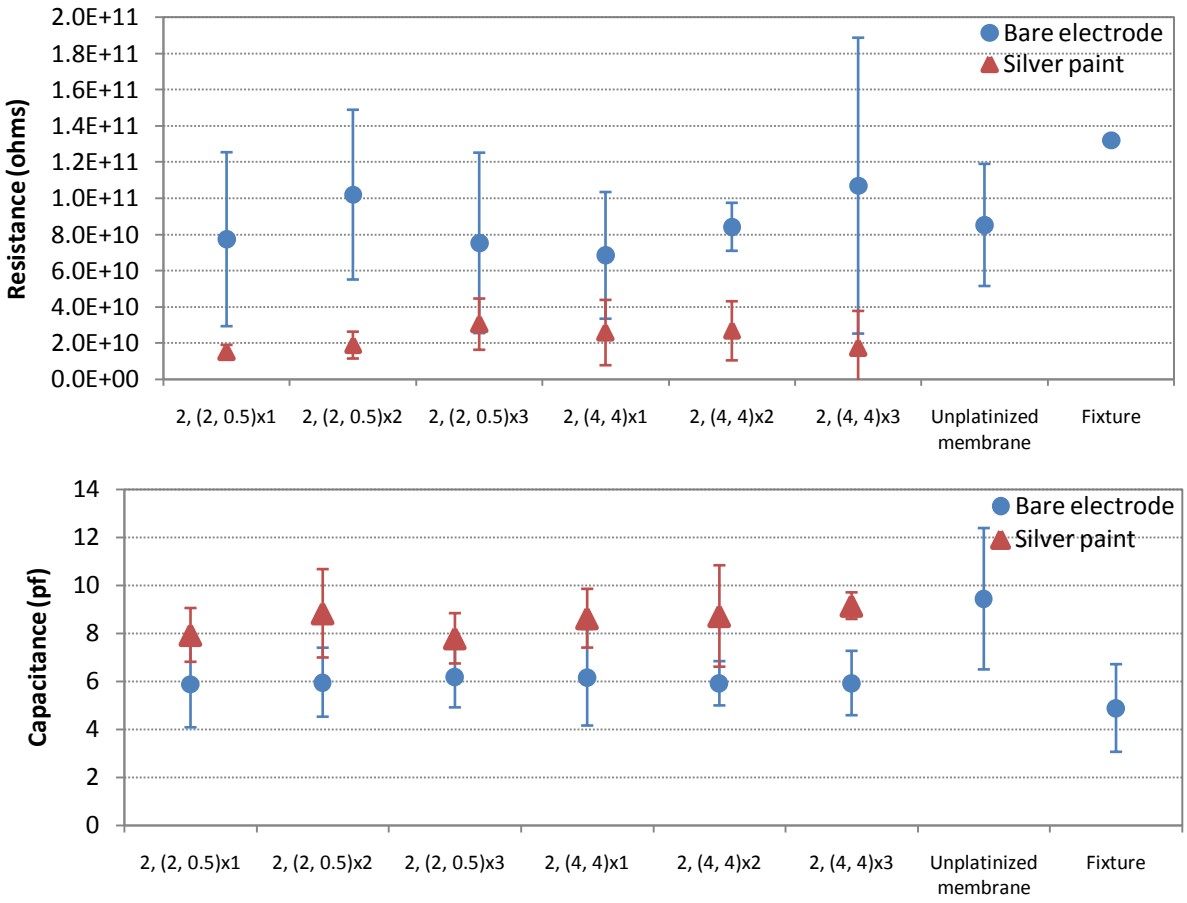

Figure 13: Average fitted resistance and capacitance from EIS data of the parametric study of the platinized polymer graft method. The individual columns on the x-axis are labeled for time (hr) of: *i*) grafting, *ii*) Pt exchange, *iii*) Pt reduction, and repetitions of exchange-reduction. The error bars represent one standard deviation.

As a remedy, the contact between the fixture and the platinized membrane was improved by applying two strips of silver paint (Fullam 14810) to the platinized samples thus allowing the brass bars of the fixture to contact the dried silver paint. The silver paint, much like the carbon grease electrodes, was able to fill the "rough" surface of the polyamide, increasing contact surface area and sensitivity of the electrical leads. The averaged results of the silver paint electrical leads are also shown in Figure 13 (labeled "Silver paint"). The resistance decreased from the bare electrodes significantly – to an average of 23 GΩ mm/mm, thus reflecting the measurement was of the electrode surface rather than the fixture or unelectroded polyamide.

Similarly, the capacitance increased an average of 40% to 8.5 pF, which more closely reflects the capacitance of the unelectroded membrane rather than that of the fixture.

Figure 13 and analysis of variance show there is no clear correlation between duration and repetition of platinization steps and the resulting surface impedance of the membrane. We anticipated that increasing membrane exposure time to grafting solution, lengthening the time of the exchange-reduction reaction and increasing the number of repetitions would increase platinum deposited and decrease surface impedance. The lack of an obvious trend of electrical properties with respect to varying the process steps and visual evidence of dissimilar degrees of platinization indicated that an alternate method was needed to assess the parametric study's platinized polymer grafts.

Unable to quantitatively evaluate the effects of varying the steps in the electroding process using EIS, SEM coupled with an EDS (Energy dispersive X-ray spectroscopy) detector was used to image the degree of platinization. The platinum detected was in concentrations less than 0.3 % atomic concentration for all samples because of the relatively large volume sampled. The EDS data failed to correlate platinum to the parameters varied. Using XPS, a more surface sensitive technique, increased the x-ray signal from deposited platinum. Figure 14 shows the concentration of platinum (Pt) plotted as a function of sulfur (S). XPS results show a significant correlation between platinum to the number of exchange-reduction repetitions (ANOVA p-value of 0.00099) and grafting time (p-value of 0.019). The average amount of platinum deposited in the samples where the exchange-reduction step was repeated three times increased 101% when compared to samples with only one exchange-reduction cycle. Since the sulfonate groups available to participate in the reaction, on average, increased with grafting time, it can be deduced that more grafted SPM would lead to more deposited platinum. As the exchange step proceeds and platinum salt ionically bonds to the sulfonate groups of the grafted SPM, the cationic platinum salt in solution is depleted and may reach chemical equilibrium with chloride anions in solution and the platinum and unexchanged K salts bound to the polymer graft. Furthermore, chemically reducing the platinum cations bound to the sulfonate groups result in the groups once again having an overall anionic state and capable of exchanging with the platinum salt upon further exposure. Changing the platinum salt concentration in the exchange solution would be one way to probe whether the chemical equilibrium or sulfonate – platinum

salt electrostatic association limits the amount of platinum deposited at each step. Indeed, the lower amount of platinum deposited on the samples indicated by the red diamonds in Figure 14 (grafted for 4 hours, exchanged-reduced for 2 hours and half an hour respectively with 4 repetitions) was due to the first two repetitions of the platinum exchange step using "old" (depleted) platinum salt solution used in previous exchange steps. Observations during the first two repetitions showed a minimal degree of platinization and the two following repetitions used "fresh" exchange solutions sufficiently platinized the membrane. This seemed to indicate that the exchange step was sensitive to platinum salt concentration.

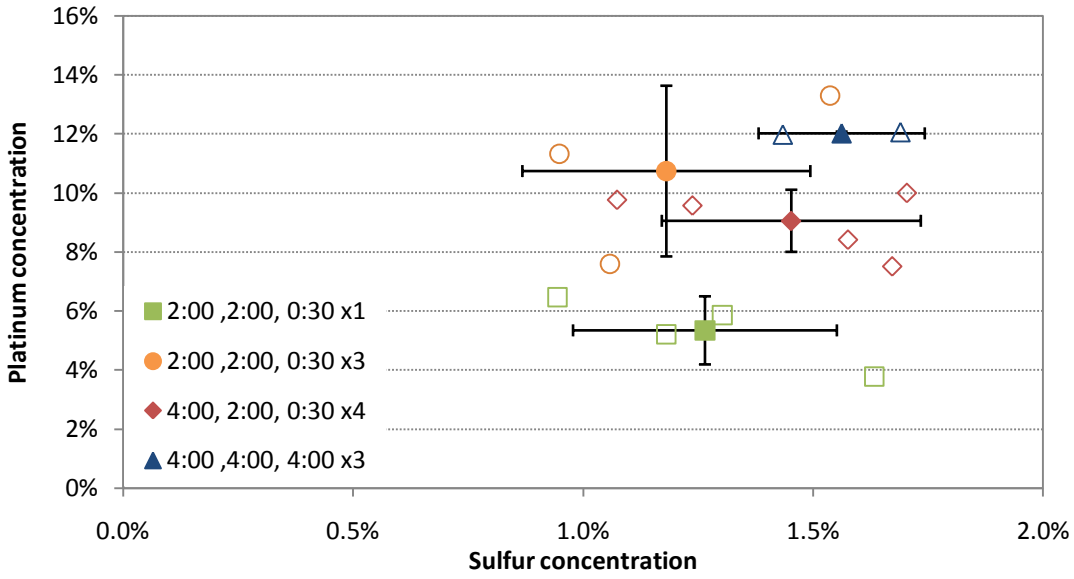

Figure 14: Results of parametric platinized polymer graft. Pt and S normalized to N atomic concentration. Solid shapes are averages of each sample (hollow shapes). Error bars are 1 standard deviation. Recipe conditions given in legend: Grafting time, Exchange time, Reducing time, number of repetitions of exchange-reduction steps, respectively.

3.4.3. Sensor viability

Along with quantifying the degree of platinization and grafting of the platinized polymer graft sensors, a preliminary investigation on the robustness of the platinized surface in cross-flow RO operating conditions was undertaken. Four areas of two BW30LE membrane samples were platinized following the recipe outlined in Section 2.5 with the grafting taking place for four hours; the exchange (two hours) and reduction (thirty minutes) steps were repeated four times. The first two exchange-reduction repetitions used "old" platinum salt solution as mentioned in

the preceding paragraph. Fresh platinum salt solution was used for the following two steps due to the minimal amount of platinum deposited using the "old" solution. One membrane sample was dried and stored in a plastic bag immediately after platinization. The other sample was placed in a cross-flow test cell connected to a lab scale RO system (described elsewhere) and operated at a pressure of 3.5 MPa (500 psi) and a flow rate of 3.8 L/min (1 gpm). These cross-flow conditions were significantly more extreme than the typical operating conditions used in fouling experiments (1 MPa and 0.75 L/min). After four hours in those conditions, XPS results indicate the atomic concentration of the platinum and sulfur (SPM) decreased on average 42% and 44% respectively as shown in Figure 15. The ratio of platinum to sulfur remained relatively constant across the platinized polymer grafted areas on both membranes; 6.5 for the membrane exposed to the cross-flow conditions and 6.2 for the one not implemented in the cross-flow test cell. The unchanged ratio of platinum to sulfur indicated the platinum remained adhered to the grafted polymer. The decrease in sulfur suggested two events may have occurred: *i*) the grafted SPM's bond to the polyamide thin film was insufficient to resist the hydrodynamic forces encountered in the RO system or *ii*) unreacted monomer with platinum deposits was being washed away. Further cross-flow experiments at longer times are required to elucidate what occurred. The loss of sulfur and platinum approaching an asymptote with time would suggest unreacted monomer is being washed away; whereas, a steady decrease would indicate the platinized polymer graft lacks durability at these operating conditions.

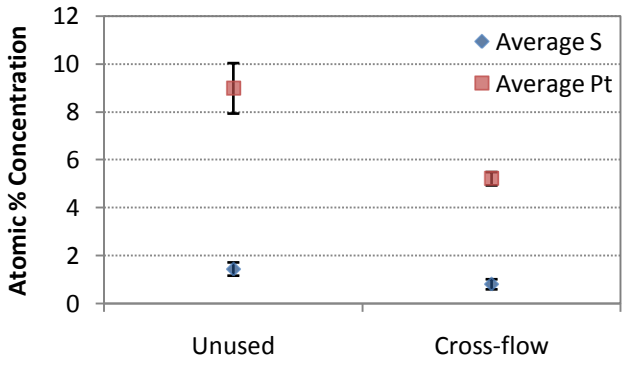

Figure 15: XPS results of viability study. Sulfur indicates the grafted SPM. "Unused" samples were dried and stored immediately after fabrication. "Cross-flow" samples were placed in RO test cell and exposed to cross-flow conditions of 3.5 MPa and 3.8 L/min for four hours. Error bars indicate one standard deviation.

3.5. Characterization Summary

In summary, the encapsulated carbon grease electrodes are durable and have a surface resistance of 30 kΩ mm/mm. The DAP electrodes RuO_2/Nafion layer had a surface resistance less than 2 kΩ mm/mm. With the addition of a melt-pressed gold foil layer, the resistance fell to well below 1 Ω mm/mm; unfortunately, the gold foil proved to be fragile upon hydration. The results of the gold exchange-reduction showed insufficient gold nanoparticles were deposited for adequate electrode conductivity. Characterization showed the gold nanoparticle size and density seemed to be affected by the presence of a coating layer on the RO membranes tested. The coating tended to increase particle size and decrease particle density. Presoaking and exchanging K ions using a strong KOH solution led to a high particle density with small gold nanoparticles. A novel electroding technique, platinized polymer grafting, exhibited a surface resistance around 23 GΩ mm/mm and a surface capacitance of 8.5 pF using EIS. A parametric study showed no significant effect of grafting time (2 and 4 hours) to the amount of SPM grafted. The amount of platinum deposited was influenced by the length of grafting time and number of exchange-reduction repetitions, and, potentially, by the platinum salt concentration of the exchange solution. The exchange-reduction times varied did not appear to influence the degree of platinization. The platinized polymer graft sensor showed a decrease in relative amounts of platinum and SPM upon being subjected to harsh cross-flow RO operating conditions but the ratio between the two remained constant. The following chapter will discuss the results of the encapsulated carbon grease and DAP electroded sensors as implemented in single and double-bath fixtures to detect changes in electrolyte concentration.

4. CONCENTRATION SENSING EXPERIMENTS

EIS was applied to the sensors to ascertain their sensitivity to electrolyte concentration. We used a single bath hydrated fixture and a double bath hydrated fixture for varying salt concentrations. A baseline sensor response to varying electrolyte concentration is required to distinguish between responses to changes in salt concentration and other phenomena (fouling, membrane degradation, etc.). Changing electrolyte concentration in our experiments also imitated concentration polarization as an RO membrane in operation will have fluctuating electrolyte concentrations at its surface depending on operating conditions (permeate flux, cross-flow rate, etc.) even with a constant bulk feedwater composition. As discussed in Section 1.6, Bason et al. showed an apparent decrease in membrane resistance with an increase in solution concentration[62]. The single bath experiments were an initial proof-of-concept step taken to determine if the electroded membrane responded to changes in salt concentration. The double bath configuration mimics the environment a sensor implemented in a RO system would encounter with the polysulfone being exposed to only the permeate (deionized water) and the polyamide to the feedwater (salt solution). The sensing mechanism is based on qualitative analysis of regional shifts in the impedance spectra.

EIS results showed the through-thickness carbon grease electroded sensor took more than 20 hours to reach a stable impedance response when placed in a salt solution of constant concentration. Varying the electrode configuration and orientation provided strong evidence that the microporous polysulfone support layer may have been responsible for transient sensor response. From the carbon grease results, we also inferred the sensors may be sensitive to electrolyte concentration due to shifting trends in impedance upon changing solution. The DAP electroded sensor impedance response lacked meaningful trends in impedance with a changing electrolyte concentration. This chapter will describe the experimental methods and fixtures used and discuss experimental results for carbon grease and DAP electroded sensors in both single and double bath configurations.

4.1. EIS testing protocol and materials

Electrical impedance spectroscopy was performed with a potentiostat/galvanostat (Autolab PGSTAT12, Eco Chemie) by applying a 50 mV (rms) sinusoidal signal from 500 kHz to 0.1 Hz with no DC bias. An Impedance/Gain-Phase Analyzer (4194A, Hewlett-Packard) was used for

higher frequency (5 MHz to 100 Hz) EIS, again applying a 50 mV (rms) sinusoidal signal. Both EIS instruments were used in a two-electrode configuration with the working electrodes and sensing electrodes sharing a common point of attachment to the sensor. Sodium chloride (Mallinckrodt) and deionized water (EASYpure II, Barnstead) were used to make salt solutions ranging from 100 to 800 mM. The concentration range was chosen to represent both brackish and seawater salinities. All other chemicals were used as supplied from the manufacturer.

The single bath experimental fixture consisted of a covered beaker on a stir plate containing the electroded membrane sample, electrolyte solution and stir bar. The samples were hydrated in deionized water for a minimum of 24 hours, then rinsed and placed in the experimental fixture. EIS was performed immediately, and the samples were rinsed with deionized water between salt solution changes. Three through-thickness and three in-plane SW30HR carbon grease samples were tested with varying salt concentration. The order of concentration exposure was initially from least to most concentrated and then rearranged to determine whether the sensor was detecting concentration rather than simply changing with time. To test for time-dependent sensor response, two through-thickness SW30HR sensors were continuously immersed in a salt solution of constant concentration while EIS was periodically run.

Double bath EIS experiments were conducted with three through-thickness carbon grease and three DAP sensors to simulate the sensor configuration in a typical RO cross-flow system with the polyamide thin film exposed to the salt solution (feedwater) while the polysulfone support remains immersed in deionized water (permeate). Figure 16 schematically shows a through-thickness carbon grease sensor mounted in the double bath fixture (note: there was no applied pressure or water flow). The salt concentrations were varied in both ascending and random orders for two separate cycles. The chambers were rinsed with deionized water between changes in solution. The double bath method followed the same sensor conditioning and EIS steps as the single bath method.

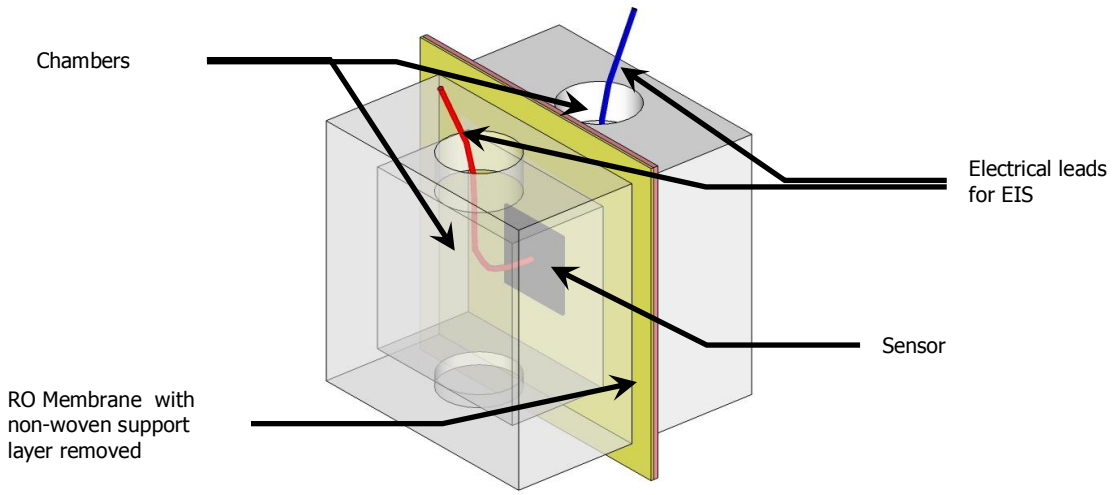

Figure 16: The double bath fixture milled from HDPE. The sensor/membrane assembly separates two chambers and allows the polyamide thin film and polysulfone to be simultaneously exposed to different solution baths. A stir bar was contained by a depression milled in the bottom of the fixture.

4.2. Carbon grease electroded sensors

Two different experimental configurations: *i*) single bath and *ii*) double bath (as described in the preceding section) were used to detect varying electrolyte concentrations with the carbon grease electroded sensors. Additionally, the carbon grease electrodes were fabricated in two different orientations: *i*) through-thickness and *ii*) in-plane. The through-thickness electrodes in single bath experiments showed a time-dependent EIS response as well as evidence of concentration sensitivity. In-plane electrodes on the polyamide thin film side of the RO membranes in the single bath experiments varied in their time-dependent response and concentration sensitivity; the variations may be correlated to defects introduced to the polyamide thin film during fabrication. Through-thickness sensors in double bath experiments showed no discernible sensitivity to varying salt concentration when the polyamide side was exposed to the electrolyte solution. The polysulfone side did exhibit a time-dependent EIS response similar to that of the single bath experiments when exposed to the electrolyte solution. A detailed discussion of the results follows.

4.2.1. Single bath: through-thickness electrode configuration

Single bath experiments were run: *i*) twice with one through-thickness carbon grease SW30HR membrane sample at a constant concentration of 400 mM and *ii*) once with another sample in an 800 mM solution to measure sensor impedance response over time at a constant concentration. Averaging the impedance over the entire frequency range measured at each time interval and normalizing with respect to the averaged impedance of the first EIS run (time zero) showed the sensors approached an asymptote but were still declining after 20 hours (Figure 17). Figure 18 shows the phase continues to shift right while the impedance falls. The results clearly show the sensor response is initially time-dependent. The epoxy covering the carbon grease electrodes is impermeable to water and strongly bonded to both the polyamide and polysulfone layers. Nevertheless, it may be expected that the salt solution slowly diffuses beneath the epoxy/carbon grease layer and through the pores of the polysulfone (Figure 19); this would change the sensor response with time until an equilibrium state is reached.

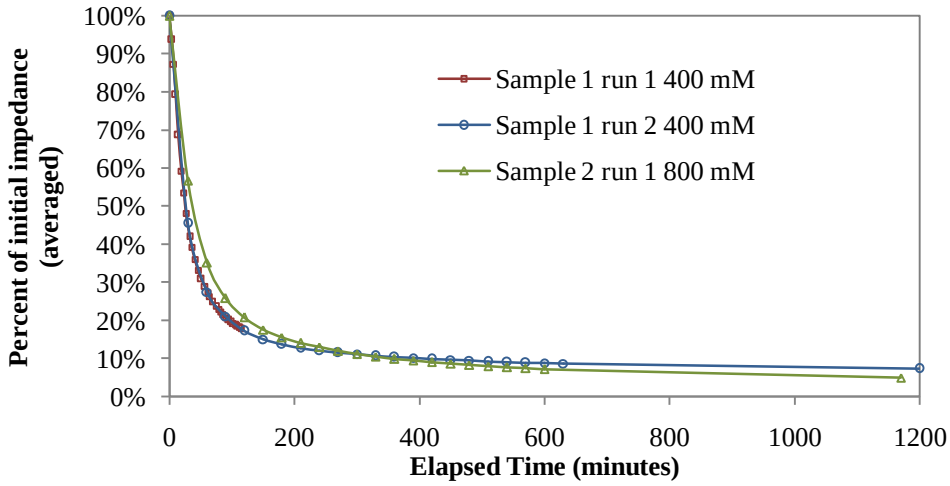

Figure 17: Transient responses of SW30HR carbon grease sensors in single baths at constant concentrations. Note: Sample 1 run 1 and 2 were performed six days apart with sample being stored in deionized water between runs.

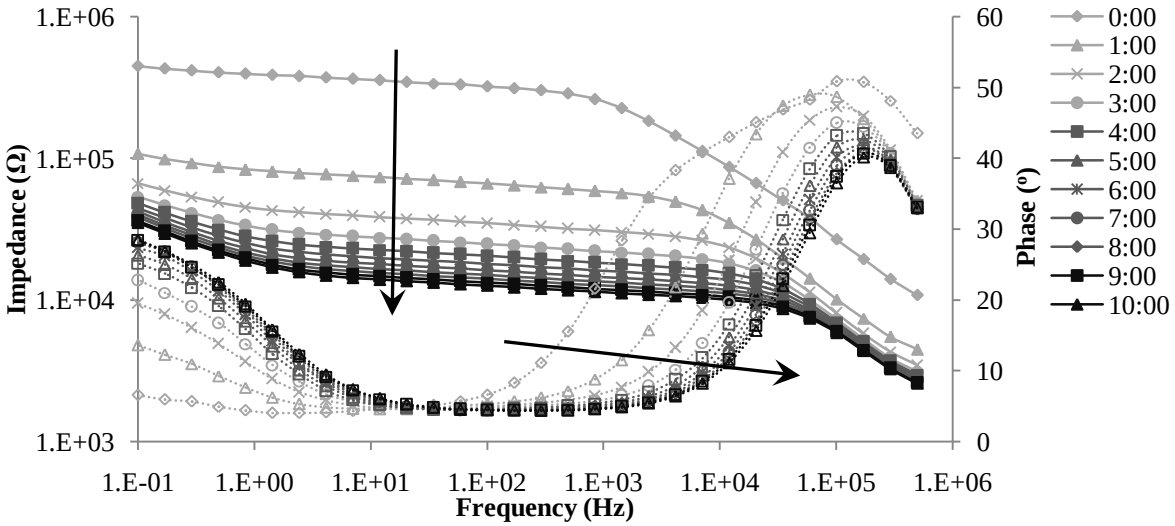

Figure 18: Transient nature of SW30HR carbon grease sensor in single bath configuration at 400 mM (Sample 1). Legend gives the corresponding elapsed time in hours. Solid shapes correspond to impedance; hollow shapes refer to phase. Arrows denote increasing exposure time.

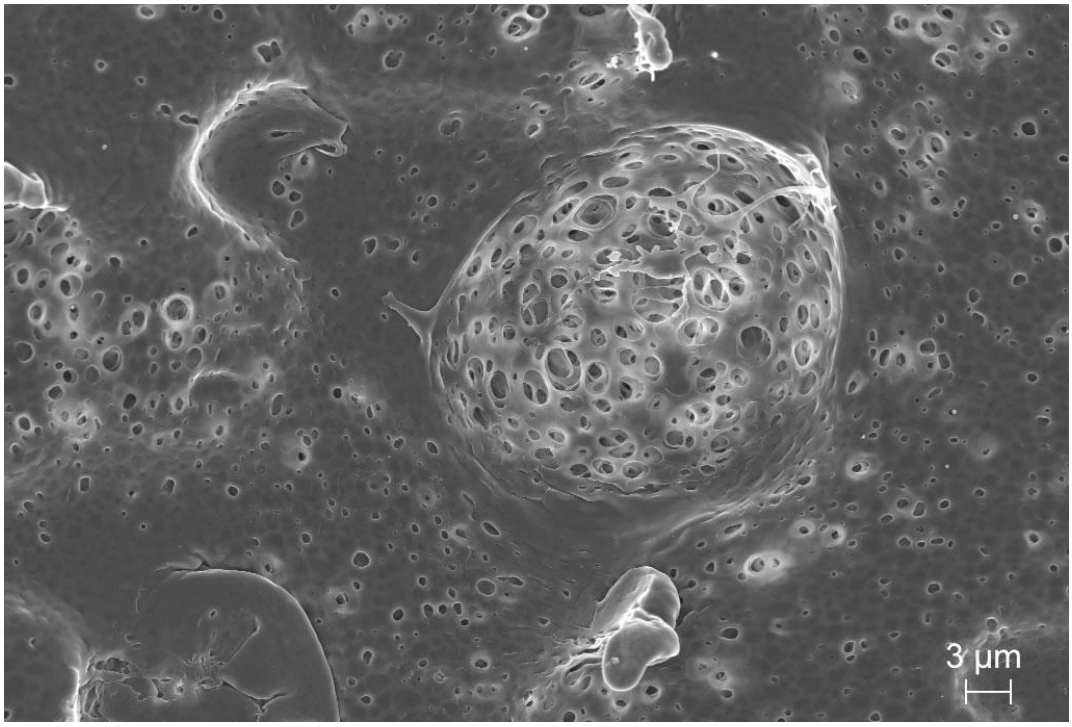

Figure 19: Microporous polysulfone support. (SEM: 5 keV, In lens detector)

In other single bath experiments, through-thickness carbon grease electroded SW30HR membranes were tested with a varying sodium chloride solution. The order of exposure was from least to greatest concentration (100 mM to 800 mM). The EIS response of three samples of the through-thickness electrode configuration, when exposed to solutions of increasing concentration, had a decrease in impedance with an increase in concentration. Figure 20 shows a representative impedance response (Sample 3) with exposure to increasing concentration. The impedance response is consistent with the literature with the "plateau" region lying between 10 Hz and 10 kHz being described as membrane resistance[62]. The range of highest sensitivity, defined as the frequency region of largest impedance shift, and the percent decrease in impedance between concentrations varied between samples and occurred at a local phase minimum. The phase peak amplitude at the higher frequencies in each spectrum decreased as the solution concentration increased while the phase peak amplitude at lower frequencies increased as solution concentration increased. The trends observed in the single bath experiments with solutions introduced in ascending concentration may not be fully attributed to changes in concentration due to their time-dependency shown previously.

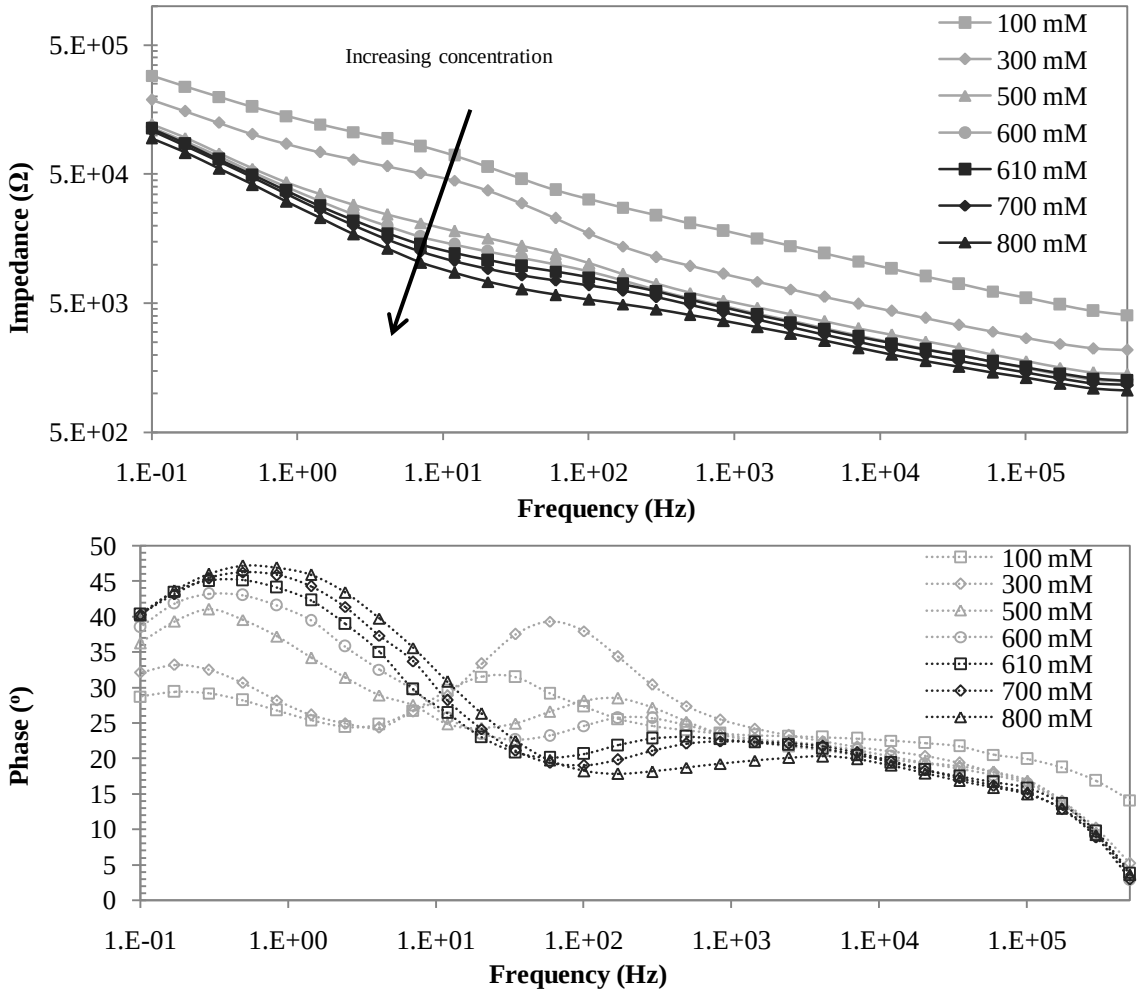

Figure 20: Impedance spectra of SW30HR through-thickness carbon grease electrode (Sample 3) in single bath configuration with concentrations introduced in ascending order. Solid shapes correspond to impedance; hollow shapes refer to phase.

An additional single bath experiment was performed to determine if the impedance and phase shifts previously observed could be attributed to sensor sensitivity to electrolyte concentration by rearranging the order of salt concentration exposure. The results of this experiment suggested the sensor might be responding to changes in salt concentration. Figure 21 shows the average normalized impedance response of a through-thickness carbon grease sample over time and with varying salt concentration. The impedance at each frequency for each EIS run of a sensor was normalized with respect to the impedance at the corresponding frequency for the first run of that sensor (time zero). The decrease in impedance was consistent between runs as shown by "Sample 1 400 mM" and "Sample 1 400 mM run 2" as the two runs were taken six days apart

with the sensor being stored in deionized water in the interim. Changing solution concentration generally led to a continued decline in impedance but with differing rates of decline. At 100 mM, the impedance response remained consistent and only began declining again after immersion in an 800 mM solution. Again, this is consistent with the decrease in membrane resistance observed in other research[62]. Although not definitive, this trend in the EIS data indicates the sensor may be responding, albeit slowly, to changes in solution concentration.

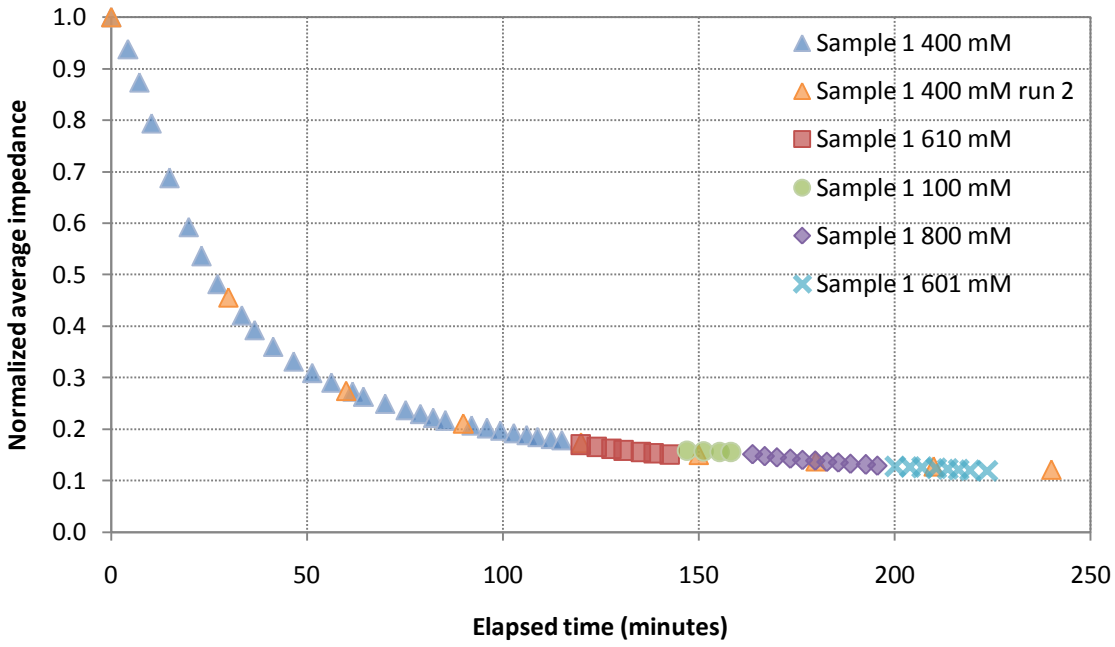

Figure 21: Average change in sensor impedance normalized to impedance (at corresponding frequency) of initial EIS response for a through-thickness carbon grease electroded SW30HR sensor (Sample 1). Elapsed time is the time sensor was immersed in sodium chloride solution when EIS was performed. Order of concentration exposure is shown in legend. For run two, the concentration remained a constant 400 mM.

The impedance spectra varied between all samples at all concentrations; Figure 22 shows the variations of three sensor impedance and phase responses between samples at 800 mM concentration. It may be expected that the impedance values would remain consistent between samples of the same electrode type and size as their dry impedances were consistent with one another; however, Bason et al. noted similar inconsistencies between identical samples of the polyamide thin film in their study[62]. It is likely that polymer and electroding heterogeneities and swelling amongst the samples would lead to these sorts of electrical inconsistencies.

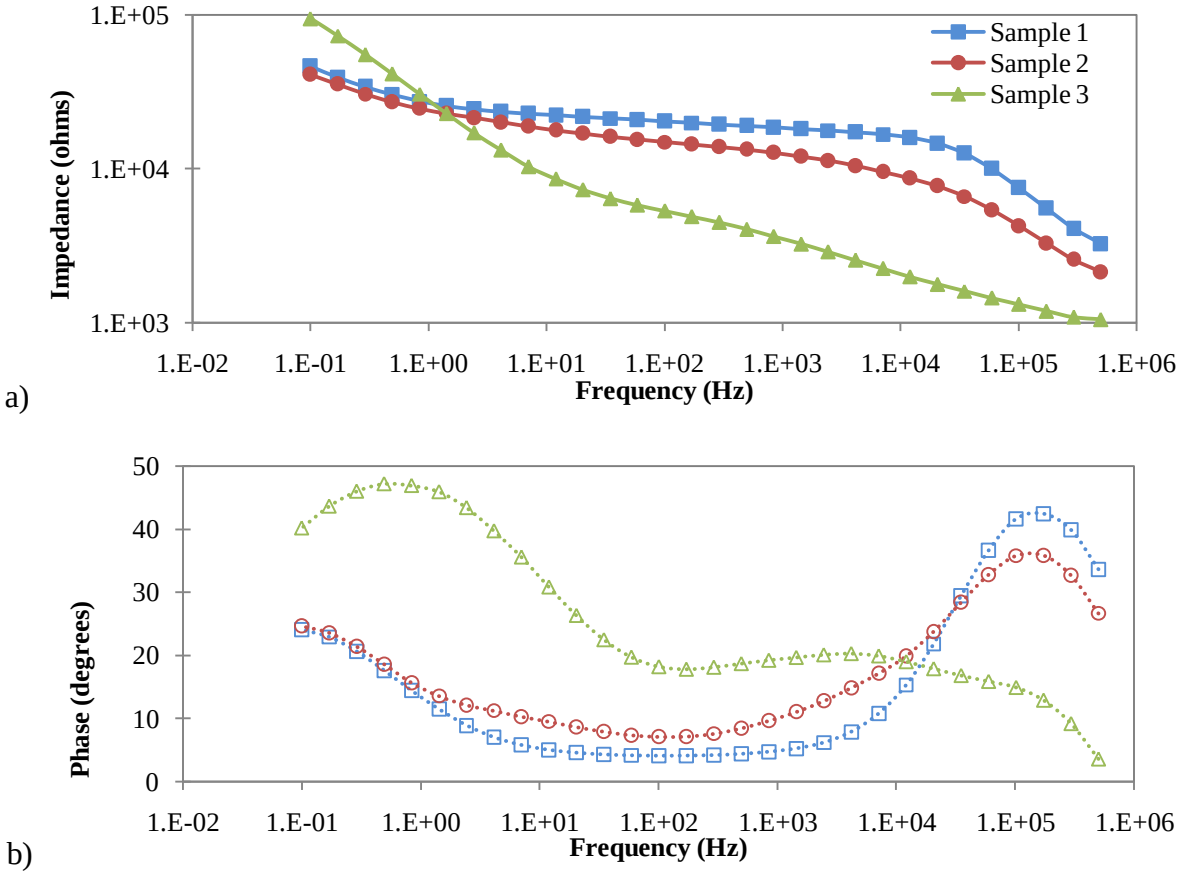

Figure 22: Impedance spectra of three SW30HR carbon grease electroded sensors in single bath configuration at 100 mM NaCl. The upper plot is impedance (Figure 22a); the lower plot is phase (Figure 22b).

4.2.2. Single bath: in-plane electrode configuration

An in-plane electrode configuration was used to provide further evidence that the polysulfone layer was responsible for the time dependent sensor response. If salt solution diffusing through the microporous support layer was responsible for EIS response of the through-thickness carbon grease electroded sensors, in-plane electrodes on the polyamide surface should lack that time-dependence as the polysulfone is now insulated from the EIS current by the polyamide thin film. The sensors were fabricated on the polyamide surface as described in Section 2.2 using SW30HR thin film composite with the non-woven backing layer removed. Single bath experiments were run with three samples; the salt concentrations were introduced in random orders. The 100 mHz to 500 kHz range measured with the Autolab frequency response analyzer was augmented with an additional frequency scan spanning 100 Hz to 1.8 MHz using the HP

4194A analyzer. Figure 23 shows the EIS data from both instruments for one sample. The Autolab results for all samples showed a deflection in the impedance slope and decrease in phase at frequencies greater than 100 kHz indicating the response might have been approaching another resistance-dominated plateau. EIS data of sensor response at higher frequencies, for which the HP 4194A is better suited, showed the capacitive impedance and phase continued to dominate. As such, EIS data from Autolab at frequencies greater than 100 kHz were excluded from the normalized impedance averages presented in the following paragraphs.

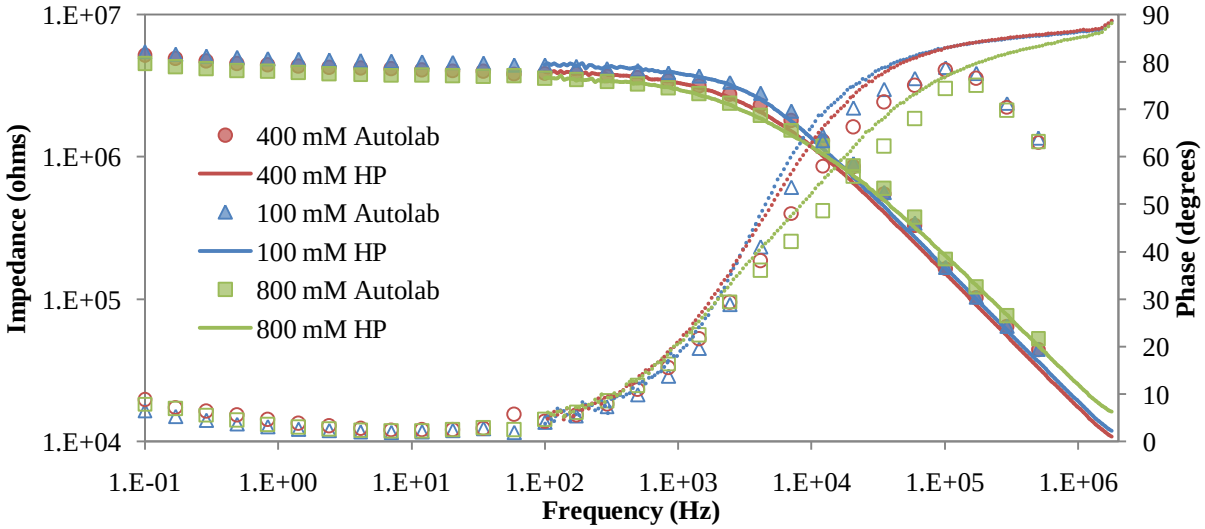

Figure 23: Averaged impedance response of an in-plane carbon grease electroded SW30HR membrane (SW3 IP): single bath experiment exposed to electrolyte concentrations in the order listed in the legend. Solid shapes and lines indicate impedance. Hollow shapes (Autolab data) and dotted lines (HP data) indicate phase.

Figure 24 shows the averages of normalized impedances for the three in-plane samples. A consistent trend in impedance indicated a time-dependent response; a change in trend slope or a sudden change in impedance matching a change in solution was interpreted as concentration sensitivity. Sample SW3 IP showed neither an obvious sensitivity to changes in salt concentration nor any time dependence. Sample SW1 IP showed a slight time dependent response while SW2 IP exhibited obvious transient behavior similar to that of the through-thickness samples (see Figure 21). The EIS results shown in Figure 24 also suggest sensors SW1 IP and SW2 IP are sensitive to salt concentration as evidenced by the trends in average normalized impedance upon changing solution. SW1 IP impedance average increases with an

increase in salt concentration; it is unclear what mechanism led to this response. SW2 IP's EIS response, more expectedly, showed a decrease in impedance with an increase in electrolyte concentration.

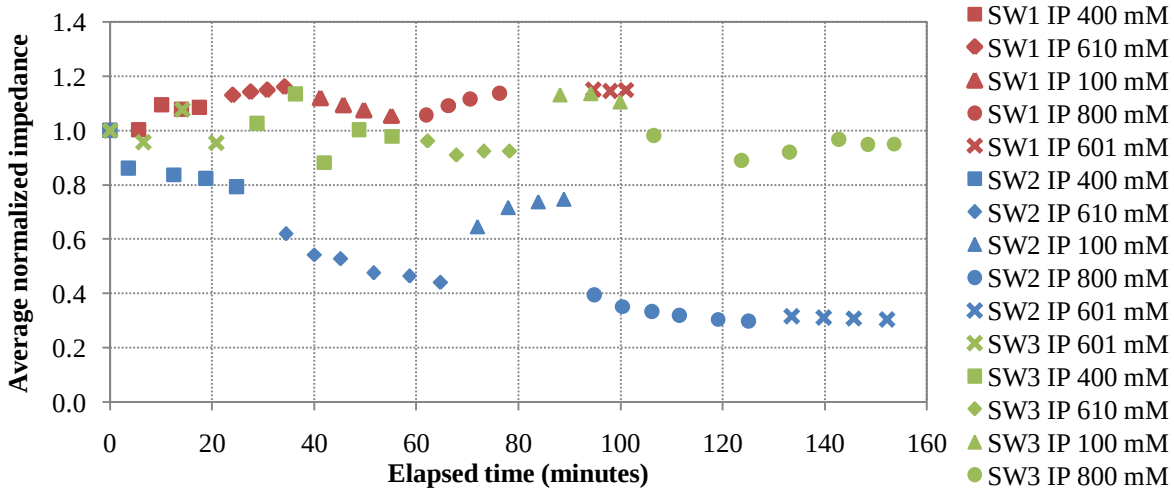

Figure 24: Average change in sensor impedance normalized to impedance (at corresponding frequency) of initial EIS response for in-plane carbon grease electroded SW30HR sensors (SW1 IP – red, SW2 IP – blue and SW3 IP – green). Elapsed time is the time sensor was immersed in sodium chloride solution when EIS was performed. Order of concentration exposure is shown in legend.

The differences in time-dependent behavior might be explained by qualitatively looking at the light transmissibility of the three samples. Figure 25 shows the three samples backlit. SW3 IP showed little to no variation in light transmissibility between electrodes suggesting the polyamide thin film remained intact throughout the fabrication process and explaining its lack of a transient response to changing salt concentration. No time dependence was expected with well-encapsulated electrodes on a defect-free polyamide surface, as minimal current would flow through the microporous polysulfone with electrodes placed on polyamide surface. Sample SW1 IP had a few slightly speckled areas of higher light transmission (polyamide defects) between the electrodes and may account for the slight transient response of the sensor. The membrane area lying between SW2 IP's two electrodes transmitted much more light than the rest of the membrane and corresponded to strongly time-dependent sensor response. This may be indicative of solution diffusing through the now exposed microporous polysulfone and providing a preferential path for EIS current. In addition, SW2 IP had an impedance response shape

similar to the through-thickness electrodes (Figure 20) an order of magnitude higher providing further evidence the polysulfone was responsible for time-dependent sensor response. The defects occurred during fabrication upon removal of the masking material used for epoxy encapsulation.

a)  b) 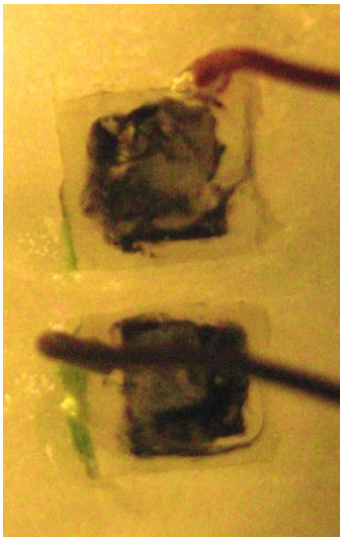 c) 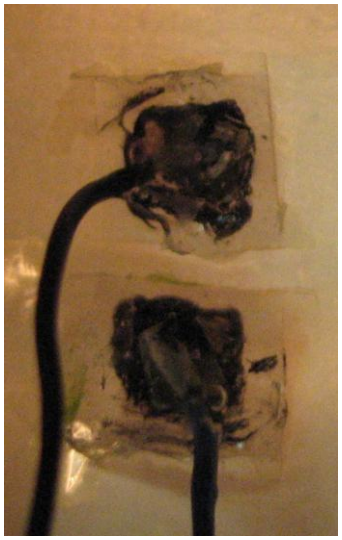

Figure 25: In-plane carbon grease electrodes: a) shows the in-plane sensor (SW2 IP) with transient EIS response to changes in salt concentration with damage to the polyamide thin film transmitting more light between electrodes, b) a sensor (SW1 IP) with a faster but still transient response with some signs of damage to thin film and c) an in-plane sensor (SW3 IP) with no time-depedent response

4.2.3. Double bath: through-thickness electrode configuration

The first set of experiments with the double bath fixture filled the chamber contacting the polyamide thin film with the salt concentration while the chamber enclosed with the polysulfone support was filled with deionized water. The impedance curves of all three carbon grease electroded samples were similar in shape to the carbon grease in-plane electrodes but with maximum magnitudes less than 1 MΩ as compared to 3.3 MΩ (in-plane) (Figure 26). Comparing the average impedance values between concentrations within the same cycle showed no consistent trends with concentration or between runs at the same concentration, nor did the order of concentration exposure appear to matter (Figure 27). The percent change between impedance measurements taken at identical conditions but in a different (random versus ascending) cycle, averaged for all frequencies, yielded decreases for all samples at all concentrations and varied from 1% to 19%. It was unclear why the impedance decreases in

subsequent cycles. Nonetheless, the lack of sensor sensitivity to concentration with only the polyamide thin film exposed to the salt solution supported the hypothesis that the polysulfone layer is responsible for the sensor response seen in the single bath experiments.

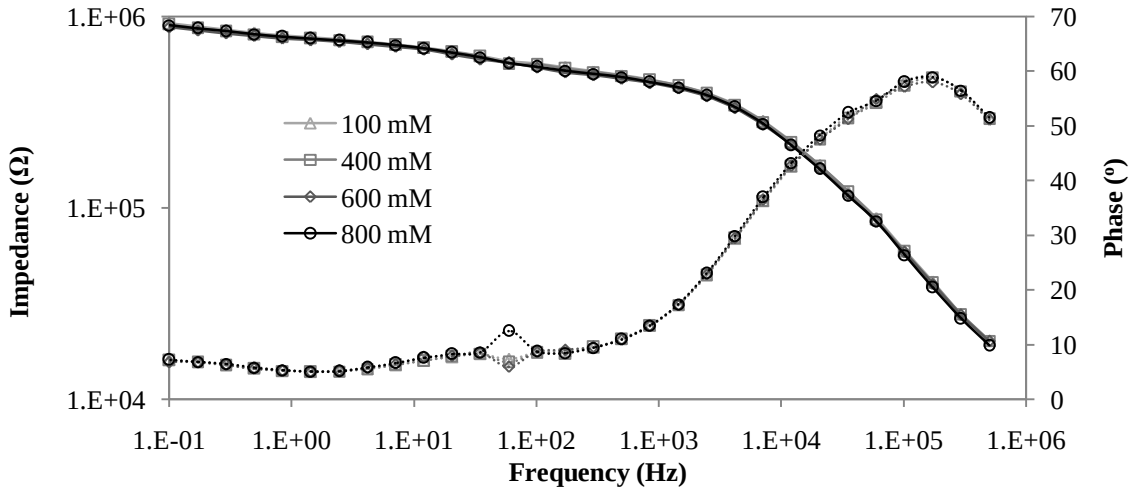

Figure 26: Representative double bath impedance spectra of SW30HR membrane with through-thickness carbon grease electrodes (Sample 1). No concentration sensitivity. Solid lines correspond to impedance; dashed lines refer to phase.

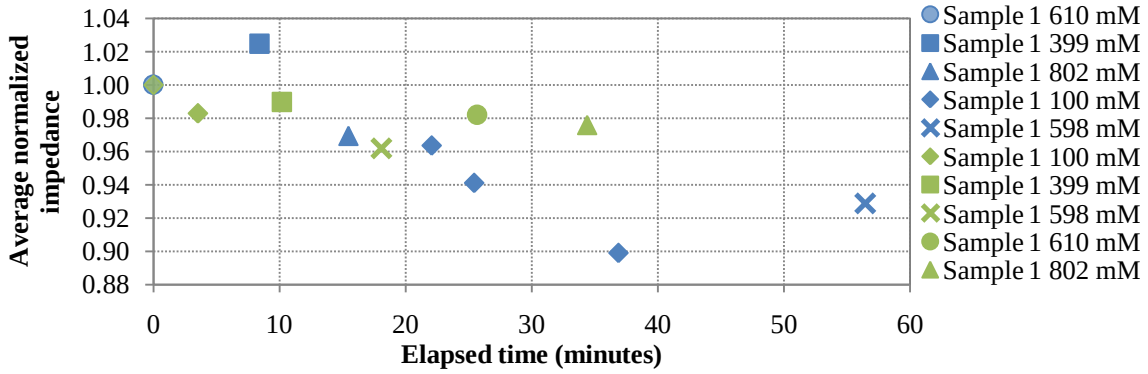

Figure 27: Average change in sensor impedance normalized to impedance (at corresponding frequency) of initial EIS response for through-thickness carbon grease electroded SW30HR sensors (Sample 1) in double bath experiment. Elapsed time was the exposure time of the polyamide side of sensor to sodium chloride solution when EIS was run. Green shapes are the first run; blue are the second. Solutions were introduced in ascending order first and then random order (shapes are consistent for each concentration).

To further support our hypothesis that the polysulfone is responsible for the transient sensor response observed in Section 4.2.1, the double bath test configuration was reversed. A carbon grease electroded sensor was mounted in the fixture so that the polysulfone side was exposed to the salt solution while the polyamide thin film only contacted deionized water. The sensor was exposed to a constant solution of 400 mM sodium chloride, and EIS measurements were taken every half hour for the first ten hours and then at longer intervals thereafter. Like the carbon grease results from the single bath, the response of the sensor in this arrangement initially fell significantly with time but appeared to approach an asymptote in a similar time scale (Figure 28). This is further evidence that the microporous polysulfone layer was responsible for the time-dependent sensor response.

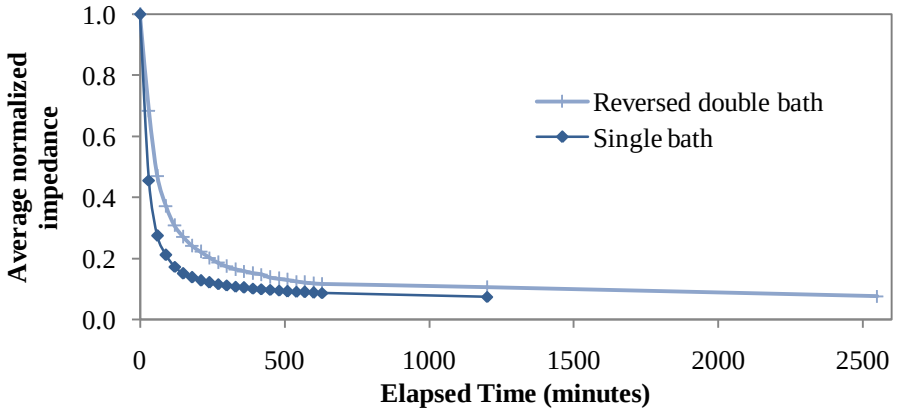

Figure 28: Normalized impedance response with time at constant concentration (400 mM) of through-thickness carbon grease electrode in reversed double bath configurations compared with single bath sensor response.

4.3. DAP electroded sensors

A series of double bath experiments with through-thickness DAP electroded sensors showed a time-dependent EIS response to changes in electrolyte concentration. The average normalized impedance trends were generally consistent when comparing the relative change between adjacent runs at different concentrations with the same sensor. Results showed a decrease in sensor impedance with an increase in salt concentration; however, the magnitude of the change in average normalized impedance did not correlated to salt concentration of solution. The experimental details and discussion follows.

4.3.1. Double bath: through-thickness electrode configuration

Three DAP electroded samples were used in double bath experiments to characterize the sensor response in comparison to the carbon grease sensors. The DAP electrodes were in direct electrical contact with the surrounding solution rather than being insulated with epoxy as the carbon grease electrodes had been. The DAP electrodes also contained Nafion ionomer as a matrix for the conducting RuO_2 particles. The electrolyte concentrations were introduced in random order from 100 mM to 800 mM NaCl with the double bath fixture and sample being rinsed twice with deionized water between solution changes. EIS was run using Autolab in a two-electrode configuration applying a 50 mV (rms) sinusoidal voltage from 100 mHz to 500 kHz.

The EIS experiments showed the sensors reached steady-state (average impedance varying by less than ± 3% between runs) in less than 30 minutes, and showed significant changes in impedance spectra between different concentrations (Figure 29 and Figure 30). However, the strength of the solution concentration did not correlate with impedance magnitude for any of the samples. For example, the impedance of DAP Sample 3 decreased an average of 41% between 399 mM to 610 mM (steady-state) but, upon exposure to 100 mM solution, only increased to an average of 80% of the sensor impedance at 399 mM. It might be expected that the sensor impedance would be much higher in a solution one-fourth the concentration of another. Whereas the carbon grease electrodes in a through-thickness configuration with the polyamide exposed to the salt solution showed no trends with respect to time dependence and concentration, the through-thickness DAP electroded sensors exhibited transient responses and, to some extent, concentration sensitivity. The differing responses between the DAP and carbon grease electrodes in the double bath experiments may be due to Nafion interacting with the salt solution through swelling or other mechanisms. The lack of a predictable and consistent change in impedance with respect to concentration may be attributed to the fragility of the DAP electrodes with the gold foil/RuO_2 interface changing (i.e. delaminating) with time and/or solution changes. Figure 31 shows the polyamide side of a DAP electroded sensor with the gold foil delaminating after hydration.

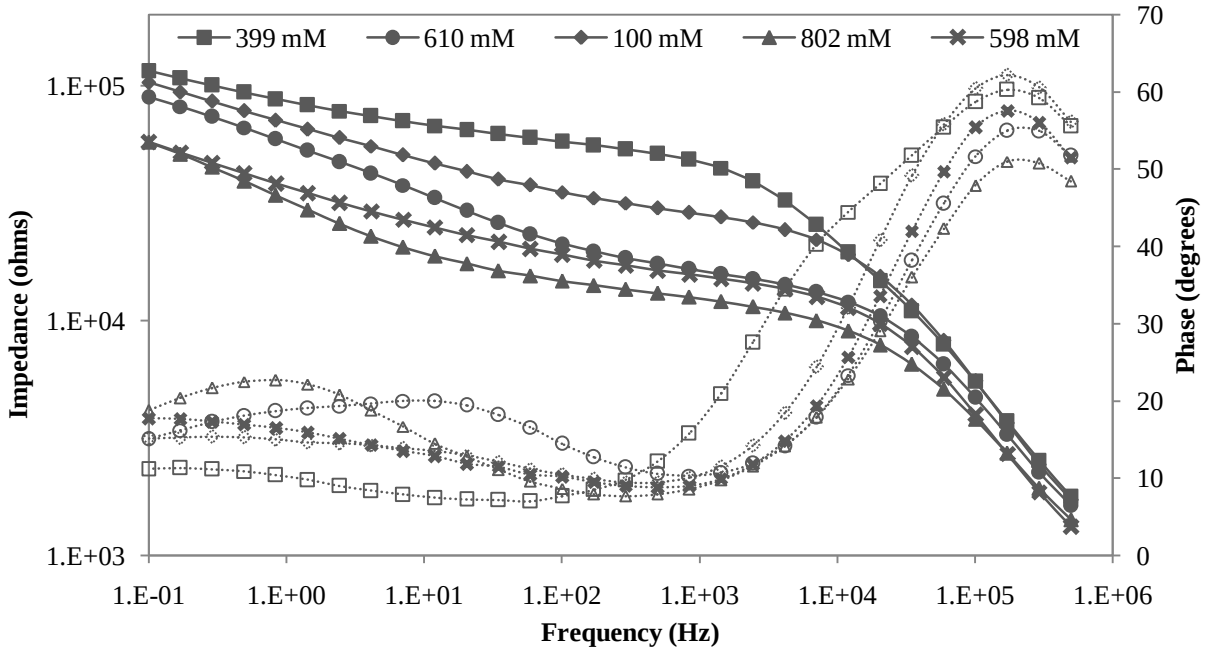

Figure 29: Typical double bath impedance spectra of SW30HR membrane with through-thickness DAP electrodes (DAP Sample 3). Steady-state sensor responses are shown (~30 minutes at each concentration). NaCl concentrations were introduced in the order: 399, 610, 100, 802, 598 mM. Solid shapes correspond to impedance; hollow shapes refer to phase.

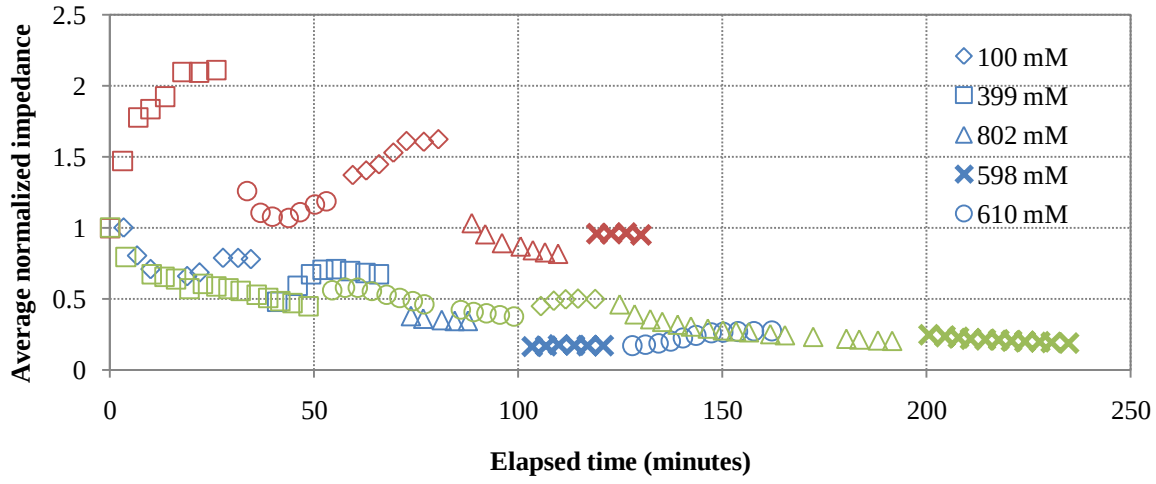

Figure 30: Average change in sensor impedance normalized to impedance (at corresponding frequency) of initial EIS response for through-thickness DAP electroded SW30HR sensors in double bath experiments. Elapsed time was the exposure time of the polyamide side of sensor to sodium chloride solution when EIS was run. Blue shapes are DAP Sample 1; green are DAP Sample 2; red are DAP Sample 3. Solutions were introduced in random order (shapes are consistent for each concentration).

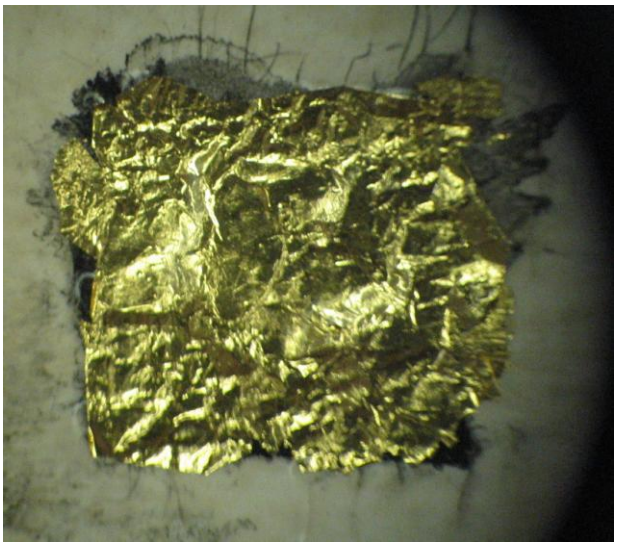

Figure 31: Micrograph a DAP electroded sensor after hydration (polyamide side). RuO_2/Nafion layer is the black areas on the edges of the delaminating gold foil. Gold foil is 5 mm by 5 mm.

4.4. Discussion of concentration sensing results

The single bath results of the carbon grease electroded sensors initially showed sensitivity to changes in salt concentration with the impedance decreasing as expected over the applied frequency range. Unfortunately, the in-plane and double bath experiments showed the polyamide thin film was not responsible for the sensor response; rather, the microporous polysulfone side of the electrode exhibited a response to concentration consistent with that of the single bath experiments. We posit this was due to the impermeability of the epoxy encapsulated carbon grease sensor. If the epoxy is sufficiently adhered to the polyamide thin film, the solution does not contact the polyamide in the area being probed by EIS. On the other hand, the polysulfone's porosity allows the solution to diffuse beneath the encapsulated electrode and fill the pores through which the electric potential is being applied. The change in electrolyte concentration manifests itself as a change in solution resistance between electrodes and a change in double layer capacitance (at low frequencies) of the electrode/solution interface where the carbon grease electrode contacts the polysulfone. Indeed, higher salt concentrations led to a decrease in sensor impedance, albeit slowly. Because the carbon grease electroded sensors failed to show sensitivity to salt concentration in the orientation required for the RO membrane to function this electroding approach is not suitable for sensing RO surface phenomena.

The DAP electroded sensors, lacking the encapsulation that prevented the carbon grease sensors from being effective, were to provide a viable alternative by allowing the electrolyte to contact the electroded area of the polyamide directly. It was thought the electrolyte concentration would affect sensor impedance through similar mechanisms seen in the carbon grease sensors, namely changes in double layer formation at the electrode and membrane resistance as the ions diffused through the polyamide[62, 76]. Unfortunately, they proved quite fragile mechanically, were time-dependent and lacked a predictable response to changes in salt concentration. The addition of Nafion (proton form), another ionomer, may have introduced unanticipated phenomena due to swelling and/or interactions with the ions in solution and may account for the transient impedance response of the sensors. The mechanical bond between the RuO_2/Nafion layer and the gold foil was another poorly understood and controlled variable introduced; imperfect or deteriorating gold foil bonding would most likely lead to inconsistent sensor responses. For these reasons, DAP electroded sensors are not suitable for RO sensor implementation.

5. PROTEIN FOULING SENSING EXPERIMENTS

Protein fouling experiments were developed to evaluate the novel *in situ* platinized polymer graft RO sensor. We utilized a custom-built lab-scale RO cross-flow system as well as dead-end experimental configurations to foul the sensors with a model protein, bovine serum albumin (BSA). This chapter will: *i*) provide background on protein fouling mechanisms and expected behavior of the sensor, *ii*) describe the experimental setups used, *iii*) present and discuss experimental results of sensor fouling, and *iv*) conclude with a summary of the experiments.

5.1. Background

Proteins constitute a significant proportion of treated secondary wastewater, and micro- and ultra-filtration pretreatments are not sufficient to completely remove protein from feedwater for downstream reverse osmosis filtration stages[35]. Numerous groups have shown that protein, typically by using BSA, forms a fouling layer on RO membranes decreasing salt rejection and permeate flux (Figure 32) [33-35, 63]. Most of these studies were meant to probe the mechanisms responsible for protein fouling. Li et al. concluded that greater membrane surface roughness and initial permeate flux (operating pressure) led to the largest flux declines attributable to fouling by BSA and sodium alginate[33]. Kim and Hoek approached fouling from a thermodynamic standpoint using experimentally determined acid-base and van der Waals energies and demonstrated foulant-membrane interfacial forces were responsible for initial fouling with foulant-foulant interactions determining additional flux decline after the initial foulant layer is formed[34]. Introducing BSA, with a NaCl as a background electrolyte, into a cross-flow system led to an initial decline in permeate flux that subsequently stabilized at about 93% of the pre-fouling flux. Ang and Elimelech investigated the influence of feedwater chemistry and composition (pH, ionic strength, calcium concentration and co-foulant (sodium alginate) on protein fouling[35]. Their experimental results correlated to foulant-foulant adhesive forces within the different feedwater compositions measured using AFM with a colloid probe attached to the AFM cantilever.

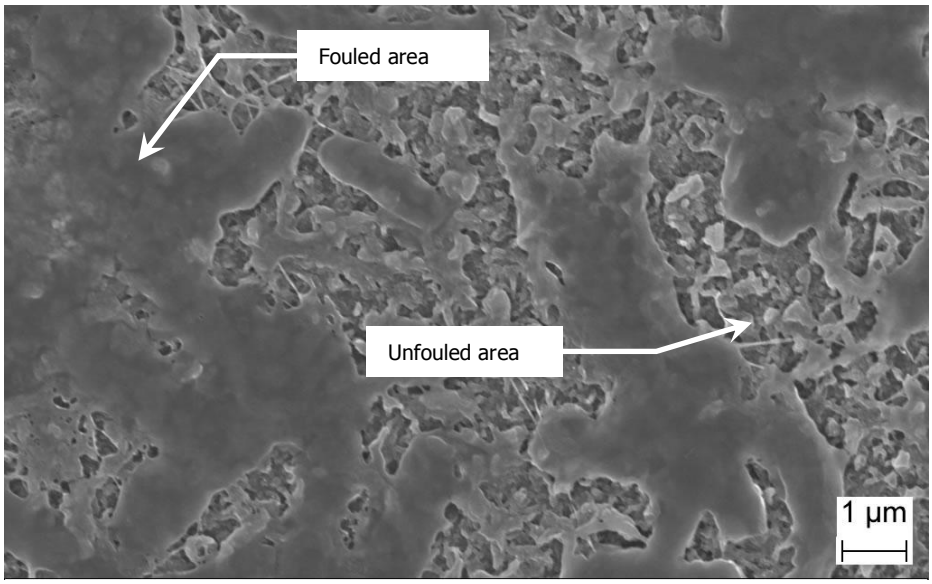

Figure 32: BW30LE membrane fouled with bovine serum albumin protein. Dead-end configuration 1 MPa, 1 mg/1 mL (BSA/deionized water)

5.2. Experimental method

The experimental setups for fouling will be described in the following sections. A cross-flow setup and a dead-end configuration were employed.

5.2.1. Cross-flow setup

A chemically inert (wetted parts: SS316 and Teflon) lab-scale RO closed cross-flow system was designed and built for membrane fouling. At the heart of the RO system is the cross-flow test cell (Sepa CF II, Sterlitech) shown in Figure 33. The cross-flow test cell held the RO membrane/sensor assembly with four bolts clamping the two halves together and sealed by two concentric o-rings. The pressurized feedwater enters through the inlet, passes through the flow channel and tangential to the membrane, and exits via the retentate outlet. The hydraulic pressure forces some of the feedwater through the membrane; this purified water is the permeate. The permeate side of the membrane is supported by sintered (porous) stainless steel, and it exits through a small outlet port in the back of the test cell (not shown in Figure 33). The test cell mimics the conditions in commercial RO systems using spiral wound modules with the feedwater passing across the membrane. This configurations limits the amount of permeate produced at any one stage but, importantly, minimizes membrane fouling due to hydraulic forces. It was observed that upon clamping the test cell, the insulation of the wires of the

sensors' electrical leads was being compressed to the point of having a resistance on the order of kΩ between themselves and the test cell. To circumvent this problem, a 1 mm thick layer of Kapton tape was placed on the clamping area to reduce the compressive forces on the electrical leads and add additional electrical insulation.

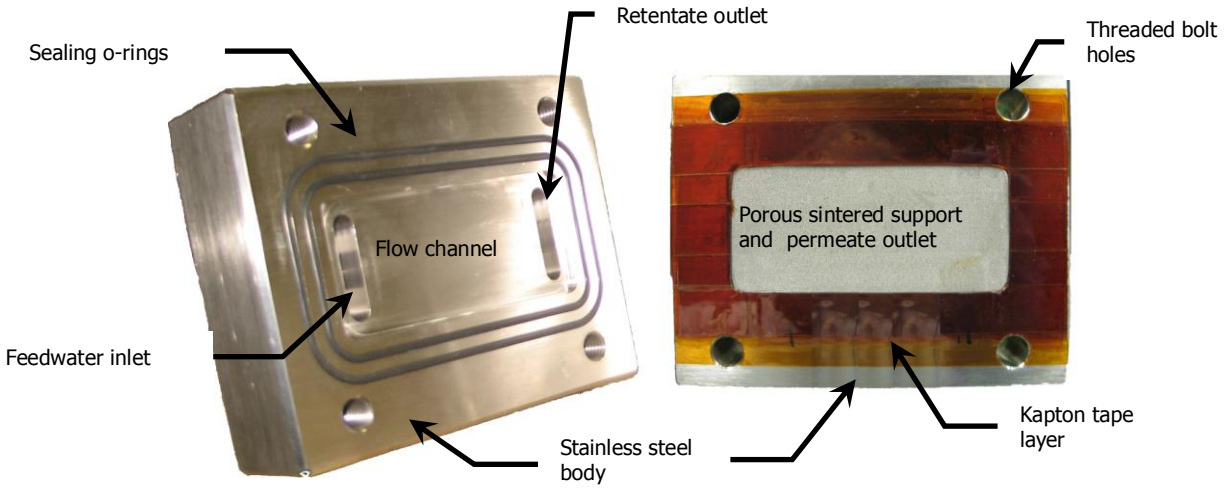

Figure 33: Picture of the cross-flow test cell used in RO fouling experiments. The membrane/sensor assembly is clamped between the two stainless steel bodies with four bolts. The assembly is described more completely in the preceding text.

Figure 34 shows the complete cross-flow system schematically. To drive the high pressure low flow diaphragm pump (Hydra-Cell D-03, Wanner Engineering, Inc.), a 2kW step-up transformer (VT 2000, Voltage-Converter-Transformer.com) supplies 220 VAC to a variable frequency drive (X200-015NFU1, Hitachi). The variable frequency drive allows the rotational speed of the 2 HP three-phase motor (116106, Leeson) it powers to be controlled by varying the output voltage frequency. The motor output shaft, in turn, connects to the pump that pressurizes the feedwater from the feed tank. The adjustability of the motor speed allows for some control of the flow rate of the feedwater.

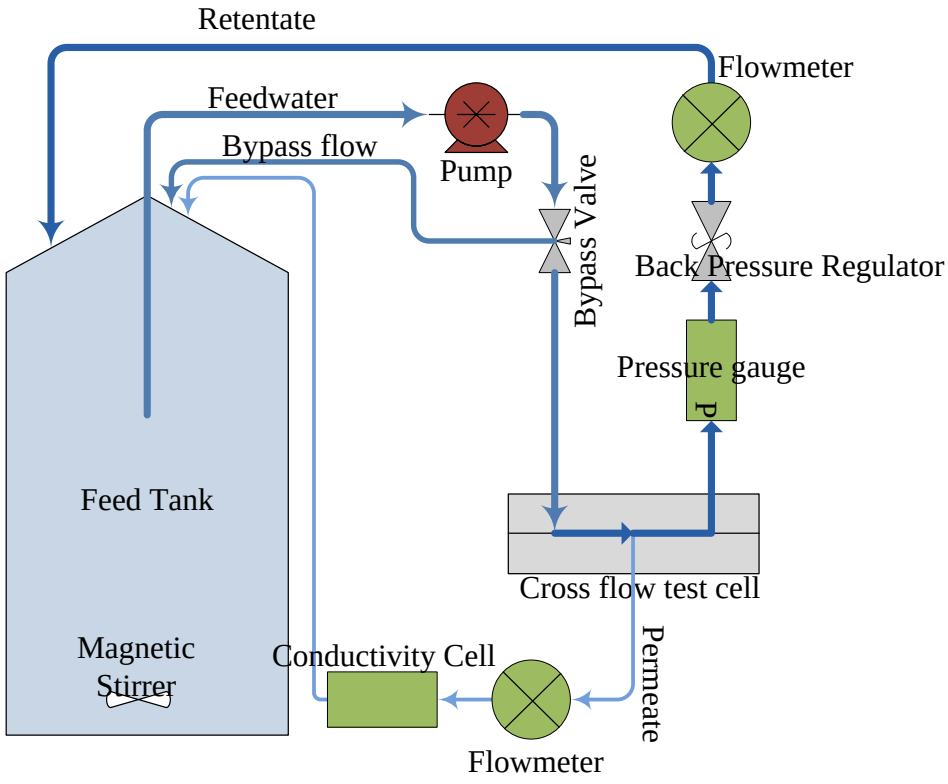

Figure 34: Schematic of the lab-scale RO system used in the cross-flow experiments

The pressurized feedwater then flows through a bypass valve that vents to the feed tank. This additional flow control allows the motor to operate in its power band whilst maintaining the desired feedwater flow rate. From the bypass valve, the feedwater enters the cross-flow test cell. The water exits as retentate and returns to the feed tank after passing through the back pressure regulator (BP-3, Go Regulator) which maintains the system pressure required to overcome the osmotic pressure and force water through the semipermeable membrane.

Several measurements were taken throughout the process to quantify RO performance and for experimental control and repeatability: *i*) hydrostatic pressure in the cross-flow test cell, *ii*) retentate and *iii*)permeate volumetric flow rate, *iv*) feed tank and *v*)permeate temperature and *vi*) permeate conductivity. The retentate flow rate was measured using a vertically mounted flowmeter (McMaster-Carr part # 8051K13, King Instrument) and was maintained at 0.75 L/min (0.2 gpm) (± 5%) by adjusting the bypass valve upstream. This flow rate produced a mean cross flow velocity within the test cell of 12 cm/s giving a Reynold's number of 0.66 indicating the

flow remained laminar through the test cell. With steady laminar flow, any electromechanical sensor response should remain invariant thus attributing any variations in response to electrochemical changes. Furthermore, establishing a baseline sensor impedance over many hours prior to fouling ensures that if flow conditions at the sensor were unsteady or localized, those effects will be averaged out over time and any further change may again be attributed to electrochemical effects. The temperature of the feed tank was monitored using a contact thermometer attached to a magnetic stirrer (RCT basic, IKAMAG) and increased to a steady-state temperature of 29°C when operating the system at 1.03 MPa (150 psi). A digital pressure transducer (DPG1000B, Omega) monitored the pressure, which was held constant (± 4%) by adjusting the back pressure regulator. The permeate temperature and flow rate were measured by a digital differential pressure flow meter (LA10-C, Flocat) and output to a LabVIEW virtual instrument (VI) program via a serial port connection. A conductivity probe (Orion 011020, Thermo Electron Corp.) with a cell constant of 0.094 cm^{-1} monitors membrane ion rejection performance with a change in conductance proportional to the change in ionic concentration of the permeate (see Figure 35). The cell constant is the ratio of distance between electrodes to surface area of electrodes. Figure 36 shows the circuit used to measure solution resistivity (inverse of conductivity). The applied voltage function was defined in a LabVIEW VI and generated with a DAQ (USB-6211, National Instruments) taking care that the current did not exceed the capabilities of the DAQ. By measuring the voltage drop across a known resistance, the conductivity of the solution was calculated using Equation (4), where R_1 is the known resistor (117.6 Ω), V_1 is the magnitude of the applied voltage, V_2 is the measured voltage drop across R_1, k is the cell constant (0.094 cm^{-1}), and $C_{solution}$ is the calculated conductivity of the solution. The conductivity was then corrected for temperature (to 25°C) using a temperature correction factor of 0.0217/degree from 25°C as measured by the permeate flow meter[77].

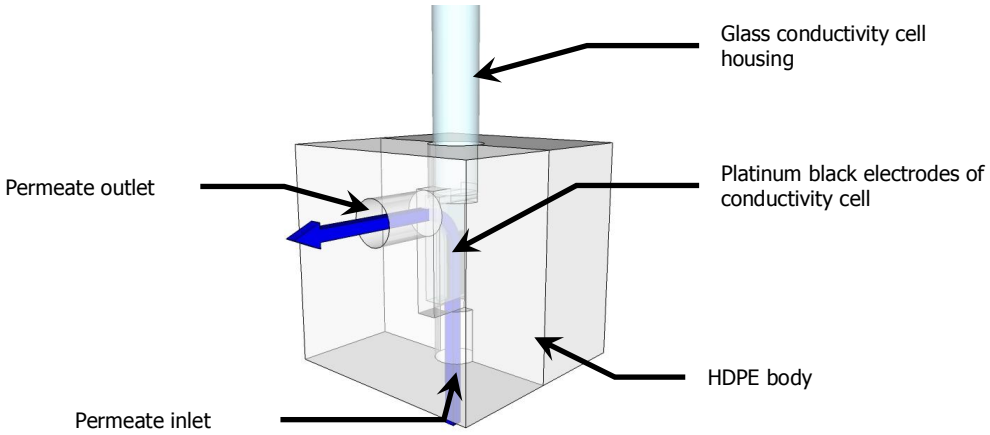

Figure 35: Conductivity cell holder constructed from HDPE. The blue arrow represents the flow of water through the cell: permeate enters from the bottom, flows between two platinum electrodes at the end of the conductivity probe and exits through the side. The platinum electrodes are used to measure the conductivity (ionic concentration) of the permeate.

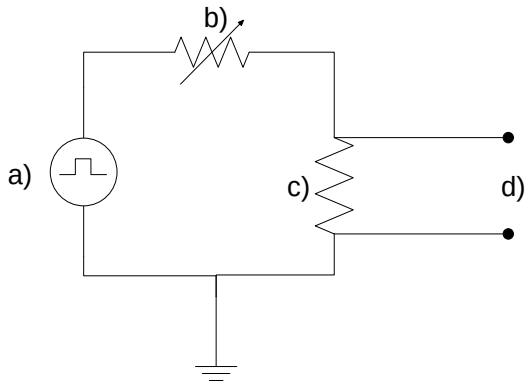

Figure 36: Circuit for the conductivity probe: a) applied voltage is a square wave (0.25 V); b) permeate resistance; c) 117.6 Ω resistor; d) measured voltage drop across resistor. Solution resistance can be calculated using Equation (4).

$$C_{solution} = \frac{1}{R_1\left(\frac{V_1}{V_2} - 1\right)}k \tag{4}$$

The experimental details of each cross-flow fouling test are outlined in Appendix A III. The cross-flow fouling experiments generally took up to a week to complete, from initial membrane compaction to post-fouling operation. In early experiments, the BSA foulant was added to 20 L of a 2000 ppm (34.2 mM) NaCl solution in the feed tank after the permeate flux had stabilized (~36 hours). Ionic concentrations greater than 10 mM have been shown to lead to an increase in

fouling (as indicated by permeate flux decline); however, in the system discussed here, the introduction of NaCl caused corrosion of a brass fitting on the back pressure regulator (Figure 37). This is representative of a real world RO system but inhibits control of feedwater composition. Therefore, the backpressure regulator was replaced with one constructed of stainless steel and future runs were performed without NaCl.

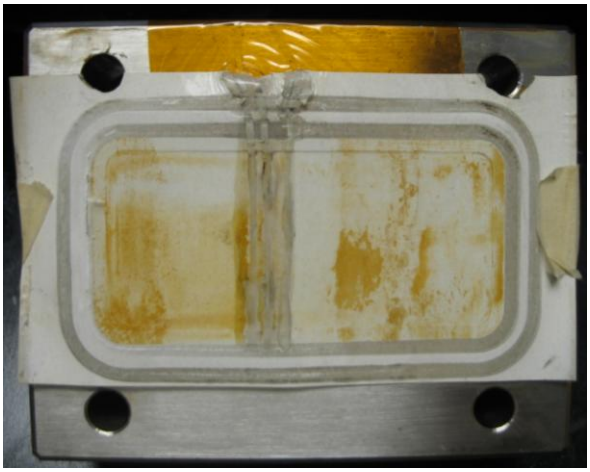

Figure 37: Deposits (orange/brown spots on membrane) from corrosion in the RO cross-flow system using NaCl solution (Sample 4). Sensor results from this sample were inconclusive as the EIS responses suggested an open circuit condition between the electrical leads and the sensor.

5.2.2. Dead-end setup

A dead-end experimental configuration was used to minimize electrical noise throughout the system and decrease the time it took to foul the membranes/sensors. As will be shown in the results section, the EIS data collected from the cross-flow experiments had a lot of electrical noise. Similar to the cross-flow experimental setup, the cross-flow test cell was used but with the outlet being blocked so that feedwater had to pass through the RO membrane. The feedwater and test cell were pressurized to 1 MPa with compressed nitrogen. Permeate was collected in a graduated cylinder and periodically measured visually as the permeate production was below the range of the flowmeter used in the cross-flow experiments. Permeate conductivity was not measured as no electrolyte was in the feedwater to minimize extraneous factors and maximize permeate production (thus the rate of fouling). Figure 38 shows the dead-end experimental setup. The red inlet hose leads to the compressed nitrogen tank.

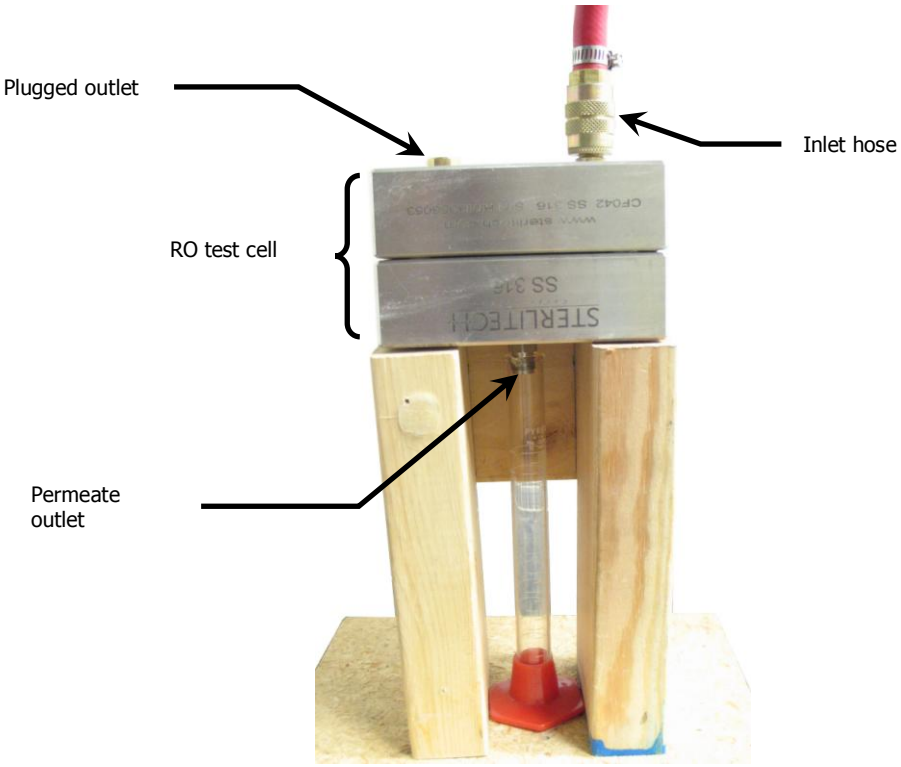

Figure 38: Dead-end test setup. Inlet hose is connected to N2 tank and is pressurized. A plug in the outlet allows the RO test cell to be used in a dead-end configuration. Permeate exits the outlet and is collected in a graduated cylinder to monitor permeate flux. Sample is clamped between the two steel halves of the test cell.

The fouling protocol for the dead-end RO experiments is as follows:

1. After mounting the membrane/sensor assembly in the test cell, the test cell and hose connected to the nitrogen are filled with ~100 mL deionized water (17 mL in test cell with the balance in hose).
2. The inlet hose connected to the test cell and nitrogen tank ensuring the water is completely placed at the end of the hose connected to the test cell.
3. System is pressurized to 1 MPa.
4. EIS is performed periodically until impedance stabilizes while monitoring permeate flow rate and refilling system as necessary.
5. Once impedance had stabilized, the system is emptied of water and 20-50 mg BSA dissolved in 100 mL deionized water is placed in test cell and hose following the method in step 2.

6. EIS and permeate flow measurements are carried out until at least 90% of the feedwater had been forced through the membrane
7. The hose is rinsed with deionized water and remaining feedwater is emptied from the test cell.
8. System is refilled with deionized water and EIS performed until impedance stabilizes or all water is filtered.

5.3. Fouling results

The following sections present fouling experiments in terms of sensor response to fouling. The specific experimental conditions and sensor fabrication recipes are given in Appendix A . EIS results indicated the platinized polymer graft sensors were sensitive to fouling, but their responses varied significantly between sensors and experimental conditions (specifically, whether or not the cross-flow system is electrically disconnected, and the fouling method used).

Three sensors on two samples fouled in dead-end experiments exhibited responses with low electrical noise and small standard deviations in the data (Figure 41, Figure 44 and Figure 45). The impedance magnitude of a *slightly fouled* and *lightly platinized* sensor increased by 7.4% at frequencies less than 2 kHz while decreasing by 10.9% at 100 kHz to 500 kHz (Figure 40). Conversely, two *more platinized* sensors on a second *highly fouled* sample responded with decreases in impedance magnitude to 14.8% at 40 Hz for one sensor and to 11.4% at 10 kHz for the other with no meaningful increase in impedance over any frequency region (Figure 43).

Opposite the dead-end fouled sensor responses, a *lightly platinized* sensor s*lightly fouled* using a cross-flow RO system decreased in impedance (up to 8.0 %) from 150 mHz to 400 Hz and increased up to 10.5% at higher frequencies (1 kHz – 200 kHz) when the system was electrically disconnected (Figure 46). EIS data taken while the cross-flow system was operating was generally too noisy for changes in response to be meaningful over most frequencies. Two sensor responses in the clean data regions showed a decrease of 62% between 200 and 650 Hz for a *lightly platinized* sensor and a decrease of 10% at 31 kHz for a *highly platinized* one. As well as percent change in impedance, the degree of platinization of the sensor appeared to affect the shape and magnitude of the response.

Due to the difficulties in quantifying the foulant layer and small number of samples tested, sensor responses were not quantitatively correlated to degree of fouling. Rather, the experiments were meant to demonstrate proof-of-concept. Two dead-end fouling runs and their sensor response will be presented and discussed followed by two of the cross-flow fouling experiments. Despite seven fouling runs with fourteen sensors, only a few produced usable data due to encapsulation defects and insulation failures. The impedance magnitudes at each frequency were averaged over each experimental "segment" (pre-foul, fouling, post-foul) for each sensor after the EIS data had stabilized (number of runs averaged varied). The standard deviation of the average at each frequency was used to determine whether the sensors' responses in that region were significant. If a sensor's average post-foul and average pre-foul impedances lay within one standard deviation of the other over a particular range of frequencies (due to electrical noise, lack of fouling sensitivity, or other phenomena), the results in that frequency range were considered inconclusive.

5.3.1. Dead-end

Three platinized polymer graft sensors fouled in a dead-end experimental configuration had quite different responses with respect to impedance trends upon fouling; this may be due to the differences in the degree of fouling. The results presented first are for a sensor whose permeate flux declined slightly, 5%, after fouling (Sample 7 1_2). Figure 39 is an SEM micrograph of the fouled sensor; both permeate flux decline and SEM images suggest the membrane sample was not highly fouled.

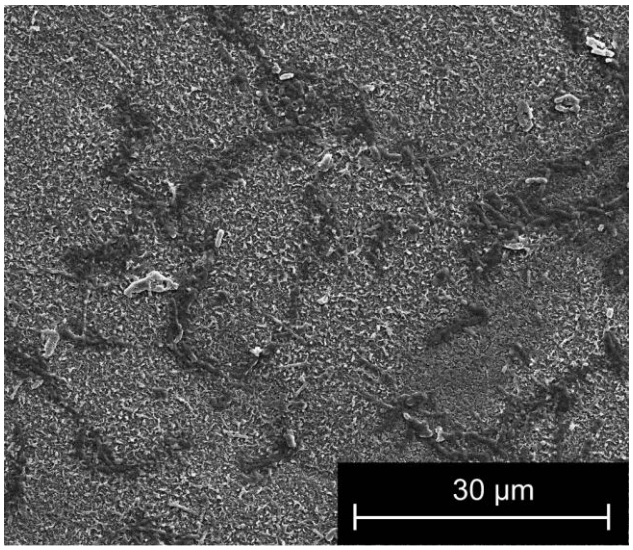

Figure 39: Micrograph of a sensor fouled in dead-end experiment (Sample 7) (20 mg BSA in 98 mL water, 89.6% of solution produced as permeate). Dark areas are the fouling deposits of protein. Permeate flux declined 5% after fouling. See Appendix A IV for experimental details.

Figure 40 shows the percent change in average impedance response of this sensor to fouling in the fouling solution and post-fouling in deionized water after the sensor had been rinsed with deionized water. Impedance increased to 8.9% at lower frequencies (50 mHz – 2 kHz) and decreased to 11.1% as frequencies went to 100 kHz. The phase of the sensor response shifted to the left upon fouling in the 100 – 100 kHz frequency range (Figure 41). The increase in impedance at lower frequencies was perhaps due to a change in sensor resistance rather than capacitance as there was a minimal shift in phase. The capacitive region (increase in phase) at the lower frequencies for all data may be attributed to the formation of a double layer. The change in impedance and shift in phase at higher frequencies post-fouling might be explained by an increase in sensor capacitance, as this would lead to a decrease in impedance and a phase shift towards lower frequencies.

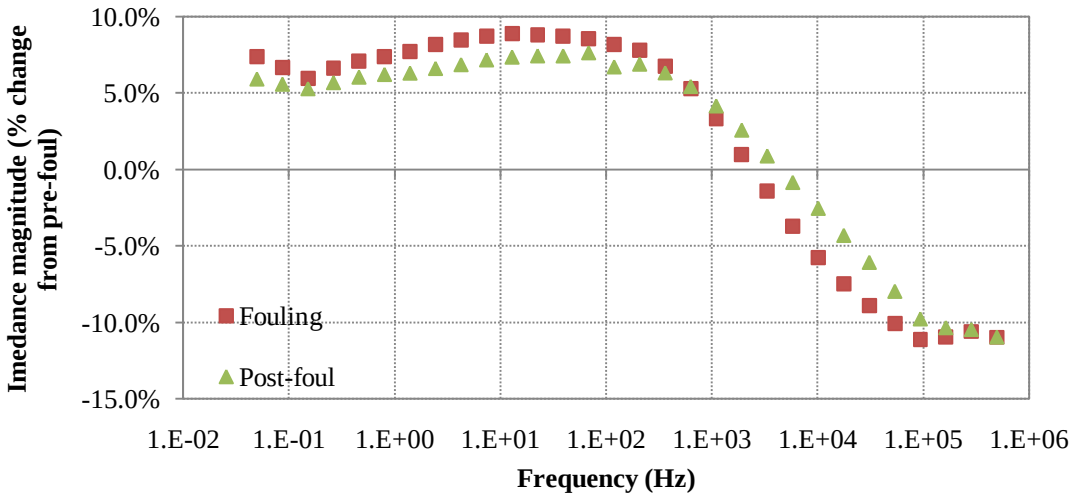

Figure 40: Percent change in average impedance magnitude of a lightly platinized sensor slightly fouled used in a dead-end experimental configuration (Sample 7 1_2). "Fouling" is the percent change of the averaged impedance at the end of the fouling run with respect to the pre-foul average impedance. "Post-foul" compares the average impedance of the sensor in deionized water after fouling to pre-foul average impedance. See Figure 41 for magnitudes and Appendix A IV for experimental conditions.

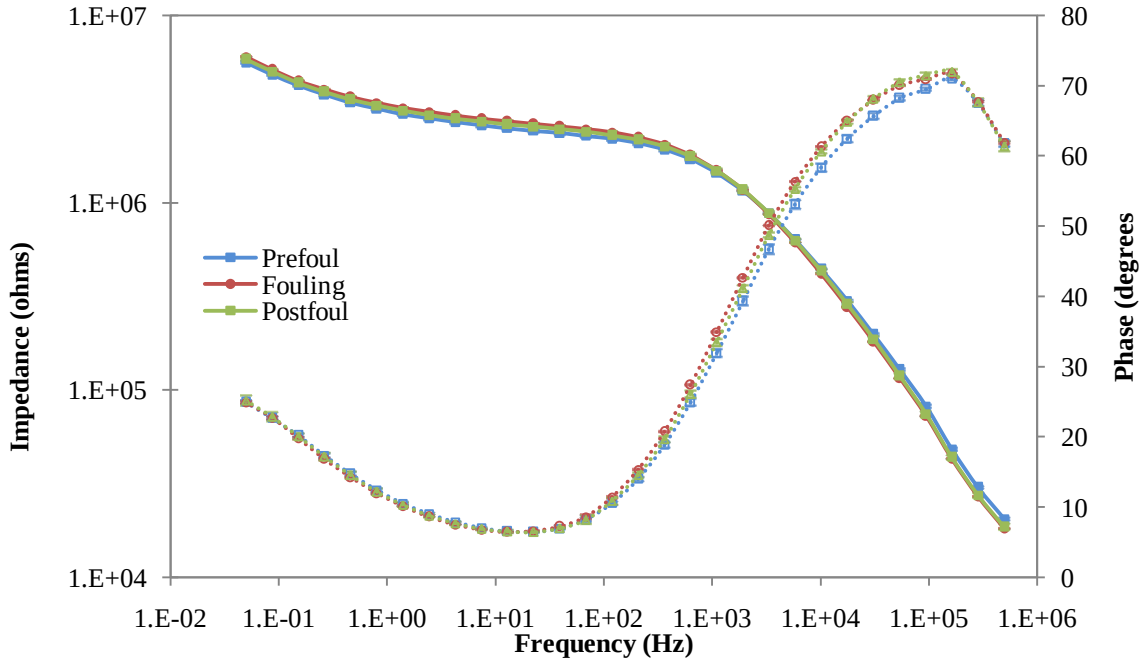

Figure 41: Averaged EIS sensor results fouled in a dead-end RO configuration (Sample 7 1_2): *i*) in deionized water pre-fouling (blue squares), *ii*) in BSA solution at the end of fouling (red circles), and *iii*) in deionized water post-fouling (green triangles). Solid lines indicate impedance, dashed lines indicate phase. Experimental conditions are given in Appendix A IV

A second sample with two sensors (Sample 11 1_2 and Sample 11 2_3), using the dead-end experimental setup, was severely fouled as seen by SEM (Figure 42); permeate flux declined by 52% (0.04 mL/min pre-foul, 0.02 mL/min post-foul). The fouling was greater than the previous dead-end experiment for several reasons: *i*) 150% more protein was used (50 mg versus 20 mg of BSA), *ii*) more feedwater was recovered (95.5% versus 89.4% recovery), and *iii*) the sample was not rinsed with deionized water between fouling and post-fouling cycles as in the previous run.

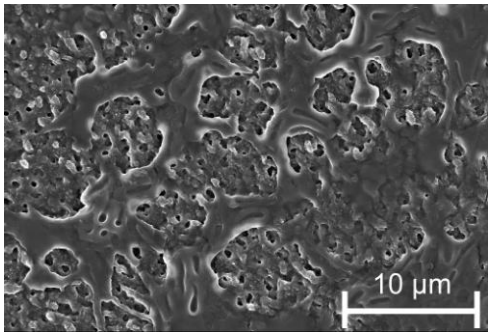

Figure 42: Micrograph of a sensor fouled with 50 mg BSA in dead-end experiment (Sample 11). Dark areas are the fouling deposits of protein. Permeate flux declined 52% after fouling. See Appendix A IV for experimental details.

Sensor 11 1_2 had a meaningful impedance decrease (less than 14.8%) between pre- and post-fouling at frequencies greater than 4 Hz (Figure 43). The phase also decreased slightly at higher frequencies (greater than 40 Hz) while increasing at frequencies less than 40 Hz. The increase in phase combined with the decrease in impedance suggests the protein layer was decreasing sensor resistance in that region. This increases the influence low frequency capacitance had on the response leading to the increase in phase. Low frequency capacitance is often associated with double layer formation, and it may be expected this would change post-fouling and contribute to the overall sensor response, too. The small decrease in phase at frequencies higher than 40 Hz along with the decrease in impedance may mean both the sensor capacitance and resistance were sensitive to fouling. In looking at the phase of the responses, both pre- and post-fouling curves showed a kink at 95 kHz that was missing from the fouling response; it was unclear what was responsible for this kink. The "Fouling" curve in Figure 44 shows the sensor response towards the end of fouling while still in the BSA solution. The significant downward shift (46.3% at 200 Hz) indicates the sensor was likely more sensitive to feedwater composition than foulant layer formation.

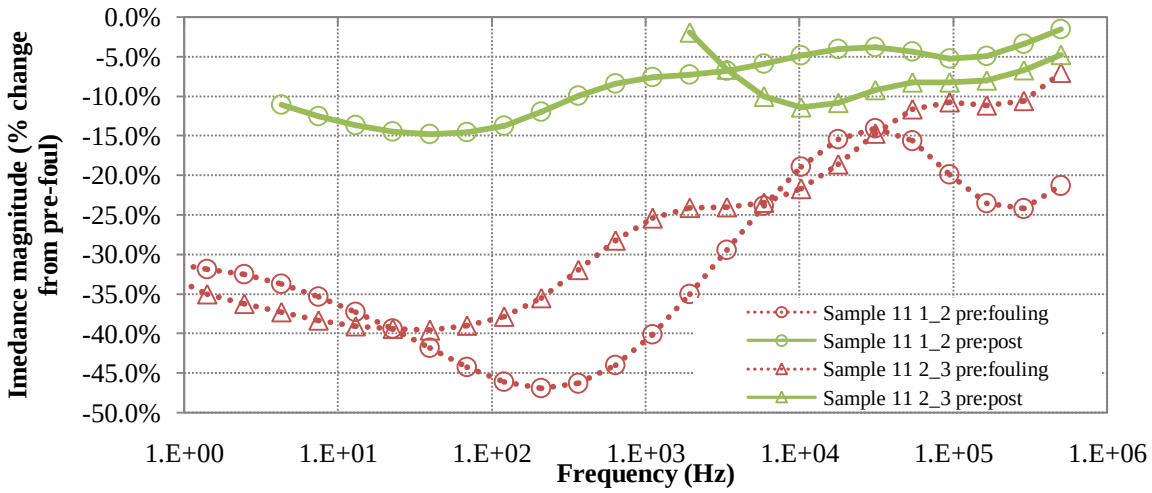

Figure 43: Change in impedance of sensors in dead-end experiment: in BSA fouling solution (pre:fouling) and deionized water (pre:post) after fouling as compared to pre-fouling (Sample 11). See Figure 44 and Figure 45 for impedance magnitudes and Appendix A IV for experimental details.

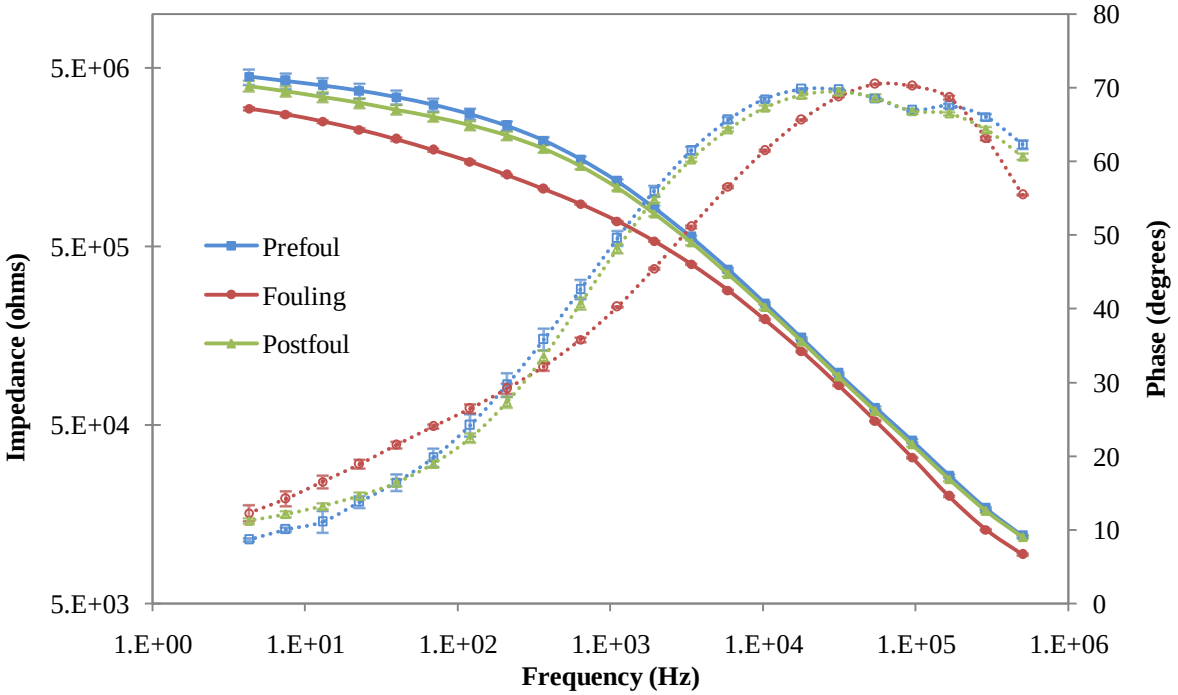

Figure 44: Averaged EIS sensor results fouled in a dead-end RO configuration (Sample 11 1_2): *i*) in deionized water pre-fouling (blue squares), *ii*) in BSA solution at the end of fouling (red circles), and *iii*) in deionized water post-fouling (green triangles). Solid lines indicate impedance, dashed lines indicate phase. Experimental conditions are given in Appendix A IV.

The second sensor (11 2_3, Figure 45) on the heavily fouled sample responded much like the first one (Figure 44) but with changes in impedance shifting to higher frequencies and decreasing in magnitude (Figure 43). The changes in impedance were only meaningful at frequencies greater than 3 kHz due to the average pre- and post-fouling values lying within one standard deviation of one another at lower frequencies. Again, the impedance decreased as much as 11.4% between the pre- and post-fouling cycles as shown in Figure 43. The phase increased at frequencies below 15 kHz while decreasing slightly at higher frequencies and had the previously observed kink at 95 kHz. This sensor did not exhibit as much sensitivity (decreasing less than 40%) to feedwater composition as compared to previously presented sensors but still appeared to change more in response to feedwater composition than to the fouling layer.

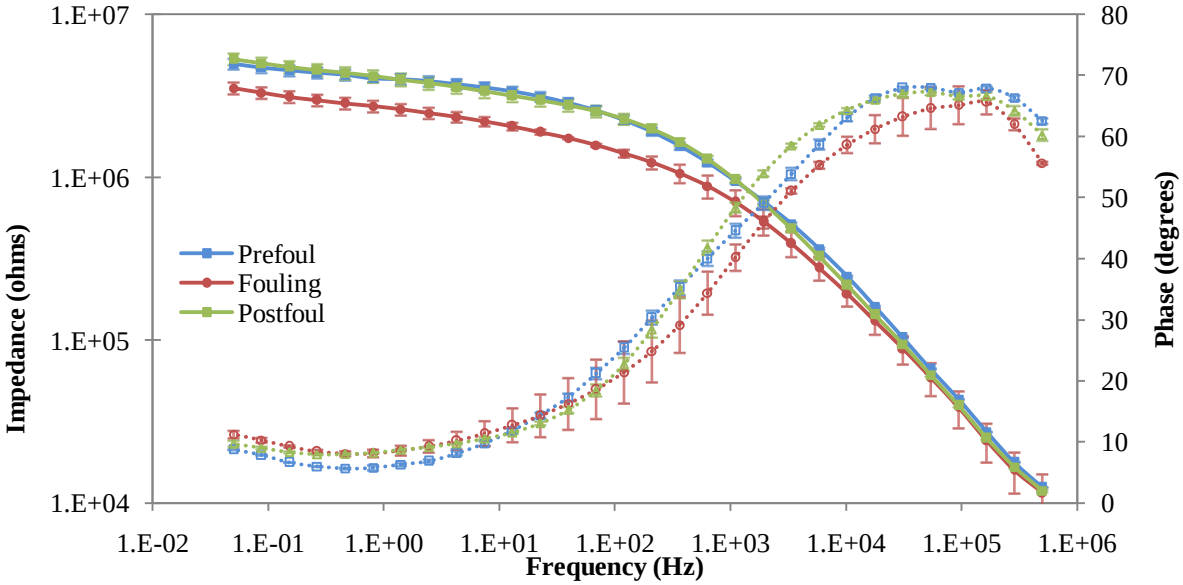

Figure 45: Averaged EIS sensor results fouled in a dead-end RO configuration (Sample 11 2_3): *i*) in deionized water pre-fouling (blue squares), *ii*) in BSA solution at the end of fouling (red circles), and *iii*) in deionized water post-fouling (green triangles). Solid lines indicate impedance, dashed lines indicate phase. Experimental conditions are given in Appendix A IV.

5.3.2. Cross-flow

Sensor response to EIS when the cross-flow system was operating led to much electrical noise and generally incoherent results for the sensors having hydrated impedances over 1 MΩ. Two sensors had regions of low electrical noise (phase with no discontinuities) from which it will be shown fouling led to sensor impedance decreasing 10-60%. EIS of the same sensor taken while

the cross-flow system was off and electrically disconnected showed a different impedance trend with the impedance decreasing 7.7% at frequencies below 360 Hz and increasing 10.5% at frequencies in the tens of kHz range (Figure 46).

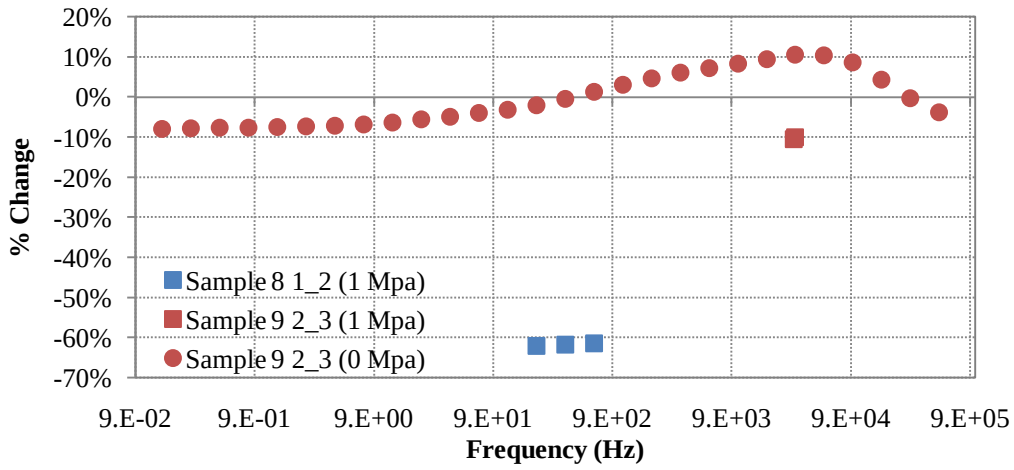

Figure 46: Percent change in impedance between averaged pre- and fouling EIS data. 1 MPa indicates the data was taken during cross-flow operating conditions. 0 MPa indicates the system was off and unplugged. Experimental details are in Appendix A III.

With the RO system operating, a lightly platinized sensor, shown in Figure 47, exhibited an impedance decrease of 60% upon fouling for the clean frequency regions (200 – 650 Hz) (Figure 46 and Figure 49). This decrease in impedance magnitude in the presence of the fouling solution was similar to responses of the Sample 11 sensors in the dead-end experiments (Figure 43 "pre:fouling" data). The permeate flux declined 40% over this same time period (from 0.53 to 0.32 mL/min) and protein fouling of the sensor was confirmed with SEM (Figure 48). Because the phase in this region was near 90°, the sensor was behaving as a capacitor and a decrease in impedance indicated the sensor capacitance is increasing. Adsorption of protein onto the platinized surface would certainly change the dielectric properties of the sensor.

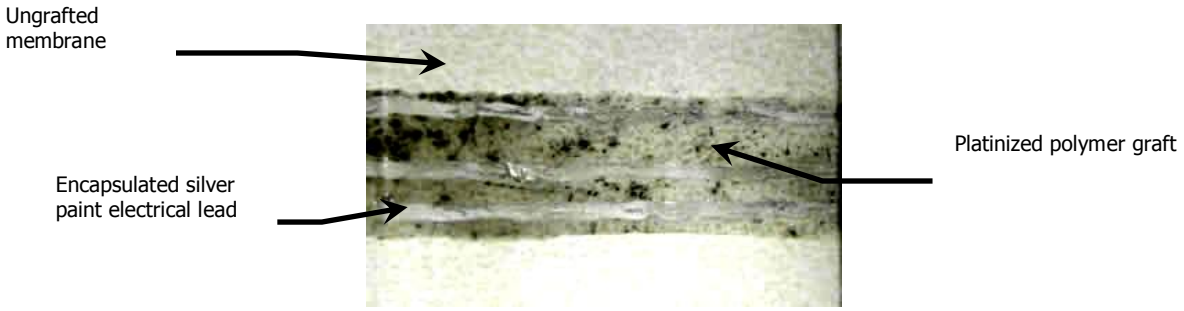

Figure 47: Lightly platinized platinized polymer graft sensor (Sample 8).

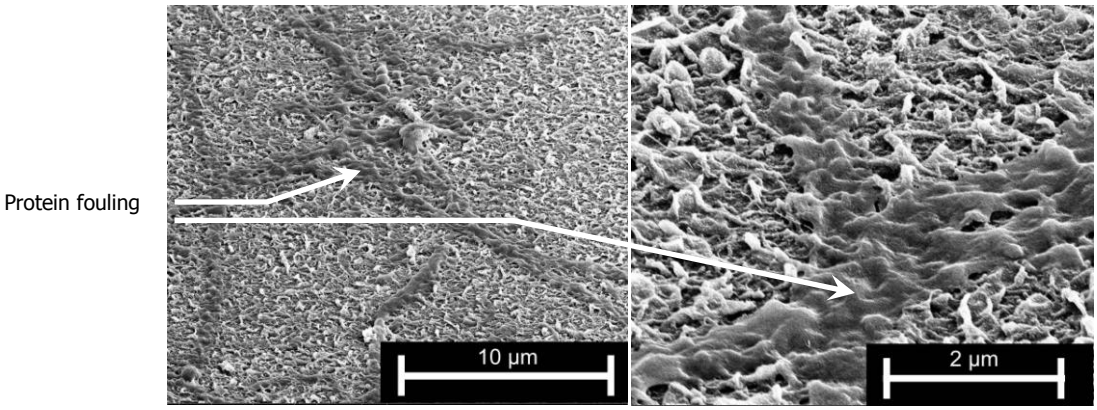

Figure 48: Micrograph of a fouled platinized graft sensor that had a 40% decline in permeate flux (Sample 8). Protein fouling appears as dark smoother areas on the membrane. The platinum nanoparticles are not visible at this scale. FIB-SEM: FEI Helios 600 5 kV.

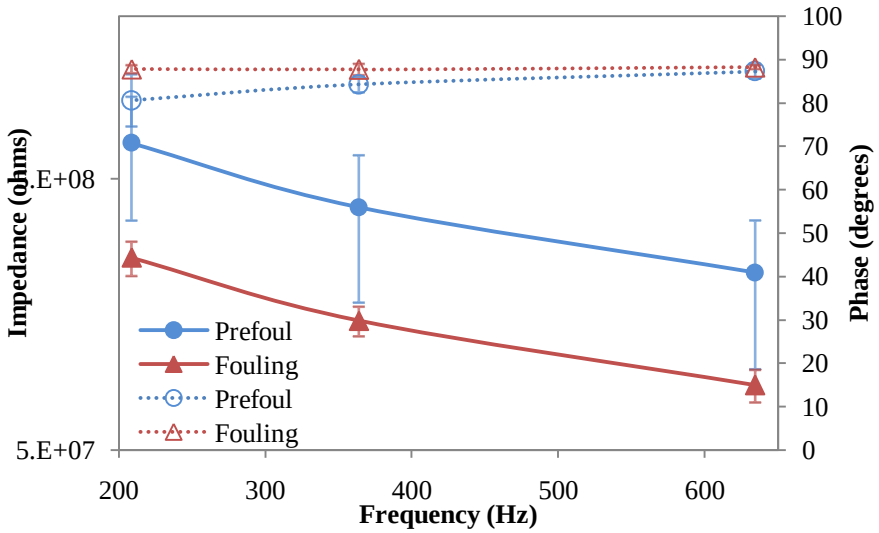

Figure 49: Lightly platinized (averaged) EIS sensor response at cross-flow *operating conditions* (Sample 8 1_2): *i*) in deionized water pre-fouling (blue squares), *ii*) in BSA solution at the end of fouling (red triangles). Solid lines indicate impedance, dashed lines indicate phase. Impedance fell 60% after fouling. This was the only frequency range that lacked significant noise. Cross-flow conditions: 1.03 MPa, 0.75 L/min, 29°C, pre-foul: 91 hours with deionized water, fouled: 80 hours with BSA (42.5 mg/L), no post-foul. Further experimental detail is in Appendix A I.

A highly platinized sensor monitored at operating conditions had, as expected, significantly lower impedance prior to fouling as compared to the less platinized sensor described above. Indeed, its impedance magnitude from 50 mHz – 31 kHz remained relatively constant at 29.5 kΩ (±2.6%) prior to fouling and fell 10% to 26.3 kΩ (2.2%) after fouling while maintaining a phase of 0 ±1°. The impedance lacked frequency dependence in that region which is indicative of resistance-dominated impedance – quite different from the capacitive response of the lightly platinized sensor. Protein adsorption decreasing sensor resistance is consistent with other research with protein adsorption to a discontinuous electrode surface[61, 64]. Figure 51 shows two SEM micrographs of the highly platinized surface of the sensor with areas of fouling. The high degree of platinization is visible as bright nodules on the surface. The lower noise level of this sensor as compared to the lightly platinized one (Figure 47) was likely due to the impedance being orders of magnitude lower; current output in response to applied potential was larger (Ohm's law) thus dominating the stray currents potentially generating noise previously. Permeate flux data for this sensor was inconclusive due to flowmeter limitations on resolving low flow rates.

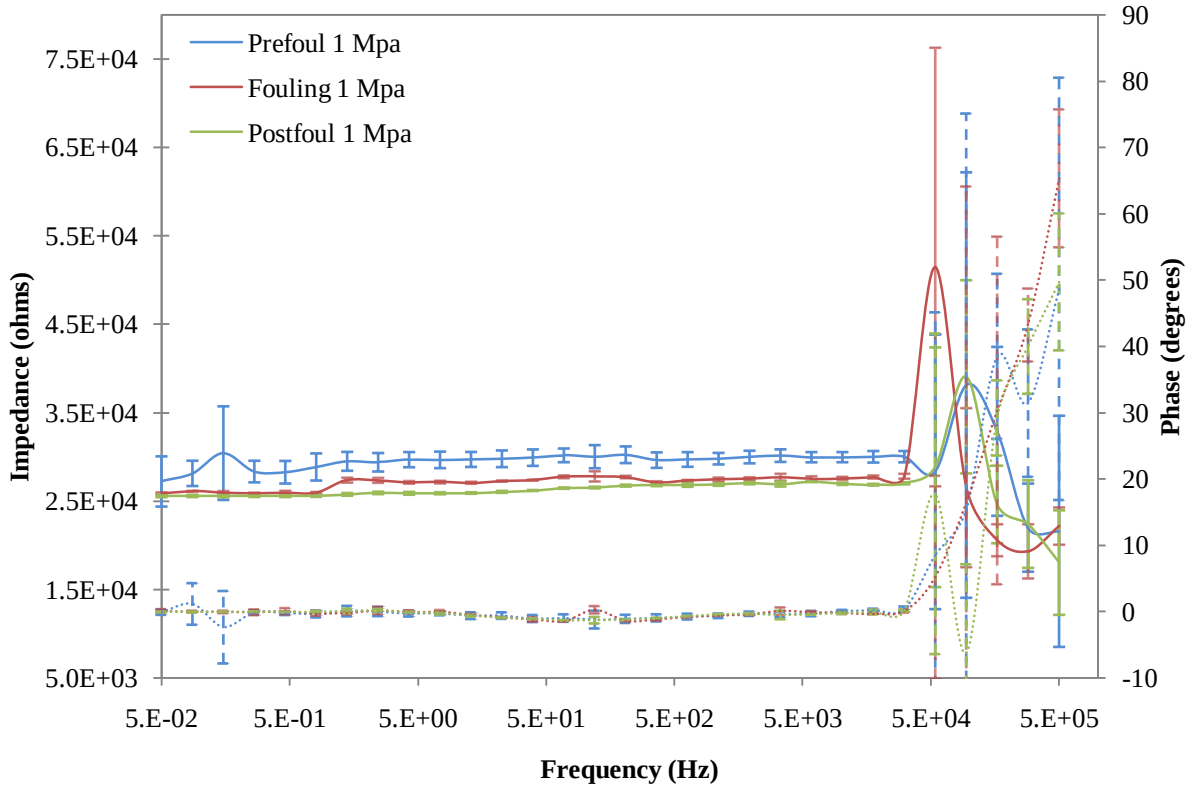

Figure 50: Highly platinized average EIS sensor response at *cross-flow operating conditions* (Sample 9 2_3): *i*) in deionized water pre-fouling (blue squares), *ii*) in BSA solution at the end of fouling (red circles), and *iii*) in deionized water post-fouling (green triangles). Solid lines indicate impedance, dashed lines indicate phase. Data averaged over a 111 hour period for pre-foul, the last 18 hours of fouling and for 28 hours post-foul. The error bars are ± one standard deviation of the averaged values. Cross-flow conditions: 1.03 MPa, 0.75 L/min, 29°C, pre-foul: 112 hrs with deionized water, fouling: 48 hrs with BSA (50. mg/L), post-foul: 54 hrs with deionized water.

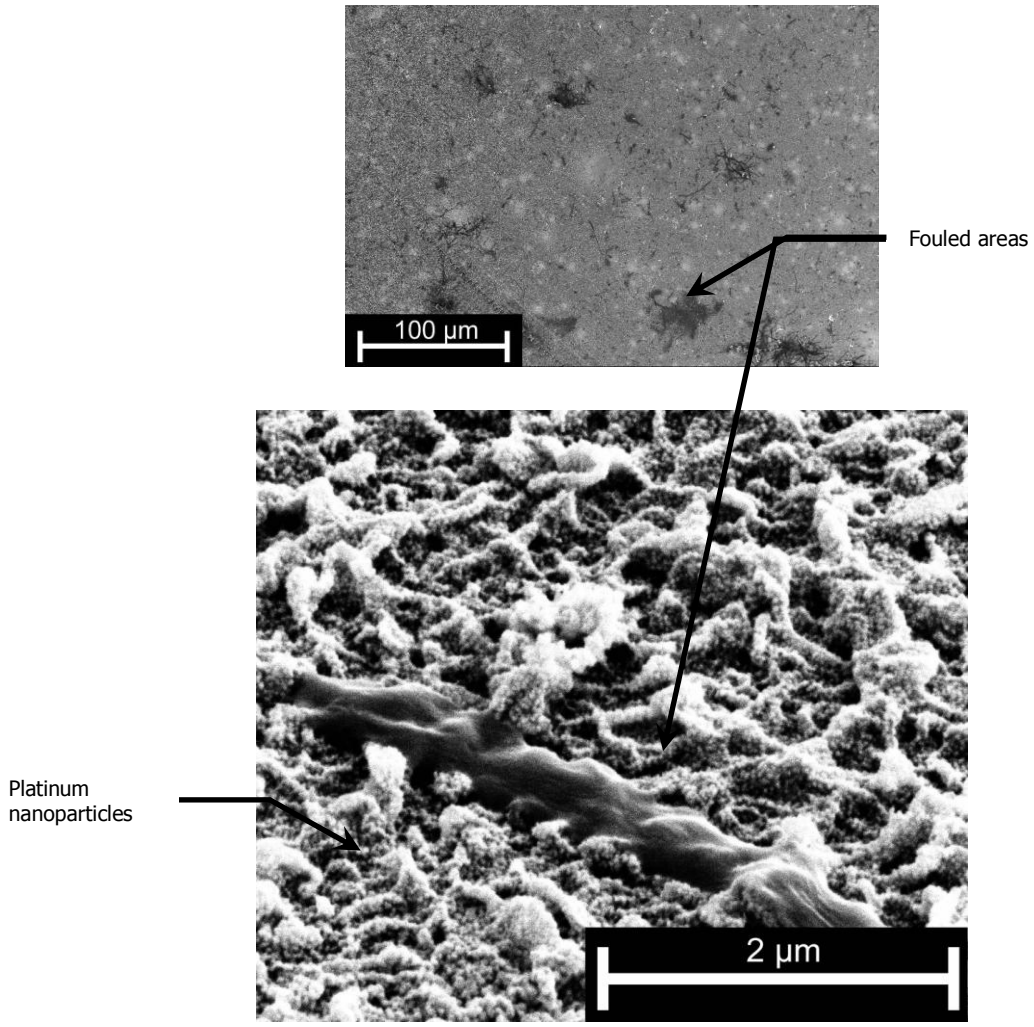

Figure 51: SEM micrograpahs showing areas of fouling on the highly platinized sensor (Sample 9 2_3). Platinum nanoparticles cover the convoluted surface of the grafted polyamide and appear as bright lumps. The protein appears as a dark areas on the surface of the two micrographs.

Electrically disconnecting the cross-flow system before measuring the impedance of the highly platinized sensor led to much "cleaner" data indicating the source of the noise observed in the EIS during system operation was from the cross-flow system. The average impedance at 50 mHz is very similar to that of the impedance measured when the system was operating (Figure 50). However, the shape of the impedance and phase spectra changed at higher frequencies to indicate capacitive elements were affecting sensor response (Figure 52). This may be due to less noise in the data as compared to Figure 49 or the cross-flow operating condition. Tangential flow of feedwater across the sensor potentially disrupts double layer formation and ion diffusion.

Membrane compaction due to hydraulic pressure may result in decreasing the mean distance between nanoparticles, increasing or otherwise affecting sensor capacitance. In comparing the averaged magnitude of the impedance spectra prior to fouling with spectra during the post-foul period, both using deionized water, the impedance at frequencies less than 500 Hz decreased as much as 7.7% upon fouling. At higher frequencies, the average impedance of the post-foul cycle increased up to 10.5% at 31 kHz. The impedance decrease at lower frequencies was consistent with the results at RO operating conditions. The increase in impedance and shifts in phase at higher frequencies in the capacitive region may be explained by research done by Eden et al. showing hydrated BSA having two dielectric dispersions separated by 1-10 kHz[78].

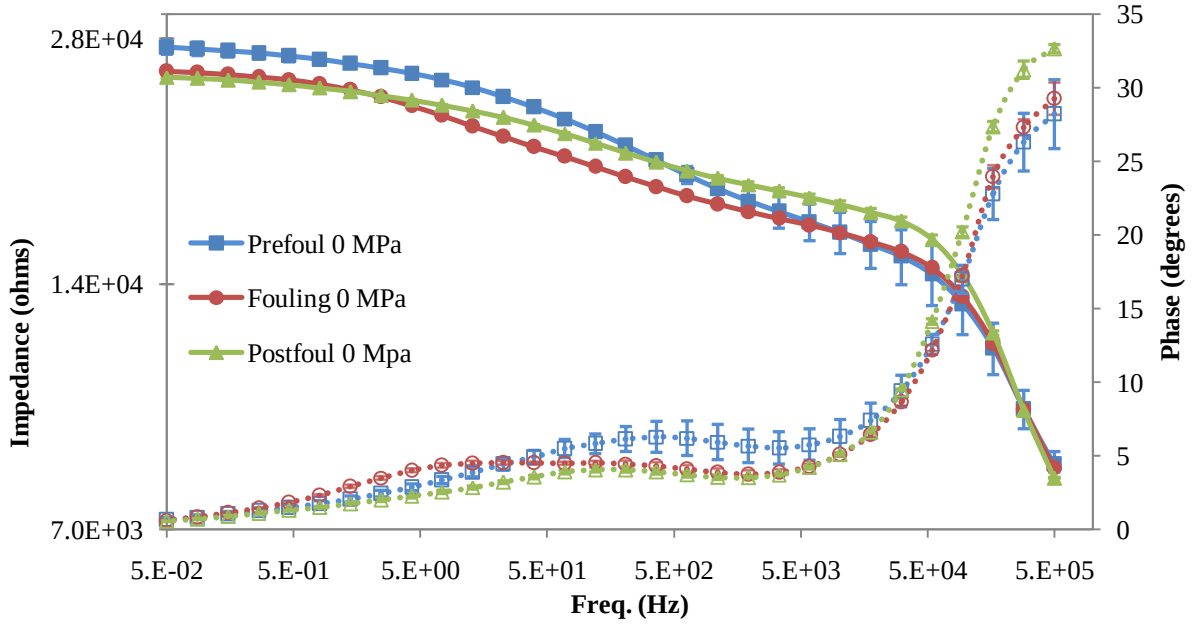

Figure 52: Highly platinized average EIS sensor response at cross-flow *electrically disconnected* (Sample 9 2_3): *i*) in deionized water pre-fouling (blue squares), *ii*) in BSA solution at the end of fouling (red circles), and *iii*) in deionized water post-fouling (green triangles). Solid lines indicate impedance, dashed lines indicate phase. Data averaged over a 111 hour period for pre-foul, the last 48 hours of fouling and for 54 hours post-foul. The error bars are ± one standard deviation of the averaged values. Cross-flow conditions: 1.03 MPa, 0.75 L/min, 29°C.

Figure 52 and Figure 53 show the average impedance during fouling increased minimally from the pre-foul average impedance (< 2.5%) from 5.5 – 500 kHz, but increased to more than 10% (from 35 – 55 kHz) during post-fouling, which has the same solution composition (deionized water) as pre-fouling. This suggests this sensor's response at higher frequencies may results from

complex interactions between feedwater composition and the fouling layer, with the effects of one countering the other during fouling. The sensor impedance during post-fouling may then represent the response of the sensor to only the fouling layer and not the fouling solution. Removing protein (as much as possible) from the RO system plumbing with deionized water between the fouling and post-fouling cycles to maintain consistent solution composition between pre- and post-fouling likely removed some of the protein foulant layer on the sensor; this may also affect the higher frequency response between fouling and post-fouling runs.

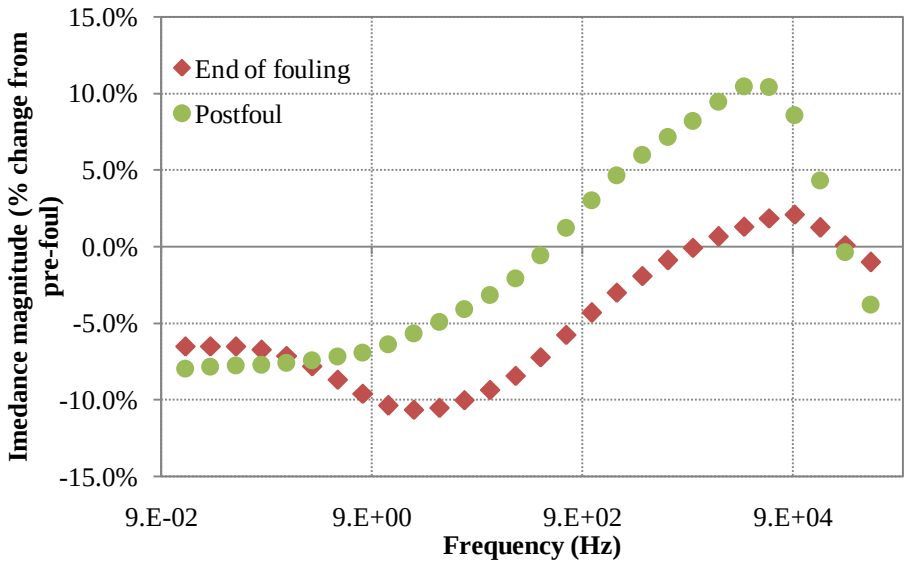

Figure 53: Comparison of change in impedance between pre-fouling and: i) the end of fouling with BSA solution and ii) postfouling with deionized water. The system was unplugged during EIS measurements (Sample 9 2_3).

It is unclear what caused the phase lag seen in all three (pre-, post-, and fouling) stages of the experiment between 500 mHz and 3 kHz (Figure 52). It may indicate Faradaic currents due to oxidation-reduction reactions of electroactive species at the platinized surface. Redox reactions behave as a Warburg element (phase of 45° with impedance inversely proportional to the square root of frequency)[76]. BSA is not known to be electroactive nor a redox species; however, it is possible the RO system wetted components contributed metal ions to the feedwater solution due to oxidation by the feedwater. Changing feedwater composition from 50 mg/L BSA to deionized water (fouling to post-fouling) certainly affects the charge transfer resistance of the solution as well as the interfacial interactions (capacitive double layer) at the sensor surface as

deionized water would lack a capacitive double layer entirely. The interplay between these phenomena may explain the trends in impedance shown in Figure 52.

The results of the cross-flow fouling experiments indicate the sensors are sensitive to protein fouling by showing a decrease in impedance at low frequencies and changes in capacitive characteristics at higher frequencies with the RO system electrically disconnected. EIS data taken while the RO system was operating generally showed a lot of noise, but frequency regions of consistent phase decreased in impedance magnitude upon fouling. SEM micrographs confirmed the presence of protein deposits on the sensor surface. The shape of the impedance response observed over the measured frequency range indicated a lightly platinized sensor behaved similar to a capacitor while a highly platinized sensor's response was closer to that of a resistor.

6. SUMMARY AND CONCLUSION

The primary purpose of this research was to develop and characterize electroding methods in the development of an *in situ* RO sensor capable of distinguishing phenomena occurring at the surface of RO membranes in operating conditions. Four electroding methodologies were explored: *i*) encapsulated carbon grease, *ii*) DAP, *iii*) gold exchange-reduction and *iv*) platinized polymer graft. The electrodes were characterized by their electrical properties, SEM and XPS. Carbon grease and DAP electroded sensors were evaluated with EIS for their sensitivity to electrolyte concentration. EIS was also used to assess the response of platinized polymer graft sensors to protein fouling in both dead-end and cross-flow RO systems. This chapter will summarize the electrode characterization, sensor results and conclusions of the research presented in the thesis. The chapter, and thesis, will conclude with a summary of contributions and suggestions for future research.

6.1. Carbon grease electroded sensors

- Prior to encapsulation, carbon grease electrodes had an average surface resistance from 27 – 32 kΩ mm/mm on the polyamide side and 16 – 30 kΩ mm/mm on the polysulfone.
- The sensors proved durable upon encapsulation.
- Through-thickness sensors in single bath and reversed double bath experiments took more than 20 hours to reach a stable EIS response in an unvarying salt concentration.
- Results of defect-free in-plane electrodes in single bath experiments and through-thickness electrodes in double bath experiments exhibited minimal time dependence.
- Shifting trends of transient normalized impedance averages were interpreted as indicating salt concentration sensitivity. Most commonly, in the through-thickness configuration, the average normalized impedance decreased with an increase in concentration strength.
- Electrolyte solution diffusion through the microporous polysulfone support layer appears responsible for the slow, time-dependent response of the sensors.
- The carbon grease electroding method was deemed unsuitable for *in situ* sensor implementation due to time-dependent response.

6.2. DAP electroded sensors

- RuO_2/Nafion layer of the DAP electrodes had surface resistances less than 2 kΩ mm/mm. After melt-pressing gold foil to the RuO_2/Nafion layer, the surface resistance fell below 0.3 Ω mm/mm.
- Gold foil adhesion to the RuO_2/Nafion layer proved to be inadequate during the concentration fouling experiments.
- Double bath experiments showed the sensors to have a time-dependent response to changes in electrolyte solution.
- Results showed a decrease in sensor impedance with an increase in salt concentration; however, the magnitude of the change in average normalized impedance did not correlated to magnitude of change in solution concentration.
- Overall, the DAP electroded sensors lacked meaningful trends in impedance with a changing electrolyte concentration, possibly due to unknown interactions between Nafion and the salt solution or gold-foil delamination.
- DAP electroding approach ultimately rejected due to poor electrode durability.

6.3. Gold exchange-reduction

- Gold exchange-reduction electrode surface resistances were out of range of the multimeter.
- Aliphatic polymeric alcohol coating appeared to inhibit gold exchange-reduction.
- Exposing RO membranes to a strong base containing potassium ions prior to the exchange-reduction process created uniformly distributed gold nanoparticles tens of nanometers in diameter.
- Our method did not produce viable sensors possibly due to the highly cross-linked nature of the polyamide thin film limiting the number of carboxyl groups available to participate in the exchange-reduction reaction.

6.4. Platinized polymer graft sensors

- Surface resistances of electrodes averaged about 23 GΩ mm/mm and had a capacitance of 8.5 pF as measured by EIS.
- Parametric study results as quantified by XPS:

    - Monomer grafted to the membrane increased 20% when doubling the length of exposure to the grafting solution.
    - Platinum deposited on the grafted area increased 101% with three repetitions of the exchange-reduction steps as compared to only doing one exchange reduction step.
    - The amount of monomer grafted to the surface correlated to the degree of platinization.
- The degree of platinization of the sensor appeared to affect the shape and magnitude of the response.
- Dead-end fouling experiments:
    - Slightly fouled and lightly platinized sensor impedance increased 7.4% at frequencies less than 2 kHz and decreased to 10.9% at higher frequencies (100 kHz – 500 kHz).
    - On a highly fouled membrane, two more platinized sensors impedances decreased to 14.8% at 40 Hz for one sensor and to 11.4% at 10 kHz for the other.
- Cross-flow fouling experiments:
    - A single sensor on a fouled membrane decreased in impedance (to 8.0 %) from 150 mHz – 400 Hz and increased up to 10.5% at higher frequencies (1 kHz – 200 kHz) when the system was electrically disconnected.
    - EIS run while the system was operating showed the impedances of two sensors in the clean data regions decreased 62% between 200 and 650 Hz for a lightly platinized sensor and decreased 10.% at 31 kHz for a highly platinized one.
- EIS results indicated the platinized polymer graft sensors were sensitive to fouling, but their responses varied significantly between sensors and experimental conditions.

6.5. Contributions

Contributions of the research presented in this thesis include the novel application of four electroding techniques in evaluating their capabilities as *in situ* RO sensors. We have shown through-thickness encapsulated carbon grease and DAP electrodes, in the geometries and

configurations tested, to be unsuitable for constructing RO sensors due to slow response time and lack of durability, respectively. A novel application of gold exchange-reduction in electroding RO membranes also failed to produce a useful sensor but succeeded in demonstrating the feasibility of utilizing RO membrane functional groups in depositing an electrode. Building on that success, we have developed a process whereby grafting a monomer with chemistry tailored to a platinum exchange-reduction reaction to an RO membrane allows for the sufficient deposition of a discontinuous electrode surface. This platinized polymer graft sensor, in preliminary results, exhibited protein-fouling sensitivity.

6.6. Future work

Building on the results of this research, future work could focus on several areas:

Exploring other means of DAP electrode fabrication may produce sufficiently durable sensors. An alternative to melt-pressing gold foil is to use platinum impregnation-reduction of the RuO_2/Nafion layer followed by gold electroplating. In trials not presented in this thesis, this method led to electrodes still lacking durability as both the deposited platinum and gold tended to rub off, but varying several parameters (RuO_2/Nafion layer thickness, melt-pressing of the dispersion, varying time and concentrations of impregnation-reduction steps, etc.) may lead to a durable sensor. It also remains to be seen whether DAP electroded membranes are capable of detecting fouling.

The platinized polymer graft method offers numerous areas of further exploration. As the fouling experimental results indicate, a larger sensor sample size is required to definitively determine the "typical" response of sensors to fouling in both dead-end and cross-flow configurations. At this time, it is unclear what is responsible for the widely varying trends in response to protein fouling and the effect the degree of platinization has on sensor response. A more comprehensive parametric study should be undertaken to determine an optimal electroding recipe, specifically shortening grafting times and optimizing the exchange-reduction concentrations to accomplish the desired degree of platinization in one step. Along those lines, a more repeatable method of attaching the electrical leads will be advantageous and may lead to results that are more consistent. Finally, investigating platinized polymer graft sensor responses to other RO membrane phenomena is required to determine the sensors viability as an *in situ* RO sensor.

BIBLIOGRAPHY

[1] "Water Supply Data at Global Level" WHO-UNICEF Joint Monitoring Programme, (2004).

[2] S. A. Avlonitis, K. Kouroumbas, and N. Vlachakis, "Energy consumption and membrane replacement cost for seawater RO desalination plants," Desalination, 157(1-3), 151-158 (2003).

[3] C. E. Reid, and E. J. Breton, "Water and ion flow across cellulosic membranes," Journal of Applied Polymer Science, 1(2), 133-143 (1959).

[4] J. Glater, "The early history of reverse osmosis membrane development," Desalination, 117(1-3), 297-309 (1998).

[5] J. W. Richter, and H. H. Hoehn, "Permselective, Aromatic, Nitrogen-containing Polymeric Membranes", United States(1971).

[6] T. A. Orofino, "Development of Hollow Filament Technology for Reverse Osmosis Desalination Systems", United States(1970).

[7] M. E. Cohen, and B. M. Riggleman, "Development of Improved Cellulose Acetate Membranes for Reverse Osmosis", United States(1969).

[8] R. Endoh, T. Tanaka, M. Kurihara *et al.*, "New Polymeric Materials for Reverse Osmosis Membranes," Desalination, 21(1), 35-44 (1977).

[9] J. E. Cadotte, "Reverse Osmosis Membrane", United States(1975).

[10] J. E. Cadotte, "Evolution of Composite Reverse Osmosis Membranes," ACS Symposium Series. 273-294.

[11] R. E. Larson, J. E. Cadotte, and R. J. Petersen, "Development of the FT-30 Thin-film Composite Membrane for Seawater Desalting Applications," NWSIA journal, 8(1), 15-25 (1981).

[12] V. Freger, J. Gilron, and S. Belfer, "TFC polyamide membranes modified by grafting of hydrophilic polymers: an FT-IR/AFM/TEM study," Journal of Membrane Science, 209(1), 283-292 (2002).

[13] J. Gilron, S. Belfer, P. Vaisanen *et al.*, "Effects of surface modification on antifouling and performance properties of reverse osmosis membranes," Desalination, 140(2), 167-179 (2001).

[14] G. Kang, M. Liu, B. Lin *et al.*, "A novel method of surface modification on thin-film composite reverse osmosis membrane by grafting poly(ethylene glycol)," Polymer, 48(5), 1165-1170 (2007).

[15] B. Freeman, "Novel Fouling-Reducing Coatings for Ultrafiltration, Nanofiltration, and Reverse Osmosis Membranes" USDOE, (2008).

[16] H. B. Park, Benny D. Freeman, Z.-B. Zhang *et al.*, "Highly Chlorine-Tolerant Polymers for Desalination13," Angewandte Chemie International Edition, 47(32), 6019-6024 (2008).

[17] M. Paul, H. B. Park, B. D. Freeman *et al.*, "Synthesis and crosslinking of partially disulfonated poly(arylene ether sulfone) random copolymers as candidates for chlorine resistant reverse osmosis membranes," Polymer, 49(9), 2243-2252 (2008).

[18] [Reverse Osmosis Membranes - Technical Manual] DOW - FILMTEC, (2009).

[19] V. Freger, "Nanoscale Heterogeneity of Polyamide Membranes Formed by Interfacial Polymerization," Sep. Sci. Technol, 34(15), 3009-3009 (1999).

[20] V. Freger, "Nanoscale Heterogeneity of Polyamide Membranes Formed by Interfacial Polymerization," Langmuir, 19(11), 4791-4797 (2003).

[21] C. Y. Tang, Y.-N. Kwon, and J. O. Leckie, "Probing the nano- and micro-scales of reverse osmosis membranes--A comprehensive characterization of physiochemical properties of uncoated and coated membranes by XPS, TEM, ATR-FTIR, and streaming potential measurements," Journal of Membrane Science, 287(1), 146-156 (2007).
[22] S. Avlonitis, W. T. Hanbury, and T. Hodgkiess, "Chlorine Degradation of Aromatic Polyamides," Desalination, 85(3), 321-334 (1992).
[23] N. P. Soice, A. C. Maladono, D. Y. Takigawa *et al.*, "Oxidative Degradation of Polyamide Reverse Osmosis Membranes: Studies of Molecular Model Compounds and Selected Membranes," Journal of Applied Polymer Science, 90, 1173-1184 (2003).
[24] Y.-N. Kwon, and O. L. James, "Hypochlorite degradation of crosslinked polyamide membranes II. Changes in hydrogen bonding behavior and performance," Journal of Membrane Science, 282, 456-464 (2006).
[25] M. Gloede, and T. Melin, "Physical aspects of membrane scaling," Desalination, 224(1-3), 71-75 (2008).
[26] C. Tzotzi, T. Pahiadaki, S. G. Yiantsios *et al.*, "A study of CaCO3 scale formation and inhibition in RO and NF membrane processes," Journal of Membrane Science, 296(1-2), 171-184 (2007).
[27] J. S. Baker, and L. Y. Dudley, "Biofouling in membrane systems -- A review," Desalination, 118(1-3), 81-89 (1998).
[28] H. C. Flemming, G. Schaule, T. Griebe *et al.*, "Biofouling - the Achilles heel of membrane processes," Desalination, 113(2-3), 215-225 (1997).
[29] X. Zhu, and M. Elimelech, "Colloidal Fouling of Reverse Osmosis Membranes: Measurements and Fouling Mechanisms," Environmental Science & Technology, 31(12), 3654-3662 (1997).
[30] M. Kumar, S. S. Adham, and W. R. Pearce, "Investigation of Seawater Reverse Osmosis Fouling and Its Relationship To Pretreatment Type," Environmental Science & Technology, 40(6), 2037-2044 (2006).
[31] H. S. Vrouwenvelder, J. A. M. van Paassen, H. C. Folmer *et al.*, "Biofouling of membranes for drinking water production," Desalination, 118(1-3), 157-166 (1998).
[32] M. Herzberg, and M. Elimelech, "Biofouling of reverse osmosis membranes: Role of biofilm-enhanced osmotic pressure," Journal of Membrane Science, 295(1-2), 11-20 (2007).
[33] Q. Li, Z. Xu, and I. Pinnau, "Fouling of reverse osmosis membranes by biopolymers in wastewater secondary effluent: Role of membrane surface properties and initial permeate flux," Journal of Membrane Science, 290, 173-181 (2007).
[34] S. Kim, and E. M. V. Hoek, "Interactions controlling biopolymer fouling of reverse osmosis membranes," Desalination, 202(1-3), 333-342 (2007).
[35] W. S. Ang, and M. Elimelech, "Protein (BSA) fouling of reverse osmosis membranes: Implications for wastewater reclamation," Journal of Membrane Science, 296, 83-92 (2007).
[36] J. S. Louie, I. Pinnau, I. Ciobanu *et al.*, "Effects of polyether–polyamide block copolymer coating on performance and fouling of reverse osmosis membranes," Journal of Membrane Science, 280(1-2), 762-770 (2006).
[37] S. Belfer, Y. Purinson, R. Fainshtein *et al.*, "Surface modification of commercial composite polyamide reverse osmosis membranes," Journal of Membrane Science, 139(2), 175-181 (1998).

[38] S. Belfer, Y. Purinson, and O. Kedem, "Surface modification of commercial polyamide reverse osmosis membranes by radical grafting: An ATR-FTIR study," Acta Polymerica, 49(10-11), 574-582 (1998).
[39] J. C. Chen, Q. Li, and M. Elimelech, "In situ monitoring techniques for concentration polarization and fouling phenomena in membrane filtration," Advances in Colloid and Interface Science, 107(2-3), 83-108 (2004).
[40] C. R. Ethier, and D. C. Lin, "Refractometric measurement of polarized layer structure: studies of hyaluronic acid ultrafiltration," Journal of Membrane Science, 68(3), 249-261 (1992).
[41] L. M. Gowman, and C. R. Ethier, "Concentration and concentration gradient measurements in an ultrafiltration concentration polarization layer Part I: A laser-based refractometric experimental technique," Journal of Membrane Science, 131(1-2), 95-105 (1997).
[42] V. L. Vilker, C. K. Colton, K. A. Smith *et al.*, "Concentration polarization in protein UF: Part II. Theoretical and experimental study of albumin ultrafiltered in unstirred cell," AIChE J, 27(4), 637–645-637–645 (1981).
[43] J. Altmann, and S. Ripperger, "Particle deposition and layer formation at the crossflow microfiltration," Journal of Membrane Science, 124(1), 119-128 (1997).
[44] M. Hamachi, and M. Mietton-Peuchot, "Experimental investigations of cake characteristics in crossflow microfiltration," Chemical Engineering Science, 54(18), 4023-4030 (1999).
[45] M. Hamachi, and M. Mietton-Peuchot, "Cake Thickness Measurement with an Optical Laser Sensor," Chemical Engineering Research and Design/Official Journal of the European Federation of Chemical Engineering: Part A, 79(A2), 151-155 (2001).
[46] S.-T. Kang, A. Subramani, E. M. V. Hoek *et al.*, "Direct observation of biofouling in cross-flow microfiltration: mechanisms of deposition and release," Journal of Membrane Science, 244(1-2), 151-165 (2004).
[47] H. Li, A. G. Fane, H. G. L. Coster *et al.*, "Direct observation of particle deposition on the membrane surface during crossflow microfiltration," Journal of Membrane Science, 149(1), 83-97 (1998).
[48] H. Li, A. G. Fane, H. G. L. Coster *et al.*, "An assessment of depolarisation models of crossflow microfiltration by direct observation through the membrane," Journal of Membrane Science, 172(1-2), 135-147 (2000).
[49] W. D. Mores, and R. H. Davis, "Direct visual observation of yeast deposition and removal during microfiltration," Journal of Membrane Science, 189(2), 217-230 (2001).
[50] D. Airey, S. Yao, J. Wu *et al.*, "An investigation of concentration polarization phenomena in membrane filtration of colloidal silica suspensions by NMR micro-imaging," Journal of Membrane Science, 145(2), 145-158 (1998).
[51] P. T. Callaghan, C. D. Eccles, and Y. Xia, "NMR microscopy of dynamic displacements: k-space and q-space imaging," Journal of Physics E: Scientific Instruments, 21(8), 820-822 (1988).
[52] J. M. Pope, S. Yao, and A. G. Fane, "Quantitative measurements of the concentration polarisation layer thickness in membrane filtration of oil-water emulsions using NMR micro-imaging," Journal of Membrane Science, 118(2), 247-257 (1996).

[53] R. M. Mc Donogh, H. Bauser, N. Stroh *et al.*, "Experimental in situ measurement of concentration polarisation during ultra- and micro-filtration of bovine serum albumin and Dextran Blue solutions," Journal of Membrane Science, 104(1-2), 51-63 (1995).
[54] J. Li, and R. D. Sanderson, "In situ measurement of particle deposition and its removal in microfiltration by ultrasonic time-domain reflectometry," Desalination, 146(1-3), 169-175 (2002).
[55] A. P. Mairal, A. R. Greenberg, W. B. Krantz *et al.*, "Real-time measurement of inorganic fouling of RO desalination membranes using ultrasonic time-domain reflectometry," Journal of Membrane Science, 159(1-2), 185-196 (1999).
[56] V. E. Reinsch, A. R. Greenberg, S. S. Kelley *et al.*, "A new technique for the simultaneous, real-time measurement of membrane compaction and performance during exposure to high-pressure gas," Journal of Membrane Science, 171(2), 217-228 (2000).
[57] E. Kujundzic, K. Cobry, A. R. Greenberg *et al.*, "Use of Ultrasonic Sensors for Characterization of Membrane Fouling and Cleaning."
[58] T. C. Chilcott, M. Chan, L. Gaedt *et al.*, "Electrical impedance spectroscopy characterisation of conducting membranes: I. Theory," Journal of Membrane Science, 195(2), 153-167 (2002).
[59] L. Gaedt, T. C. Chilcott, M. Chan *et al.*, "Electrical impedance spectroscopy characterisation of conducting membranes: II. Experimental," Journal of Membrane Science, 195(2), 169-180 (2002).
[60] E. Barsoukov, and J. R. Macdonald, "Impedance Spectroscopy Theory, Experiment, and Applications" John Wiley and Sons, Inc, Hoboken, New Jersey(2005).
[61] E. Katz, and I. Willner, "Probing Biomolecular Interactions at Conductive and Semiconductive Surfaces by Impedance Spectroscopy: Routes to Impedimetric Immunosensors, DNA-Sensors, and Enzyme Biosensors," Electroanalysis, 15(11), 913-947 (2003).
[62] S. Bason, Y. Oren, and V. Freger, "Characterization of ion transport in thin films using electrochemical impedance spectroscopy: II: Examination of the polyamide layer of RO membranes," Journal of Membrane Science, 302(1-2), 10-19 (2007).
[63] J. S. Park, T. C. Chilcott, H. G. L. Coster *et al.*, "Characterization of BSA-fouling of ion-exchange membrane systems using a subtraction technique for lumped data," Journal of Membrane Science, 246(2), 137-144 (2005).
[64] M. S. DeSilva, Y. Zhang, P. J. Hesketh *et al.*, "Impedance based sensing of the specific binding reaction between Staphylococcus enterotoxin B and its antibody on an ultra-thin platinum film," Biosensors and Bioelectronics, 10(8), 675-682 (1995).
[65] J. W. Fox, and N. C. Goulbourne, "A study on the effect of flexible electrodes and passive layers on the performance of dielectric elastomer membranes," American Society of Mechanical Engineers, Aerospace Division (Publication) AD. 9-9.
[66] R. E. Pelrine, R. D. Kornbluh, and J. P. Joseph, "Electrostriction of polymer dielectrics with compliant electrodes as a means of actuation," Sensors and Actuators A: Physical, 64(1), 77-85 (1998).
[67] F. Carpi, P. Chiarelli, A. Mazzoldi *et al.*, "Electromechanical characterisation of dielectric elastomer planar actuators: comparative evaluation of different electrode materials and different counterloads," Sensors and Actuators A: Physical, 107(1), 85-95 (2003).

[68] B. Akle, M. Bennett, D. Leo *et al.*, “Direct assembly process: a novel fabrication technique for large strain ionic polymer transducers,” Journal of Materials Science, 42(16), 7031-7041 (2007).
[69] M. Shahinpoor, and K. J. Kim, “Ionic polymer-metal composites: I. Fundamentals,” Smart Materials and Structures, 10(4), 819-833 (2001).
[70] K. Oguro, N. Fujiwara, K. Asaka *et al.*, "Polymer electrolyte actuator with gold electrodes." 3669, 64-71.
[71] M. Le Guilly, "Flemion actuator array" Ph. D. Dissertation, University of Washington, Seattle, WA, (2004).
[72] J. W. Fox, "Electromechanical Characterization of the Static and Dynamic Response of Dielectric Elastomer Membranes" Virginia Polytechnic Institute and State University, Blacksburg VA(2007).
[73] C. M. Harris, “136. Nitrogenous chelate complexes of transition metals. Part I. The constitution and properties of the 1 : 10-phenanthroline complexes of tervalent gold,” Journal of the Chemical Society (Resumed), 682-687 (1959).
[74] M. Le Guilly, C. Xu, V. Cheng *et al.*, "Flemion based actuator for mechanically controlled microwave switch." 5051, 362-362.
[75] O. Coronell, B. J. Mariñas, X. Zhang *et al.*, “Quantification of Functional Groups and Modeling of Their Ionization Behavior in the Active Layer of FT30 Reverse Osmosis Membrane,” Environmental Science & Technology, 42(14), 5260-5266 (2008).
[76] V. Freger, and S. Bason, “Characterization of ion transport in thin films using electrochemical impedance spectroscopy: I. Principles and theory,” Journal of Membrane Science, 302(1-2), 1-9 (2007).
[77] F. Paparone, "Understanding Low-Conductivity/High-ResistivityMeasurements", (2009).
[78] J. Eden, P. R. C. Gascoyne, and R. Pethig, “Dielectric and electrical properties of hydrated bovine serum albumin,” Journal of the Chemical Society, Faraday Transactions 1, 76, 426-434 (1980).

Appendix A Platinized polymer graft electroded sensors

I ANOVA of parametric study

i) Mathematica code for running analysis of variance

```
Needs["ANOVA`"]

{FileNameSetter[Dynamic[file]],Dynamic[file]}

Partition[Flatten[Import[file]],5]

data={{}}; (*copy and paste output from previous line*)

model={graft,impreg,reduct,reps,All};

vars={graft,impreg,reduct,reps};

ANOVA[data,model,vars]
```

ii) ANOVA of XPS data to correlate amount of sulfur to parameters varied

Out[17]=

ANOVA →	DF	SumOfSq	MeanSq	FRatio	PValue
graft	1	0.0000638252	0.0000638252	4.04376	0.0694919
impreg	1	0.0000480344	0.0000480344	3.04331	0.108908
reps	1	1.20693×10^{-6}	1.20693×10^{-6}	0.0764671	0.78727
Error	11	0.00017362	0.0000157836		
Total	14	0.000286686			

CellMeans →		
	All	0.0144945
	graft[2.]	0.0122894
	graft[4.]	0.0164241
	impreg[2.]	0.0132213
	impreg[4.]	0.0195875
	reduct[0.5]	0.0132213
	reduct[4.]	0.0195875
	reps[1.]	0.012649
	reps[3.]	0.0156987
	reps[4.]	0.014526
	graft[2.] impreg[2.]	0.0122894
	graft[4.] impreg[2.]	0.014526
	graft[4.] impreg[4.]	0.0195875
	graft[2.] reduct[0.5]	0.0122894
	graft[4.] reduct[0.5]	0.014526
	graft[4.] reduct[4.]	0.0195875
	graft[2.] reps[1.]	0.012649
	graft[2.] reps[3.]	0.0118099
	graft[4.] reps[3.]	0.0195875
	graft[4.] reps[4.]	0.014526
	impreg[2.] reduct[0.5]	0.0132213
	impreg[4.] reduct[4.]	0.0195875
	impreg[2.] reps[1.]	0.012649
	impreg[2.] reps[3.]	0.0118099
	impreg[2.] reps[4.]	0.014526
	impreg[4.] reps[3.]	0.0195875
	reduct[0.5] reps[1.]	0.012649
	reduct[0.5] reps[3.]	0.0118099
	reduct[0.5] reps[4.]	0.014526
	reduct[4.] reps[3.]	0.0195875
	graft[2.] impreg[2.] reduct[0.5]	0.0122894
	graft[4.] impreg[2.] reduct[0.5]	0.014526
	graft[4.] impreg[4.] reduct[4.]	0.0195875
	graft[2.] impreg[2.] reps[1.]	0.012649
	graft[2.] impreg[2.] reps[3.]	0.0118099
	graft[4.] impreg[2.] reps[4.]	0.014526
	graft[4.] impreg[4.] reps[3.]	0.0195875
	graft[2.] reduct[0.5] reps[1.]	0.012649
	graft[2.] reduct[0.5] reps[3.]	0.0118099
	graft[4.] reduct[0.5] reps[4.]	0.014526
	graft[4.] reduct[4.] reps[3.]	0.0195875
	impreg[2.] reduct[0.5] reps[1.]	0.012649
	impreg[2.] reduct[0.5] reps[3.]	0.0118099
	impreg[2.] reduct[0.5] reps[4.]	0.014526
	impreg[4.] reduct[4.] reps[3.]	0.0195875
	graft[2.] impreg[2.] reduct[0.5] reps[1.]	0.012649
	graft[2.] impreg[2.] reduct[0.5] reps[3.]	0.0118099
	graft[4.] impreg[2.] reduct[0.5] reps[4.]	0.014526
	graft[4.] impreg[4.] reduct[4.] reps[3.]	0.0195875

The column of data on the right is the mean % atomic concentration of sulfur at each condition

iii) ANOVA of XPS data to correlate amount of platinum to parameters varied

Out[22]=

ANOVA →		DF	SumOfSq	MeanSq	FRatio	PValue
	graft	1	0.00190503	0.00190503	7.54482	0.0189996
	impreg	1	0.000988235	0.000988235	3.91387	0.0734761
	reps	1	0.00498766	0.00498766	19.7534	0.00098766
	Error	11	0.00277745	0.000252495		
	Total	14	0.0106584			

CellMeans →		
	All	0.0885684
	graft[2.]	0.0765208
	graft[4.]	0.0991101
	impreg[2.]	0.0823458
	impreg[4.]	0.113459
	reduct[0.5]	0.0823458
	reduct[4.]	0.113459
	reps[1.]	0.0534039
	reps[3.]	0.110401
	reps[4.]	0.0905009
	graft[2.] impreg[2.]	0.0765208
	graft[4.] impreg[2.]	0.0905009
	graft[4.] impreg[4.]	0.113459
	graft[2.] reduct[0.5]	0.0765208
	graft[4.] reduct[0.5]	0.0905009
	graft[4.] reduct[4.]	0.113459
	graft[2.] reps[1.]	0.0534039
	graft[2.] reps[3.]	0.107343
	graft[4.] reps[3.]	0.113459
	graft[4.] reps[4.]	0.0905009
	impreg[2.] reduct[0.5]	0.0823458
	impreg[4.] reduct[4.]	0.113459
	impreg[2.] reps[1.]	0.0534039
	impreg[2.] reps[3.]	0.107343
	impreg[2.] reps[4.]	0.0905009
	impreg[4.] reps[3.]	0.113459
	reduct[0.5] reps[1.]	0.0534039
	reduct[0.5] reps[3.]	0.107343
	reduct[0.5] reps[4.]	0.0905009
	reduct[4.] reps[3.]	0.113459
	graft[2.] impreg[2.] reduct[0.5]	0.0765208
	graft[4.] impreg[2.] reduct[0.5]	0.0905009
	graft[4.] impreg[4.] reduct[4.]	0.113459
	graft[2.] impreg[2.] reps[1.]	0.0534039
	graft[2.] impreg[2.] reps[3.]	0.107343
	graft[4.] impreg[2.] reps[4.]	0.0905009
	graft[4.] impreg[4.] reps[3.]	0.113459
	graft[2.] reduct[0.5] reps[1.]	0.0534039
	graft[2.] reduct[0.5] reps[3.]	0.107343
	graft[4.] reduct[0.5] reps[4.]	0.0905009
	graft[4.] reduct[4.] reps[3.]	0.113459
	impreg[2.] reduct[0.5] reps[1.]	0.0534039
	impreg[2.] reduct[0.5] reps[3.]	0.107343
	impreg[2.] reduct[0.5] reps[4.]	0.0905009
	impreg[4.] reduct[4.] reps[3.]	0.113459
	graft[2.] impreg[2.] reduct[0.5] reps[1.]	0.0534039
	graft[2.] impreg[2.] reduct[0.5] reps[3.]	0.107343
	graft[4.] impreg[2.] reduct[0.5] reps[4.]	0.0905009
	graft[4.] impreg[4.] reduct[4.] reps[3.]	0.113459

The column of data on the right is the mean % atomic concentration of platinum at each condition

II Recipes and fabrication

i) Sample 7

1. Boiled membrane in Di water – 0:45
2. Mix 3 mL of grafting solution, stir and pour in "well" – 3:00
    a. Unstirred and uncovered
3. Rinsed well with DI water
    a. Dried out over the weekend
4. Resoaked in DI water – 5:18
5. Soaked in 3.0 mL tetraammineplatinum(II) chloride solution (5.4 mg) – 6:53
6. Remove solution and rinsed well with DI water without spraying membrane directly
7. Add 3 mL of 0.1 wt% $NaBH_4$ – 12:00
    a. Slight graying of certain areas of the membrane
8. Rinsed well and stored in DI water
9. Dried prior to encapsulation

Space between encapsulated electrical leads: Sensor 1_2 ~2.5 mm, Sensor 2_3 ~1.9 mm

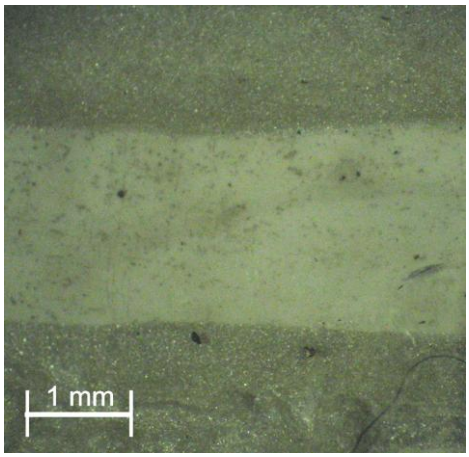

Figure 54: Sample 7 platinized polymer graft. Lightly platinized area lies between the two darker encapsulated silver paint electrical leads.

ii) Sample 8

1. Boiled dry membrane in Di water – 0:45
2. Mix 3 mL of grafting solution, stir and pour in "well" – 2:00
    a. Unstirred and covered
3. Rinsed well with DI water 0:05
4. Soaked in 3.0 mL tetraammineplatinum(II) chloride solution (5.0 mg) – 7:09
5. Remove solution and rinsed well with DI water without spraying membrane directly – 0:06
6. Add 3 mL of 0.1 wt% NaBH4 – 4:54
    a. Slight graying of certain areas of the membrane
7. Rinsed well and stored in DI water

Space between encapsulated electrical leads: Sensor 1_2 ~2.5 mm, Sensor 2_3 ~1.9 mm

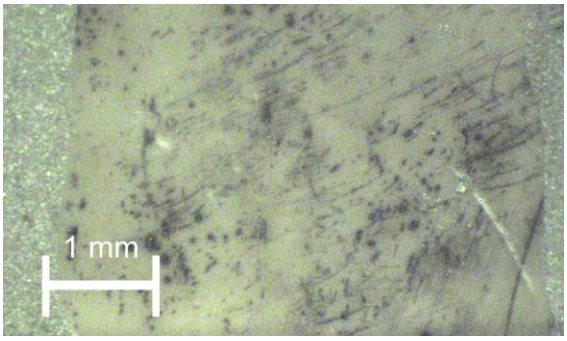

Figure 55: Sample 8 platinized polymer graft. Lightly platinized area (clusters of platinum appear dark) lies between the two encapsulated silver paint electrical leads.

iii) Sample 9

1. 3mL grafting solution - 4:00
2. Rinse 3x with DI water
3. 3mL "previously used" 5mg/mL Pt salt solution - 2:13
4. Rinse 1x indirectly
5. 3mL 0.1 wt% NaBH4 - 0:33
6. Rinse 3x with DI water
    a. Minimal platinization
7. Stored in DI water overnight
8. 3mL "previously used" 5mg/mL Pt salt solution - 2:02
9. Rinse 1x indirectly
10. 3mL 0.1 wt% NaBH4 - 0:30
11. Rinse 3x with DI water
    a. Minimal platinization
12. Stored in DI water overnight
13. 3mL fresh 5mg/mL Pt salt solution - 2:00
14. Rinse 1x indirectly
15. 3mL 0.1 wt% NaBH4 - 0:30
16. Rinse 3x with DI water
    a. Slight platinization
17. 3mL "previously used" 5mg/mL Pt salt solution (UNCOVERED to allow evaporation and increased solution concentration) - 2:00
18. Rinse 1x indirectly
19. 3mL 0.1 wt% NaBH4 - 0:30
20. Rinse 3x with DI water
    a. Quite platinized

Space between encapsulated electrical leads: Sensor 1_2 ~2.0 mm, Sensor 2_3 ~3.0 mm

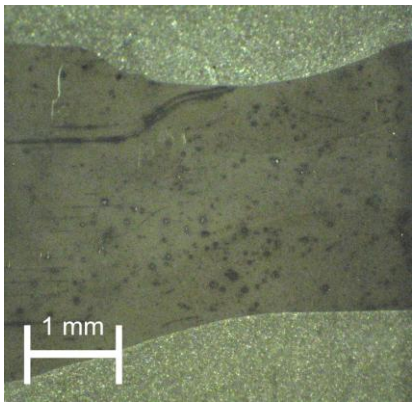

Figure 56: Sample 9 platinized polymer graft. Highly platinized area (clusters of platinum appear dark) lies between the two encapsulated silver paint electrical leads.

iv) Sample 11

1. Boiled in DI water 0:45
2. 3mL grafting solution - 4:02
3. Rinse 3x with DI water
4. 2mL 5mg/mL Pt salt solution (previously used) - 2:41
5. Rinse 1x indirectly
6. 3mL 0.1 wt% NaBH4 - 0:30
7. Rinse 3x with DI water
    a. Minimal platinization
8. Stored in DI water overnight
9. 3mL 5mg/mL Pt salt solution (previously used) – 1:59
10. Not rinsed
11. 3mL 0.1 wt% NaBH4 - 0:31
12. Rinse 3x with DI water
    a. Minor platinization
13. 2mL 5mg/mL Pt salt solution – 5:50
14. Rinse 1x indirectly
15. 3mL 0.1 wt% NaBH4 - 0:30
16. Rinse 3x with DI water
    a. Uneven platinization
17. Boiled in DI water 0:15 to remove reactants
18. Dried in vacuo @ 30C
19. Stored in plastic bag prior to encapsulation

Space between encapsulated electrical leads: Sensor 1_2 ~3.0 mm, Sensor 2_3 ~3.5 mm

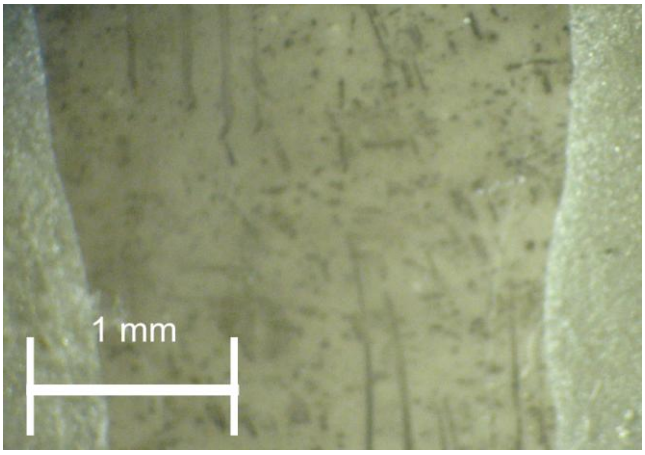

Figure 57: Sample 11 platinized polymer graft. Platinized area (clusters of platinum appear darker) lies between the two encapsulated silver paint electrical leads.

III Fouling experiments: cross-flow configuration

i) Sample 8

Cross-flow fouling experiment (9/15/09 – 9/22/09):

1. Sensor mounted in test cell using Kapton to further insulate electrical leads.
2. 20 L of deionized water was poured into the cleaned feed tank, and the system was primed.
3. Operating conditions were set to 1.03 MPa, 0.75 L/min. Steady state temperature was 29°C.
4. At hour 87.6, 85 mL of 1g/100mL BSA stock solution was added to the feed tank (BSA concentration is 42.5 mg/L)
5. System was shut down after 167 hours of operation.

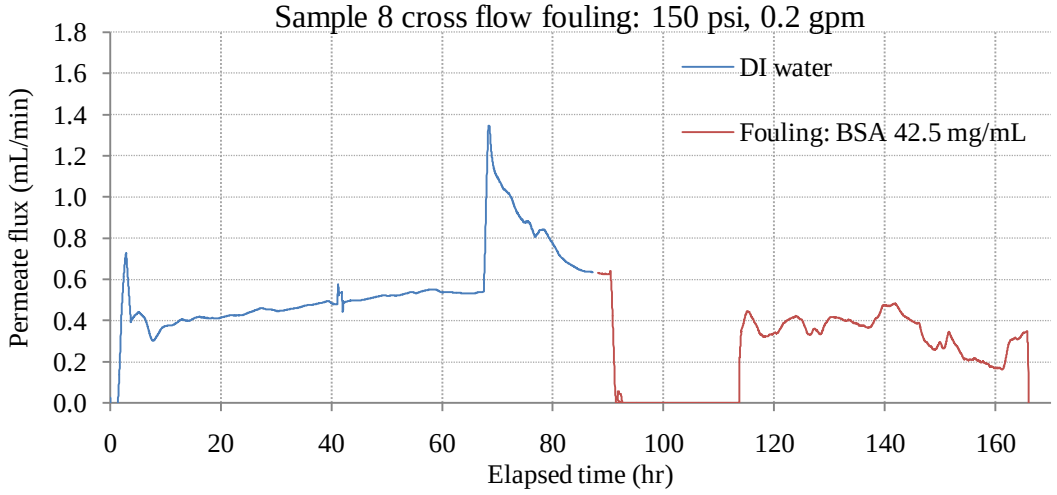

Figure 58: Cross-flow permeate flux data, blue line was measured pre-fouling, red line was during fouling. Lines are 50 minute moving averages.

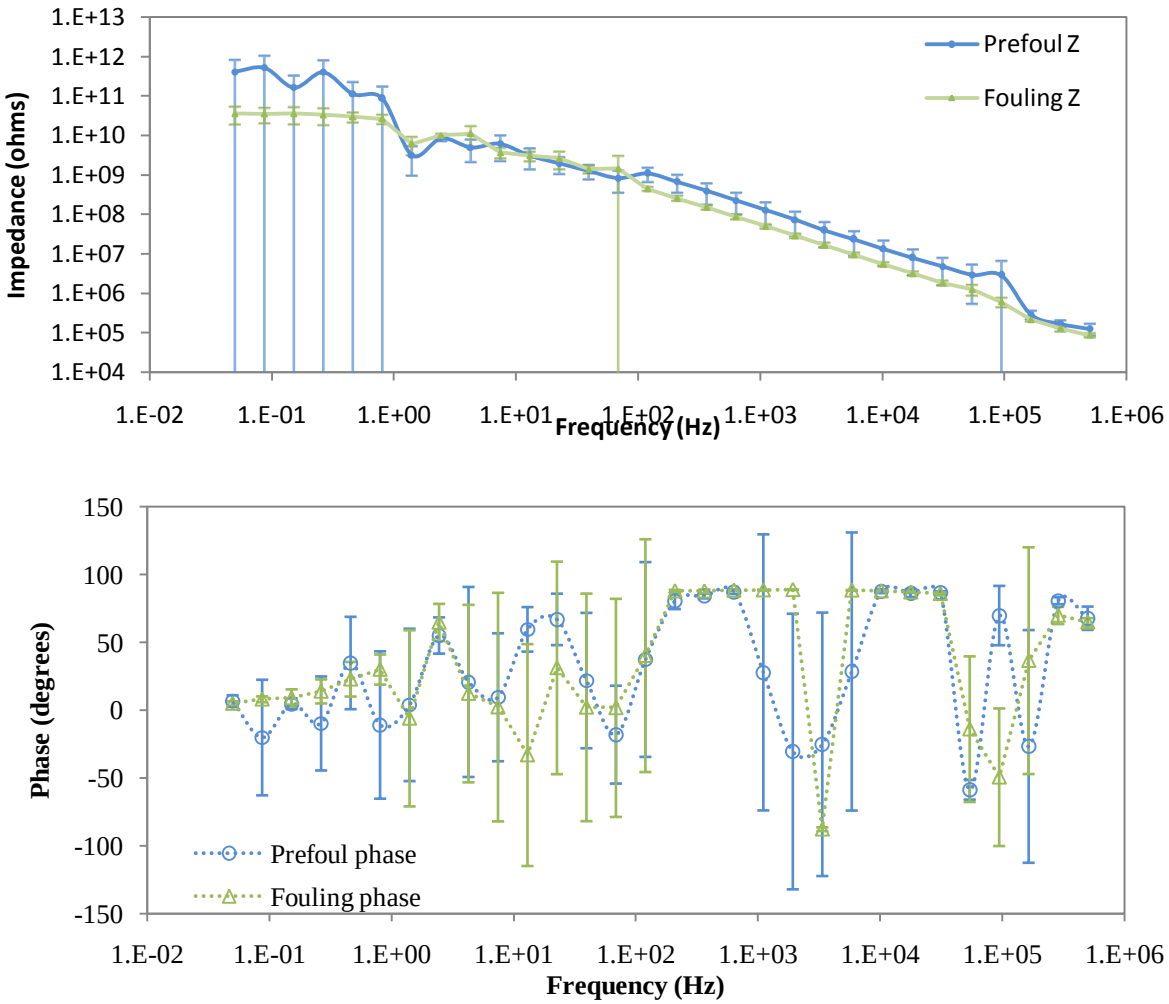

Figure 59: Averaged impedance response of sensor (Sample 8 1_2) to fouling with cross-flow system. Consecutive runs with similar impedances were averaged: the last 40 hours of deionized water for "Prefoul" and the last 24 hours of protein fouling. Error bars indicate one standard deviation. BSA was introduced into 20L of water at a concentration of 42.5 mg/L after 87.5 hours of the cross-flow system operating at 1.03 MPa and a flow rate of 0.2 gpm.

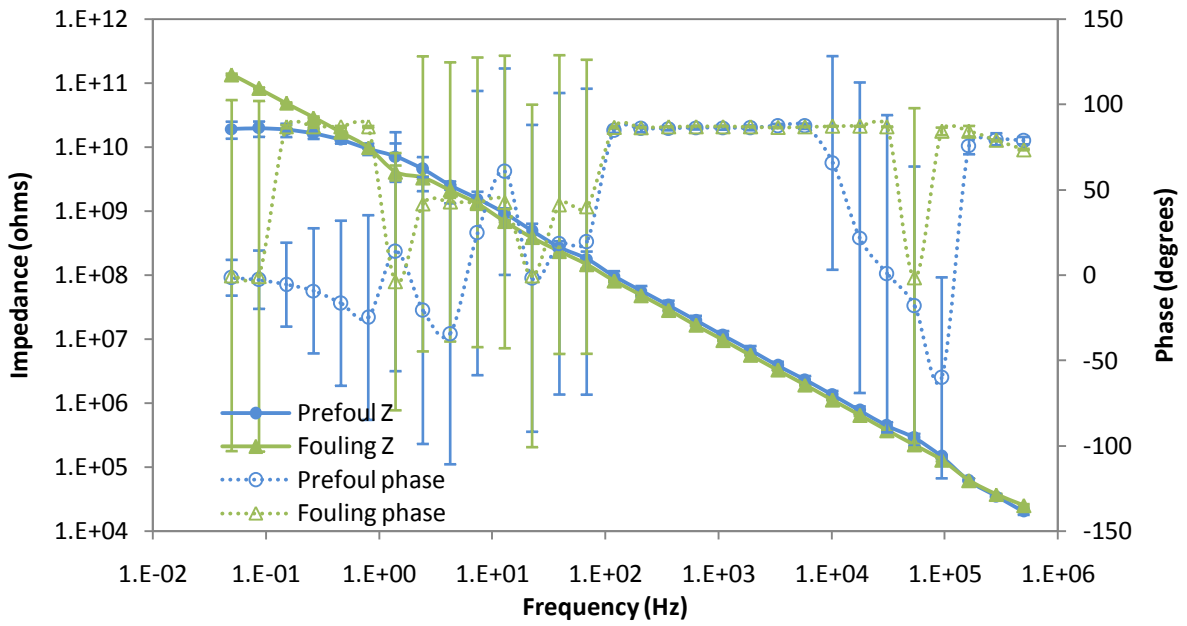

Figure 60: Averaged impedance response of sensor (Sample 8 2_3) to fouling with cross-flow system. Consecutive runs with similar impedances were averaged: the last 40 hours of deionized water for "Prefoul" and the last 24 hours of protein fouling. BSA was introduced into 20L of water at a concentration of 42.5 mg/L after 87.5 hours of the cross-flow system operating at 1.03 MPa and a flow rate of 0.2 gpm.

ii) Sample 9

Cross-flow fouling experiments (9/23/09 – 10/2/09):

1. Sensor mounted in test cell using Kapton to further insulate electrical leads.
2. 20 L of deionized water was poured into the cleaned feed tank, and the system was primed.
3. Operating conditions were set to 1.03 MPa, 0.75 L/min. Steady state temperature was 29°C.
4. At hour 112.2, 100 mL of 1g/100mL BSA stock solution was added to the feed tank (BSA concentration is 50 mg/L)
5. At hour 160, system was drained and fresh deionized water was run through for 5 minutes to remove as much BSA as possibly from the RO system.
6. System drained again and 20 L fresh deionized water added for the post-fouling run.
    a. Permeate flux data was not zeroed correctly and so post-fouling data is erroneous.
7. System was shut down after 214 hours of operation.

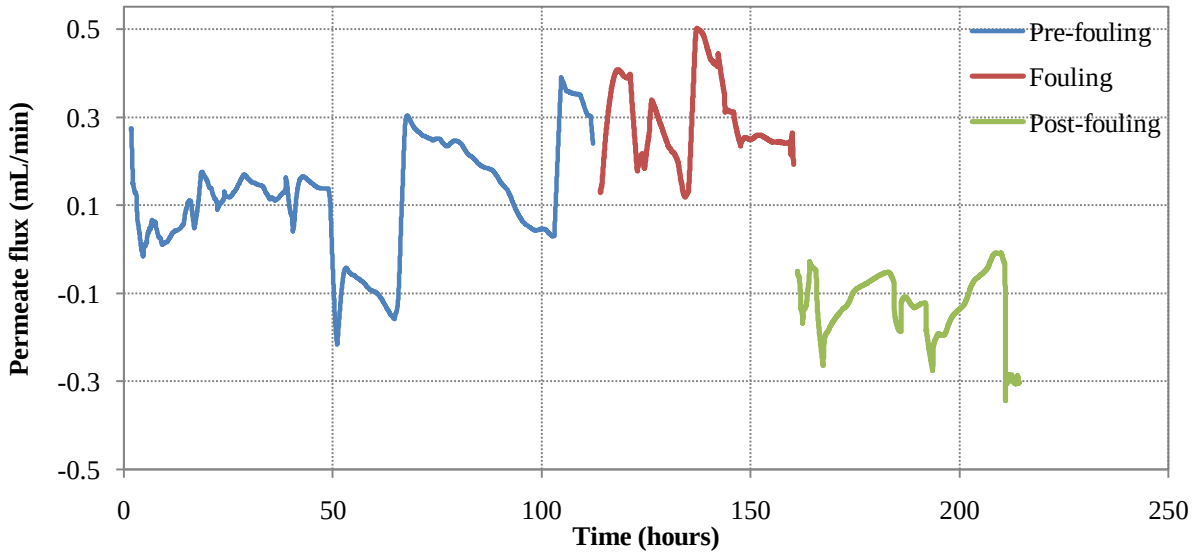

Figure 61: Cross-flow permeate flux data, blue line was measured pre-fouling, red line was during fouling. Lines are 100 minute moving averages. Significant drops in flux occurred when system was shut off to take electrically disconnected EIS measurements.

IV Fouling experiments: dead-end configuration

i) Sample 7

Dead-end fouling experiments (8/26/09 – 8/31/09):

1. 100 mL DI water added to system and pressurized with N_2 to 1 MPa (~ 145 psi)
2. After all water had been produced as permeate, the membrane was rinsed membrane 1x.
3. System filled with another 100mL DI water.
4. Pressure off and system sat in DI water over the weekend
5. Drained test cell of water, filled with another ~95mL DI water
6. Rinsed 1x DI water.
7. Added 98mL DI water + 20mg BSA (2 mL of stock solution: 2000mg BSA/100mL DI water)
8. Pressure off - 10.4 mL of fouling solution remained in test cell
9. Rinsed 3x, filled with 75 mL DI water for post-fouling, pressurized to 1 MPa.
10. Overnight in DI water, rinsed 1x, 95 mL DI water added before pressurizing to 1 MPa
11. Removed from test cell and rinsed well with DI water.
12. Dried in vacuo for 12+ hours.

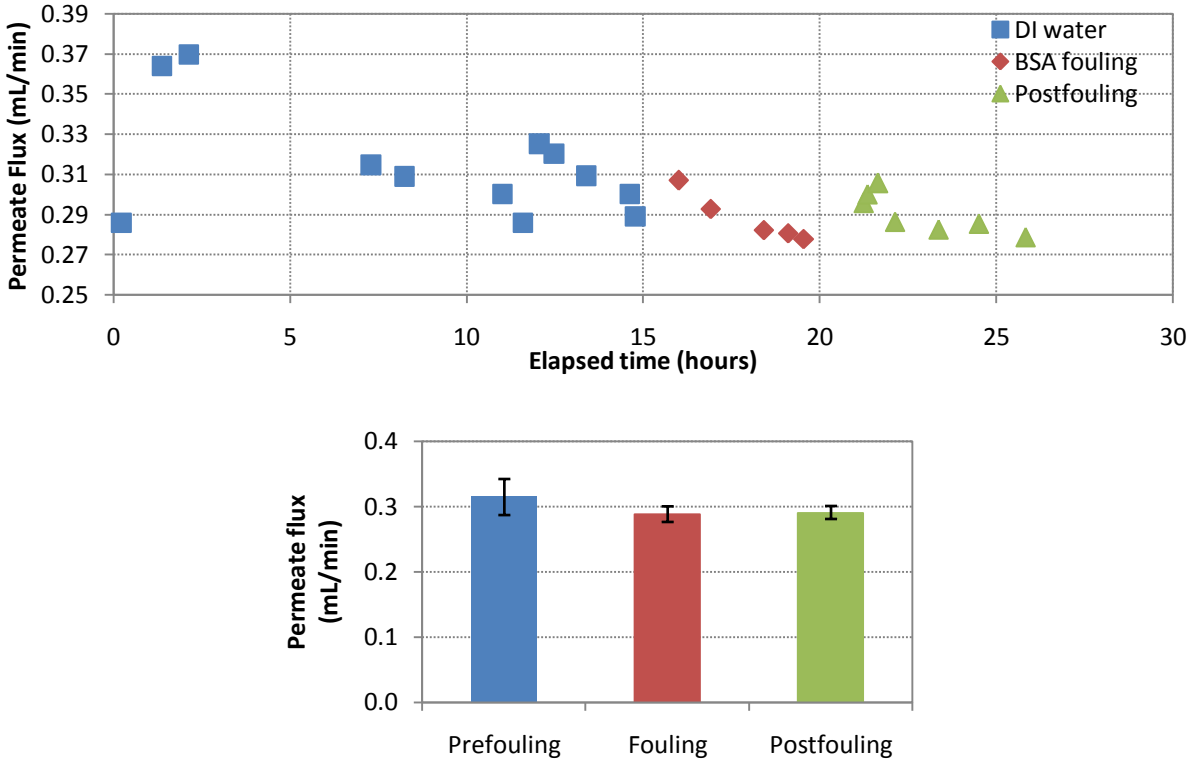

Figure 62: Dead-end permeate flux data. The upper graph plots the individual points of data calculated from volumetric and time data. The lower graph shows the averages of each segment of the experiment with the error bars representing one standard deviation.

ii) Sample 11

Dead-end fouling experiments (10/28/09 – 11/05/09):

1. 102 mL DI water added to system and pressurized with N_2 to 1 MPa (~ 145 psi)
2. Pressure off and system sat in DI water overnight.
3. At hour 15.9, 50 mg BSA was added to 100mL DI water and system was filled with solution
4. Pressure off – 4.5 mL of fouling solution remained in test cell
5. Test cell not rinsed, pressurization hose rinsed once with deionized water.
6. 95 mL DI water added before pressurizing to 1 MPa
7. Removed from test cell and stored in sealed plastic bag.

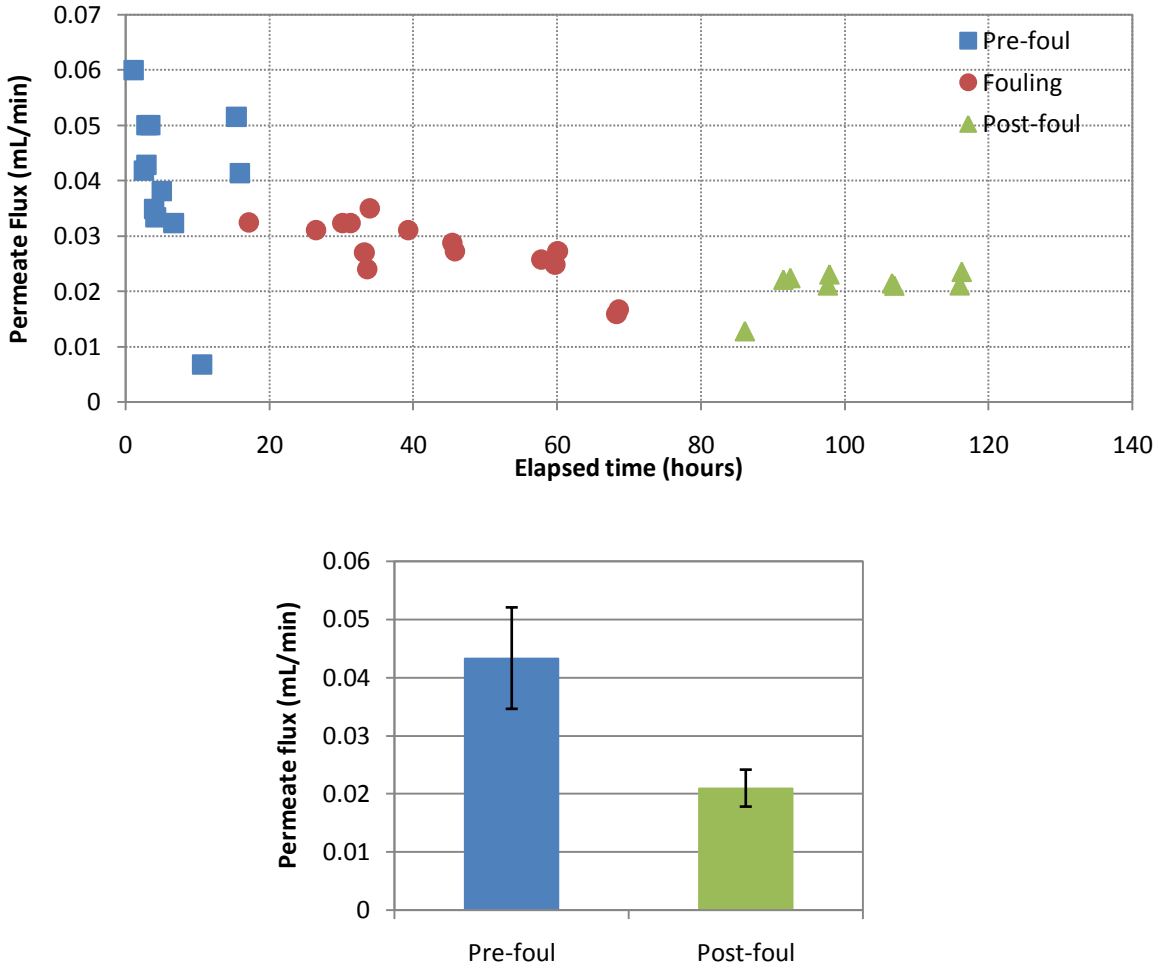

Figure 63: Dead-end permeate flux data. The upper graph plots the individual points of data calculated from volumetric and time data. The lower graph shows the averages of each segment of the experiment with the error bars representing one standard deviation.